

**A STUDY ON DESIGN OF
ORTHOGONAL DTCWTS WITH
IMPROVED PROPERTIES**

by

Daiwei Wang

A Dissertation Submitted in Partial Fulfillment of
the Requirements for the Degree of
Doctor of Engineering

at

THE UNIVERSITY OF
ELECTRO-COMMUNICATIONS TOKYO-JAPAN

July 2014

**A STUDY ON DESIGN OF
ORTHOGONAL DTCWTS WITH
IMPROVED PROPERTIES**

APPROVED BY SUPERVISORY COMMITTEE:

Chairman: Prof. Xi ZHANG

Member: Prof. Wataru MITSUHASHI

Prof. Takayuki NAGAI

Associate Prof. Kota TAKAHASHI

Associate Prof. Hideyuki NOMURA

Copyright

by

Daiwei Wang

2014

各種の性質を改善した直交 DTCWT の設計 に関する研究

王 戴維

概要

双対木複素ウェーブレット変換 (DTCWT: Dual Tree Complex Wavelet Transform) は信号処理や画像処理などの多くの分野で応用されている。DTCWT は、二つの実係数フィルタバンクを用いたウェーブレット変換で実行され、それぞれ複素数の実部と虚部に対応する。二つのウェーブレット基底はヒルベルト変換対となる必要がある。その結果、双対木複素ウェーブレット変換は近似的にシフト不変性であり、高次元信号の場合、より良い方向選択性を持つ。本論文では、改善された特性を持つ二種類の双対木複素ウェーブレット変換を提案する。

第二章では、まず双対木複素ウェーブレット変換の基礎について簡潔に述べる。ウェーブレット変換は時間と周波数領域において信号を同時に解析できる有効なツールである。スケーリング係数とウェーブレット係数を効率よく得るため、離散ウェーブレット変換が導入され、離散ウェーブレット変換は 2 チャネルフィルタバンクを用いて実現できる。次に、2 チャネルフィルタバンクの設計条件：完全再構成条件と直交条件を説明し、ウェーブレット関数の直交性、対称性やバニシングモーメント等の性質について述べる。さらに、双対木複素ウェーブレット変換の構造を説明し、二つのウェーブレット基底がヒルベルト変換対となることを必要であることを明らかにする。ヒルベルト変換対になるために、二つのスケーリングローパスフィルタが半サンプル遅延条件を満たすことが要求される。最後に、複素ウェーブレット変換の性能を評価するための評価基準を示す。

第三章では、異なる次数の分子と分母を持つ一般的な IIR フィルタを用いて、改善された解析性と周波数選択性を持つ双対木複素ウェーブレット変換を提案する。Selesnick により提案された共通因子法では、半サンプル遅延条件を満たすために、最大平坦オールパスフィルタが使用された。しかし、得られた複素ウェーブレット変換の解析性が良くなかった。複素ウェーブレット変換の解析性を改善するために、平坦度を指定して近似帯域で等リプル位相特性を持つオールパスフィルタの設計法を提案する。また、スケーリングローパスフィルタの周波数選択性を改善するために、 $z=-1$ における零点の数を指定して阻止域の振幅誤差を最小化する。Remez アルゴリズムを用いて、等リプル特性を近似

する．よって，固有値問題を解くことで，簡単にフィルタ係数が得られる．さらに，双対木複素ウェーブレット変換の性能を調査し，近似帯域と阻止域の適切な与え方を示す．Selesnick により提案された DTCWT は本論文で提案された DTCWT の特殊なケースにすぎないことを明らかにする．

第四章では，任意の対称中心を持つ近似的に対称な双対木複素ウェーブレット変換を提案する．複素ウェーブレット変換の解析性を改善するために，まずスケールリングローパスフィルタの群遅延の平坦度とバニシングモーメントを指定し，二つのスケールリングローパスフィルタの間の周波数応答の差を最小化する．次に，Remez アルゴリズムを用いて定式化し，わずかに数回の反復計算で，誤差関数の等リプル特性を得る．よって，二つのスケールリングローパスフィルタを同時に設計することができる．得られた複素ウェーブレット変換は，直交であり，対称性と解析性が改善できる．さらに，スケールリングローパスフィルタの群遅延が任意に指定できるため，スケールリング関数は任意の対称中心を持つ．いくつかの設計例を通じて，本論文で提案された DTCWT の設計手法の有効性を示す．最後に，ノイズ低減の応用例を通じて，本論文で設計された DTCWT が優れたノイズ除去性能を達成できることを明らかにする．

A STUDY ON DESIGN OF ORTHOGONAL DTCWTS WITH IMPROVED PROPERTIES

DAIWEI WANG

Abstract

The Dual tree complex wavelet transforms (DTCWTs) have been found to be successful in many applications of signal and image processing. DTCWTs employ two real wavelet transforms, where one wavelet corresponds to the real part of complex wavelet and the other is the imaginary part. Two wavelet bases are required to be a Hilbert transform pair. Thus, DTCWTs are nearly shift invariant and have a good directional selectivity in two or higher dimensions with limited redundancies. In this dissertation, we propose two new classes of DTCWTs with improved properties.

In Chapter 2, we review the Fourier transform at first and then introduce the fundamentals of dual tree complex wavelet transform. The wavelet transform has been proved to be a successful tool to express the signal in time and frequency domain simultaneously. To obtain the wavelet coefficients efficiently, the discrete wavelet transform has been introduced since it can be achieved by a tree of two-channel filter banks. Then, we discuss the design conditions of two-channel filter banks, i.e., the perfect reconstruction and orthonormality. Additionally, some properties of scaling and wavelet functions including orthonormality, symmetry and vanishing moments are also given. Moreover, the structure of DTCWT is introduced, where two wavelet bases are required to form a Hilbert transform pair. Thus, the corresponding scaling lowpass filters must satisfy the half-sample delay condition. Finally, the objective measures of quality are given to evaluate the performance of the complex wavelet.

In Chapter 3, we propose a new class of DTCWTs with improved analyticity and frequency selectivity by using general IIR filters with numerator and denominator of different degree. In the common-factor technique proposed by Selesnick, the maximally flat allpass filter was used to satisfy the half-sample delay condition, resulting in poor analyticity of complex wavelets. Thus, to improve the analyticity of complex wavelets, we present a method for designing allpass filters with the specified degree of flatness and equirip-

ple phase response in the approximation band. Moreover, to improve the frequency selectivity of scaling lowpass filters, we locate the specified number of zeros at $z = -1$ and minimize the stopband error. The well-known Remez exchange algorithm has been applied to approximate the equiripple response. Therefore, a set of filter coefficients can be easily obtained by solving the eigenvalue problem. Furthermore, we investigate the performance on the proposed DTCWTs and dedicate how to choose the approximation band and stopband properly. It is shown that the conventional DTCWTs proposed by Selesnick are only the special cases of DTCWTs proposed in this dissertation.

In Chapter 4, we propose another class of almost symmetric DTCWTs with arbitrary center of symmetry. We specify the degree of flatness of group delay, and the number of vanishing moments, then apply the Remez exchange algorithm to minimize the difference between two scaling lowpass filters in the frequency domain, in order to improve the analyticity of complex wavelets. Therefore, the equiripple behaviour of the error function can be obtained through a few iterations. Moreover, two scaling lowpass filters can be obtained simultaneously. As a result, the complex wavelets are orthogonal and almost symmetric, and have the improved analyticity. Since the group delay of scaling lowpass filters can be arbitrarily specified, the scaling functions have the arbitrary center of symmetry. Finally, several experiments of signal denoising are carried out to demonstrate the efficiency of the proposed DTCWTs. It is clear that the proposed DTCWTs can achieve better performance on noise reduction.

Contents

Chapter 1	Introduction	5
1.1	Background	5
1.2	Previous Design Methods	7
1.3	Contributions and Organizations of the Dissertation	9
Chapter 2	Fundamentals of Dual Tree Complex Wavelet Transform	13
2.1	Introduction	13
2.2	Fourier Analysis	13
2.2.1	Fourier Transform	13
2.2.2	Short-Time Fourier Transform	14
2.3	Wavelet Theory	15
2.3.1	Wavelet Series Expansion and Multiresolution	15
2.3.2	Discrete Wavelet Transform	18
2.3.3	Two Channel Filter Banks	19
2.3.3.1	Basic Structure	19
2.3.3.2	Perfect Reconstruction	20
2.3.3.3	Orthonormality	21
2.3.3.4	Symmetry	22
2.3.3.5	Vanishing Moments	23
2.4	Dual Tree Complex Wavelet Transform	24
2.4.1	Basic Structure	24
2.4.2	Half-sample Delay Condition	26
2.4.3	Error Function	26
2.5	Objective Measures of Analyticity	27
2.6	Summary	27
Chapter 3	Orthogonal DTCWTs with Improved Analyticity and Frequency Selectivity	29
3.1	Introduction	29
3.2	The Common-Factor Technique	30
3.2.1	Hilbert Transform Pairs by Allpass Filter	30
3.2.2	FIR Orthonormal Solution	32
3.2.3	IIR Orthonormal Solution	33
3.2.4	General IIR Orthonormal Solution	35
3.2.5	Design Examples	38

3.3	DTCWTs with Improved Analyticity	50
3.3.1	Flatness Condition	50
3.3.2	Phase Error Minimization	52
3.3.3	Design Algorithm	54
3.3.4	Design Examples	55
3.4	DTCWTs with Improved Frequency Selectivity	69
3.4.1	Formulation using Remez exchange algorithm	69
3.4.2	Design Algorithm	72
3.4.3	Design Examples	73
3.5	Performance Investigation	86
3.6	Summary	89
Chapter 4	Almost Symmetric DTCWTs with Arbitrary Center of Symmetry	91
4.1	Introduction	91
4.2	Q-Shift Filters	92
4.3	DTCWTs with Arbitrary Center of Symmetry	94
4.3.1	Approximation of Flat Group Delay	95
4.3.2	Orthonormality and Vanishing Moments	97
4.3.3	Linearization of the Design Problem	98
4.3.4	Design Algorithm	100
4.3.5	Design Examples	101
4.4	DTCWTs with Improved Analyticity	113
4.4.1	Initial Solution	113
4.4.2	Formulation using Remez exchange algorithm	115
4.4.3	Design Algorithm	117
4.4.4	Design Examples	118
4.5	Signal Denoising Application	138
4.5.1	Denoising Using Wavelet Thresholding	138
4.5.2	Denoising Using DTCWT Thresholding	139
4.5.3	Experiments on Signal Denoising	142
4.6	Summary	154
Chapter 5	Conclusion	155
	References	157
	Acknowledgements	163
	List of Publications	167

Notation

$\phi(t)$	scaling function
$\psi(t)$	wavelet function
$\psi_c(t)$	complex wavelet function
$\psi_1(t)$	wavelet function of Tree A (real part of $\psi_c(t)$)
$\psi_2(t)$	wavelet function of Tree B (imaginary part of $\psi_c(t)$)
$\Phi(\omega)$	Fourier transform of $\phi(t)$
$\Psi(\omega)$	Fourier transform of $\psi(t)$
$\Psi_c(t)$	Fourier transform of $\psi_c(t)$
$\Psi_1(t)$	Fourier transform of $\psi_1(t)$ of Tree A
$\Psi_2(t)$	Fourier transform of $\psi_2(t)$ of Tree B
$c_{j,n}$	scaling coefficient
$d_{j,n}$	wavelet coefficient
$d_{j,n}^c$	complex wavelet coefficient
$d_{j,n}^A$	wavelet coefficient of Tree A (real part of $d_{j,n}^c$)
$d_{j,n}^B$	wavelet coefficient of Tree B (imaginary part of $d_{j,n}^c$)
$\hat{d}_{j,n}$	wavelet coefficient after thresholding
$\hat{d}_{j,n}^c$	complex wavelet coefficient after thresholding
$h(n)$	impulse response of lowpass filter in analysis filter
$h_1(n)$	impulse response of lowpass filter of Tree A
$h_2(n)$	impulse response of lowpass filter of Tree B

$H(z)$	transfer function of lowpass filter in analysis filter
$\tilde{H}(z)$	transfer function of lowpass filter in synthesis filter
$H_1(z)$	transfer function of lowpass filter of Tree A
$H_2(z)$	transfer function of lowpass filter of Tree B
$g(n)$	impulse response of highpass filter in analysis filter
$G(z)$	transfer function of highpass filter in analysis filter
$\tilde{G}(z)$	transfer function of highpass filter in synthesis filter
$\mu(r)$	moment of impulse response of highpass filter
$m(r)$	moment of wavelet function
K	number of vanishing moment
$\theta(\omega)$	phase response of lowpass filter
$\theta_1(\omega)$	phase response of lowpass filter of Tree A
$\theta_2(\omega)$	phase response of lowpass filter of Tree B
$\theta_d(\omega)$	desired phase response of lowpass filter
$\theta_1^d(\omega)$	desired phase response of lowpass filter of Tree A
$\theta_2^d(\omega)$	desired phase response of lowpass filter of Tree B
$\theta_e(\omega)$	error phase response of lowpass filter
$\theta_1^e(\omega)$	error phase response of lowpass filter of Tree A
$\theta_2^e(\omega)$	error phase response of lowpass filter of Tree B
τ	group delay of lowpass filter
τ_1	group delay of lowpass filter of Tree A
τ_2	group delay of lowpass filter of Tree B
$A(z)$	transfer function of allpass filter

$a(n)$	coefficient of allpass filter
J	degree of allpass filter
L	degree of flatness of group delay
N	degree of FIR filter or numerator of IIR filter
M	number of integer delay in half-sample delay condition
$P(z)$	product filter
ω_c	cutoff frequency of approximation band of allpass filter
ω_s	cutoff frequency of stopband of lowpass filter
T	threshold value
$E(\omega)$	error function
E_p	objective measure of analyticity of complex wavelet
$H\{\cdot\}$	Hilbert transform
$\lfloor \cdot \rfloor$	largest integer not greater than \cdot
$\mathcal{D}(\cdot, \cdot)$	thresholding operator

Chapter 1 Introduction

1.1 Background

A *wavelet* is a locally oscillating function that can be used to capture informative, efficient, and useful descriptions of a signal. Despite of its short history, wavelet theory has been proved to be a powerful mathematical tool for analysis and synthesis of signals and has been used in a remarkable diversity of disciplines such as physics, geophysics, numerical analysis, signal processing, biomedical engineering, statistics, and computer graphics [1] ~ [3], [26].

Why have wavelets been proved so useful in such a wide range of applications? The primary reason is because they collect information from both temporal and frequency domain simultaneously while cutting up data into different frequency components, and then study each component with a resolution matched to its scale. Therefore, they can provide an extremely efficient representation for many types of signals, that appear often in practice but are not well matched by the Fourier basis, which is ideally meant for periodic signals. Another reason encourages us is that the coefficients from a fine-scale representation can be easily obtained from two octave-band, discrete-time filter banks that recursively apply a discrete-time lowpass filter, a highpass filter, and upsampling and downsampling operations [1] ~ [3]. However, the wavelet transform itself also suffer four fundamental shortcomings in spite of its efficient signal representation and multiscale analysis [26];

1. OSCILLATION

It is attractive that if wavelet coefficients could be large at the edge or the sharp position. Generally, the wavelet coefficients tend to oscillate positive and negative around these areas.

2. **SHIFT VARIANCE** A small shift of signal would generate a great difference of wavelet coefficients, especially the wavelet coefficients oscillate around singularities.

3. ALIASING

As mentioned above, the wavelet coefficients can be computed from the signal via iterated discrete-time downsampling operations from lowpass and highpass filters, resulting in substantial aliasing.

4. LACK OF DIRECTIONAL SELECTIVITY

In two or higher dimensions, the wavelet produces a checkerboard pattern that is oriented along 4 directions, i.e., 0° , 45° , 90° , 135° . This lack of directional selectivity greatly complicates modelling and processing of geometric image features like edges.

The undecimated wavelet transform [10] seems to be a good solution to these four DWT shortcomings, since downsampling and upsampling operations have not been adopted. However, the undecimated wavelet transform leads in a huge redundancy as the output of each level of signal contains the same number of samples as the input. Therefore, a better solution between shift invariance and redundancies in the wavelet coefficients is to use a complex wavelet instead, in which one of the most successful and widely-used approaches is dual-tree complex wavelet transform (DTCWT).

DTCWT was originally introduced by Kingsbury [13], and has been found to be successful in many applications of signal and image processing [13] ~ [29]. DTCWT provides the following significant improvements over the conventional discrete wavelet transform (DWT) in [1], i.e., it is of approximate shift invariance, enhanced directional selectivity for multidimensional signals and gives the explicit phase information [26]. Generally, the DTCWT is constructed by a Hilbert transform pair of wavelets (90° out of phase with each other). It has been shown in [20], [23] and [27] ~ [30] that the necessary and sufficient condition for two wavelet bases to be a Hilbert transform pair is that the two corresponding lowpass filters should satisfy the half-sample delay condition.

1.2 Previous Design Methods

Several design procedures for constructing DTCWTs had been presented in [13] ~ [48]. In [20], Selesnick had proposed a common-factor design technique, where the scaling lowpass filters are constructed by using allpass filters to satisfy the half-sample delay condition. This method is simple and effective, since the approximation accuracy of the half-sample delay is controlled only by the allpass filter. Selesnick had adopted the maximally flat allpass filter and given a class of FIR orthonormal and biorthogonal solutions, and IIR orthonormal solution, where the scaling lowpass filters have as many zeros at $z = -1$ as possible to obtain the maximum number of vanishing moments of wavelets, resulting in the maximally flat magnitude responses of the scaling lowpass filters. It is well known that frequency selectivity is a useful property for many applications of signal processing. However, the maximally flat filters have poor frequency selec-

tivity [2]. In addition, the resulting IIR scaling lowpass filters have the numerator and denominator of the (almost) same degree. In [25], a new class of Hilbert transform pairs of orthonormal wavelet bases has been proposed by using general IIR filters, where the degree of numerator is larger than that of the denominator, but only the maximally flat design has been discussed. The maximally flat allpass filters have a larger phase error as $|\omega|$ increases, resulting in a poor analyticity of complex wavelet.

The wavelet filters obtained by the common-factor method have non-linear phase responses, resulting in asymmetric wavelet bases. Generally, the symmetric wavelet bases are widely used in image processing since the perceptually objectionable distortions around image edges can be effectively reduced. Therefore, several methods have been proposed for obtaining symmetric wavelet bases. Q-shift filters were proposed by Kingsbury in [16], [17], [22]. In [16], two scaling lowpass filters were selected to be the time-reversed versions of each other. Therefore, the group delay of lowpass filter is required to be $1/4$ (quarter) or $3/4$ sample from the half-sample delay condition, and then the filter was called as Q-shift filter. Some design methods for Q-shift filters have been also proposed in [17], [22], [41], [42] to improve the vanishing moments, symmetry and so on. In addition, SSH (symmetric self-Hilbertian) filter had been proposed by Tay in [30] and its design had been discussed in [31], [45], [47]. In principle, SSH filters are the same as Q-shift filters, and have a group delay of $1/4$ sample.

In many applications of signal and image processing, digital filters with the specified (fractional or integer) group delay are often needed [3], [6]. For the conventional DWTs, nearly symmetric orthogonal wavelets, e.g.,

coiflets, had been proposed in [1, chapter 8.2], and the original coiflets had also been generalized by varying the group delay at $\omega = 0$, i.e., the center of symmetry of scaling function, where non-integer group delay was used to obtain a rich class of new wavelets [11], [12]. Therefore, it is reasonable to design a class of almost symmetric DTCWTs with arbitrarily specified group delay responses.

1.3 Contributions and Organizations of the Dissertation

This dissertation proposes two new classes of DTCWTs with different improved properties. First of all, we propose a new class of DTCWTs with improved analyticity and frequency selectivity by using general IIR filters with numerator and denominator of different degree based on common-factor method. Next, we propose another class of almost symmetric DTCWTs with arbitrary center of symmetry. The scaling lowpass filters can have the specified group delay responses, resulting in the scaling functions having arbitrary center of symmetry. The resulting DTCWTs are orthogonal and almost symmetric, and have the improved analyticity.

In Chapter 2, we first review Fourier transform and short time Fourier transform, and then introduce the theory of wavelet transform including wavelet series expansion and multiresolution. It is shown that the signal can be easily constructed from a single wavelet by its shift and scaling. The discrete wavelet transform is introduced to obtain the wavelet coefficients efficiently, since the coefficients can be calculated by a tree of two-channel filter banks. Next, we discuss the properties of wavelets in-

cluding orthonormality, symmetry and vanishing moments. Moreover, the structure of Dual tree complex wavelet transforms (DTCWTs) is given, which is consisted from two conventional discrete wavelet transform. Two wavelet bases are required to form a Hilbert transform pair, thus, the corresponding scaling lowpass filters must satisfy the half-sample delay condition. Finally, two objective measures are introduced to evaluate the performance of complex wavelet.

In Chapter 3, we propose a new class of DTCWTs with improved analyticity and frequency selectivity by using general IIR filters with numerator and denominator of different degree. To improve the analyticity of complex wavelet, we present a method for designing allpass filters with the specified degree of flatness at $\omega = 0$ and equiripple phase response in the approximation band. To improve the frequency selectivity of the scaling lowpass filters, we specify the number of zeros at $z = -1$ from the viewpoint of vanishing moments and then minimize the stopband error by using the remaining degree of freedom. The proposed design procedures are based on the well-known Remez exchange algorithm, thus, a set of filter coefficients can be easily obtained by solving the eigenvalue problem. The optimal solution is attained through a few iterations. It is shown that the conventional FIR and IIR orthonormal solutions proposed in [20] are only the special cases of DTCWTs proposed in this dissertation. Moreover, we investigate the performance on the proposed DTCWTs and indicate how to choose the approximation band properly.

In Chapter 4, we propose another class of almost symmetric DTCWTs with arbitrary center of symmetry. We design simultaneously two scaling lowpass filters with the specified flat group delay at $\omega = 0$, which sat-

isfy the half-sample delay condition. In addition to specifying the number of vanishing moments, we apply the Remez exchange algorithm to minimize the difference between two scaling lowpass filters in the frequency domain, in order to improve the analyticity of complex wavelets. The equiripple behaviour of the error function can be obtained through a few iterations. As a result, the complex wavelets are orthogonal and almost symmetric, and have the improved analyticity. Differently from Q-shift filters, the group delay responses of scaling lowpass filters can be arbitrarily specified, resulting in the scaling functions having the arbitrary center of symmetry. Moreover, it is shown that DTCWTs proposed in this dissertation can achieve better analyticity than Q-shift filters. Finally, we introduce wavelet thresholding scheme to investigate the performance of noise reduction by using the proposed DTCWTs.

In Chapter 5, we conclude the dissertation.

Chapter 2 Fundamentals of Dual Tree Complex Wavelet Transform

2.1 Introduction

In this chapter, we briefly review the theory of Fourier analysis and short time Fourier transform, and then introduce the fundamentals of wavelet theory, from wavelet series expansion, to two-channel filter bank. Next, a newly-developed technique referred as dual tree complex wavelet transform (DTCWT) is introduced. Two measures used for evaluating the performance of complex wavelet are given at the end of this chapter.

2.2 Fourier Analysis

2.2.1 Fourier Transform

The Fourier transform is one of the most significant mathematical tool for decomposing the signal into a sum of sines and cosines basis functions. Each of these basis functions is a complex exponential of a different frequency. Therefore, the Fourier transform maps the signal in time domain to the frequency domain.

Generally, the Fourier transform of a signal $x(t)$ can be expressed as

$$X(\omega) = \int_{-\infty}^{\infty} x(t)e^{-j\omega t} dt. \quad (2.1)$$

In addition, $x(t)$ can be obtained from $X(\omega)$ via the inverse Fourier transform:

$$x(t) = \frac{1}{2\pi} \int_{-\infty}^{\infty} X(\omega)e^{j\omega t} d\omega. \quad (2.2)$$

According to Eq.(2.1), we can not obtain the frequency spectrum for the signal in accurate time position. According to Eq.(2.2), it is difficult to extract the time information corresponding to the specified frequency spectrum. That is to say, the Fourier transform can only provide either time or frequency domain information. Therefore, short-time Fourier transform (STFT) had been proposed to obtain the local information in both time and frequency domains.

2.2.2 Short-Time Fourier Transform

The concept of STFT is obvious that it uses a window function (e.g., Hann window or Gaussian window), which is nonzero for only a short period of time, to provide the local information of time and frequency as the window slides along the time axis. The STFT can be expressed as

$$X(\omega, t_0) = \int_{-\infty}^{\infty} x(t)w(t - t_0)e^{-j\omega t} dt, \quad (2.3)$$

where $w(t)$ is the window function and t_0 is the local position. Thus, STFT is time and frequency localized, which can provide both time and frequency information.

However, the STFT only provides the equal resolution in time for lower and higher frequencies since the resolution is determined by the window size in advance. For the practical usage, it is reasonable to provide multiresolution for time-frequency analysis. Therefore, the wavelet transform had been proposed and proved to be a successful tool instead of STFT.

2.3 Wavelet Theory

2.3.1 Wavelet Series Expansion and Multiresolution

In the previous section, the Fourier transform is employed to transform signals between time and frequency domains. However, the signal can not contain information in both time and frequency domains simultaneously. In order to overcome the limitation of Fourier transform, another transform referred as *wavelet transform* had been proposed and proved to be a successful tool instead of Fourier transform. Differently from basis functions (sines and cosines) in Fourier transform, the wavelet bases are a set of locally oscillating functions, which are constructed from a single mother (or father) wavelet by its shift and scaling. Therefore, the scaling functions $\phi(t)$ and wavelet functions $\psi(t)$ at scale j with n shift are expressed as,

$$\begin{cases} \phi_{j,n}(t) = 2^{j/2}\phi(2^j t - n) \\ \psi_{j,n}(t) = 2^{j/2}\psi(2^j t - n) \end{cases} \quad (2.4)$$

Generally, a signal $x(t)$ can be represented as a linear combination of

the wavelet bases as

$$x(t) = \sum_n c_{j_0,n} \phi_{j_0,n}(t) + \sum_{j=j_0}^{\infty} \sum_n d_{j,n} \psi_{j,n}(t), \quad (2.5)$$

where $c_{j_0,n}$ are the *scaling coefficients* at scale 2^{j_0} and $d_{j,n}$ are the *wavelet coefficients* at scale 2^j . Eq.(2.5) is regarded as *wavelet series expansion*.

The scaling coefficients $c_{j_0,n}$ can be obtained by

$$c_{j_0,n} = \int_{-\infty}^{+\infty} x(t) \phi_{j_0,n}(t) dt, \quad (2.6)$$

while the wavelet coefficients $d_{j,n}$ can be obtained by

$$d_{j,n} = \int_{-\infty}^{+\infty} x(t) \psi_{j,n}(t) dt. \quad (2.7)$$

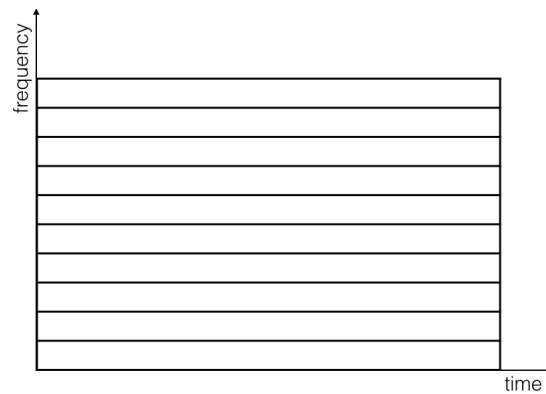
The first term in Eq.(2.5) represents the approximation of the signal $x(t)$ at level j_0 by the linear combination of the scaling functions $\phi_{j_0,n}(t)$ and the second term represents the details in different levels of the signal $x(t)$ by the linear combination of the wavelet functions $\psi_{j,n}(t)$. Thus, the scaling function has the characteristic of lowpass nature (“smooth” the signal) whereas the wavelet function has the characteristic of highpass nature (take “difference” of signal).

It should be noted that at each given resolution (level j) of the signal, the approximation plus the detail, the $\phi_{j,n}(t)$'s plus the $\psi_{j,n}(t)$'s, combine into a **multiresolution** of the signal at the finer level $j + 1$,

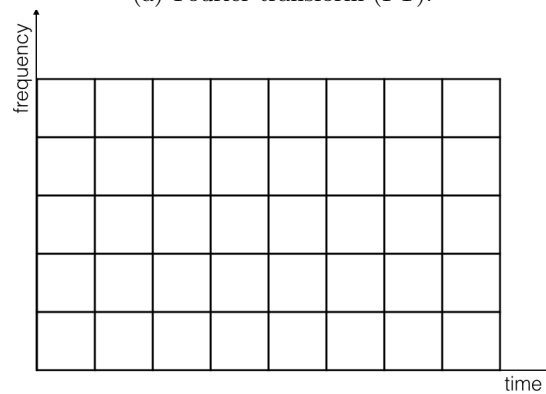
$$\sum_n c_{j+1,n} \phi_{j+1,n}(t) = \sum_n c_{j,n} \phi_{j,n}(t) + \sum_n d_{j,n} \psi_{j,n}(t). \quad (2.8)$$

Thus, the signal is usually expressed by the wavelet series expansion in its multiresolution representation. Fig.2.1 shows each mentioned-above trans-

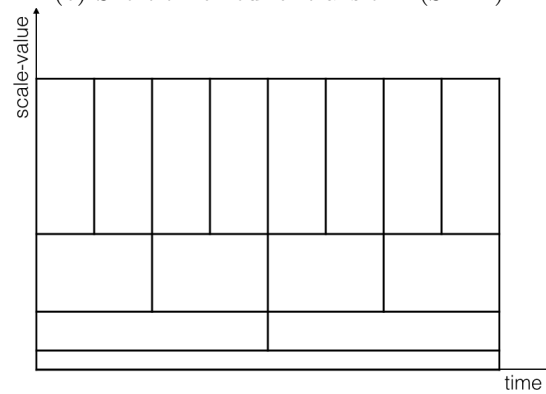
form in time-frequency representation. The Fourier transform only provides information about either time or frequency; The short-time Fourier transform provides local time-frequency information, but with the same resolution; The wavelet transform provides information about the time and frequency with different resolution.



(a) Fourier transform (FT).



(b) Short-time Fourier transform (STFT).



(c) Wavelet transform (WT).

Fig.2.1 Comparison of FT, STFT and WT

2.3.2 Discrete Wavelet Transform

For the practical usage of the wavelet transform and its multiresolution analysis, *discrete wavelet transform* had been proposed to compute the coefficients $c_{j,n}$ and $d_{j,n}$ quickly and efficiently. In the discrete time, the scaling function $\phi(t)$ satisfy **dilation equation**:

$$\phi(t) = \sqrt{2} \sum_n h(n) \phi(2t - n), \quad (2.9)$$

and the wavelet function $\psi(t)$ satisfy **wavelet equation**:

$$\psi(t) = \sqrt{2} \sum_n g(n) \phi(2t - n). \quad (2.10)$$

where $h(n)$ and $g(n)$ are lowpass filter and highpass filter from a **two-channel filter bank**, respectively.

Thus, multiresolution analysis in discrete time can be achieved by a tree of two-channel filter banks. The scaling and wavelet coefficients at scale 2^j can be computed from the scaling coefficients at the finer scale 2^{j+1} through a discrete-time filtering followed by a downsampling operations, while the scaling coefficients at the scale 2^{j+1} can be synthesized from the scaling and wavelet coefficients at the scale 2^j via a up-sampling operation followed by a discrete-time filtering. For instance, we start with $c_{j_1+1,n}$ and perform the decomposition $(j_1 - j_0 + 1)$ times:

$$\begin{array}{ccccccc} c_{j_1+1,n} & \longrightarrow & c_{j_1,n} & \longrightarrow & c_{j_1-1,n} & \longrightarrow & \cdots & \longrightarrow & c_{j_0,n} \\ & \searrow & & \searrow & & \searrow & & \searrow & \\ & & d_{j_1,n} & & d_{j_1-1,n} & & \cdots & & d_{j_0,n} \end{array},$$

while we can recover $c_{j_1+1,n}$ by performing the reconstruction $(j_1 - j_0 + 1)$

times:

$$\begin{array}{ccccccc}
 c_{j_0,n} & \longrightarrow & c_{j_0+1,n} & \longrightarrow & \cdots & \longrightarrow & c_{j_1,n} & \longrightarrow & c_{j_1+1,n} \\
 & \nearrow & & \nearrow & & \nearrow & & \nearrow & . \\
 d_{j_0,n} & & d_{j_0+1,n} & & \cdots & & d_{j_1,n} & &
 \end{array}$$

Thus, it is obvious that the discrete wavelet transform provides an efficient discrete-time approach to compute the wavelet series expansion by its recursive process.

2.3.3 Two Channel Filter Banks

2.3.3.1 Basic Structure

The basic structure of two-channel filter bank is shown in Fig.2.2. In the analysis bank, $H(z)$ is a lowpass filter and $G(z)$ is a highpass filter. In the synthesis bank, $\tilde{H}(z)$ is a lowpass filter and $\tilde{G}(z)$ is a highpass filter. The down-sampling operators (\downarrow) are decimators and the upsampling operators (\uparrow) are expanders. Basically, the properties (orthogonality, symmetry, vanishing moments and so on) of scaling and wavelet function are determined by the filter banks.

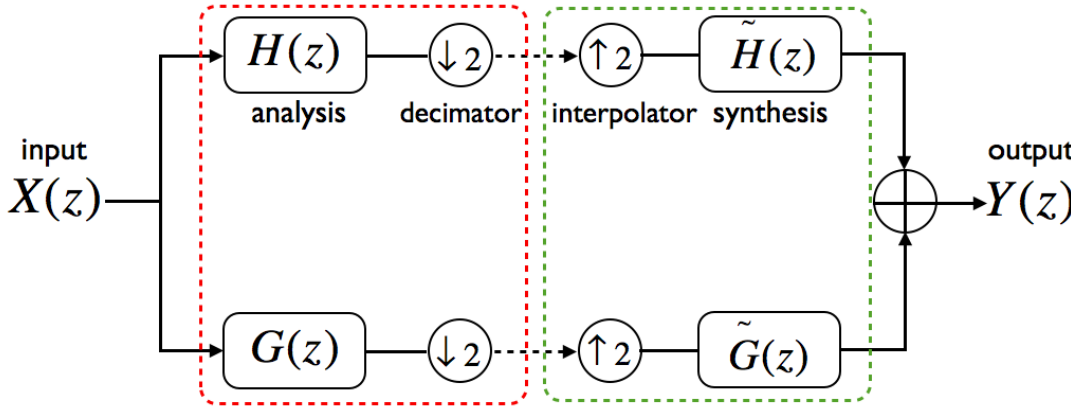


Fig.2.2 Two-channel filter bank.

2.3.3.2 Perfect Reconstruction

Consider the input signal is $X(z)$, then the output $Y(z)$ is consisted from lowpass and highpass channels,

$$\text{lowpass output} = \frac{1}{2} \tilde{H}(z) [H(z)X(z) + H(-z)X(-z)]$$

$$\text{highpass output} = \frac{1}{2} \tilde{G}(z) [G(z)X(z) + G(-z)X(-z)]$$

Therefore, the output $Y(z)$ can be expressed as

$$\begin{aligned} Y(z) &= \frac{1}{2} [H(z)\tilde{H}(z) + G(z)\tilde{G}(z)]X(z) \\ &\quad + \frac{1}{2} [H(-z)\tilde{H}(z) + G(-z)\tilde{G}(z)]X(-z). \end{aligned} \quad (2.11)$$

For perfect reconstruction with N sample delays, $Y(z) = X(z)z^{-N}$. So the first term in Eq.(2.11) should cancel the signal distortion and the second

term must be zero. Thus, the corresponding filter banks should satisfy

$$\begin{cases} H(z)\tilde{H}(z) + G(z)\tilde{G}(z) = 2z^{-N} \\ H(-z)\tilde{H}(z) + G(-z)\tilde{G}(z) = 0 \end{cases}, \quad (2.12)$$

where N is odd. Thus, the synthesis bank $\tilde{H}(z), \tilde{G}(z)$ can be directly derived from analysis bank $H(z), G(z)$ as

$$\tilde{H}(z) = G(-z) \quad \text{and} \quad \tilde{G}(z) = -H(-z). \quad (2.13)$$

Then, Eq.(2.12) becomes

$$H(z)G(-z) - H(-z)G(z) = 2z^{-N}. \quad (2.14)$$

which is **perfect reconstruction condition**.

2.3.3.3 Orthonormality

It is well-known that the orthonormal wavelets form a tight Riesz basis, and the corresponding transform has the l^2 -norm-preserving property. In applications, the orthogonality has several advantages such as noise decorrelation in denoising, energy preservation and so on [46]. Therefore, we restrict ourself to the case of orthonormal wavelet bases in this dissertation. The corresponding filter banks should satisfy the orthonormality condition, i.e., the synthesis filter bank should be time-reversed of analysis filter banks,

$$\tilde{H}(z) = z^{-N}H(z^{-1}) \quad \text{and} \quad \tilde{G}(z) = z^{-N}G(z^{-1}). \quad (2.15)$$

According to Eq.(2.13), Eq.(2.15) becomes

$$H(-z) = -z^{-N}G(z^{-1}) \quad \text{and} \quad G(-z) = z^{-N}H(z^{-1}). \quad (2.16)$$

Then the orthonormality condition can be derived from Eq.(2.14), Eq.(2.15) and Eq.(2.16),

$$\begin{cases} H(z)H(z^{-1}) + H(-z)H(-z^{-1}) = 2 \\ G(z)G(z^{-1}) + G(-z)G(-z^{-1}) = 2 \\ H(z)G(z^{-1}) + H(-z)G(-z^{-1}) = 0 \end{cases} . \quad (2.17)$$

2.3.3.4 Symmetry

If the scaling function $\phi(t)$ and wavelet function $\psi(t)$ are symmetric and their center of symmetry are located at τ_0 and $\frac{N}{2}$, respectively,

$$\begin{cases} \phi(t - \tau_0) = \phi(\tau_0 - t) \\ \psi(t - \frac{N}{2}) = \psi(\frac{N}{2} - t) \end{cases} . \quad (2.18)$$

Eq.(2.18) requires that the corresponding scaling lowpass filter must have a linear phase response;

$$\theta(\omega) = -\tau_0\omega, \quad (2.19)$$

where τ_0 is the constant.

2.3.3.5 Vanishing Moments

The moment of the wavelet function is defined by

$$m(r) = \int_{-\infty}^{\infty} t^r \psi(t) dt, \quad (2.20)$$

and the moment of impulse response $g(n)$ is given by

$$\mu(r) = \sum_n n^r g(n). \quad (2.21)$$

Generally, the wavelets function is required to have K vanishing moments,

$$\begin{cases} m(r) = \int_{-\infty}^{\infty} t^r \psi(t) dt = 0 \\ \mu(r) = \sum_n n^r g(n) = 0 \end{cases} \quad (r = 0, 1, \dots, K - 1). \quad (2.22)$$

According to Eq.(2.16), we have

$$g(n) = (-1)^n h(N - n). \quad (2.23)$$

Therefore, the scaling lowpass filter $H(z)$ must have K zeros at $z = -1$;

$$H(z) = Q(z)(1 + z^{-1})^K, \quad (2.24)$$

where $Q(z)$ is a FIR or IIR filter.

2.4 Dual Tree Complex Wavelet Transform

In the previous section, the wavelet theory and filter banks have been introduced. However, the conventional wavelet transform has some unavoidable shortcomings, like shift variance, lack of directionality and so on. Therefore, the dual-tree complex wavelet transform is proposed to overcome the shortcomings of DWT.

2.4.1 Basic Structure

Dual-Tree Complex Wavelet Transform (DTCWT) was originally proposed by Kingsbury [13], and has been found to be successful in many applications of signal and image processing [13] ~ [29]. It not only inherits the merit of DWT, like multiresolution analysis, time-frequency representation and so on, but also makes a comparable improvement to the shortcomings of DWT, i.e., it is of approximate shift invariance, enhanced directional selectivity for multidimensional signals and gives the explicit phase information [26]. Besides, it achieves these with a redundancy factor of only 2^d for d -dimensional signals, which is substantially lower than the undecimated DWT.

DTCWT employs two real DWTs, as shown in Fig.2.3, where the first DWT is the real part of DTCWT and the other one is the imaginary part. Each DWT is consisted from two-channel filter bank. Let $\{\phi_i(t), \psi_i(t)\}$ be the scaling and wavelet functions of two DWTs, where $i = 1, 2$. Then, the

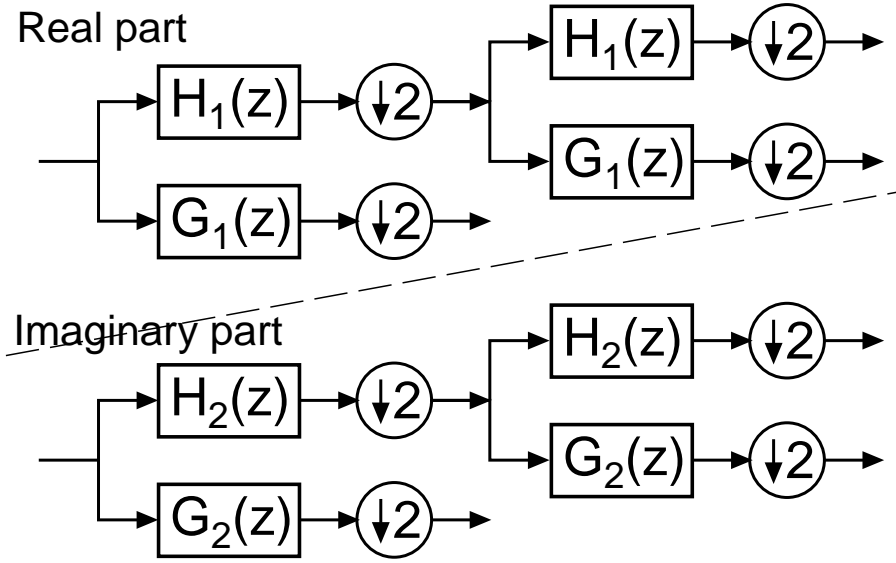


Fig.2.3 Dual tree complex wavelet filter bank.

complex wavelet $\psi_c(t)$ is expressed as

$$\psi_c(t) = \psi_1(t) + j\psi_2(t). \quad (2.25)$$

Generally, two wavelet functions $\psi_1(t)$ and $\psi_2(t)$ are required to be a pair of *Hilbert transform*. Thus the complex wavelet $\psi_c(t)$ is analytic, i.e., the spectrum is one-sided:

$$\Psi_c(\omega) = \Psi_1(\omega) + j\Psi_2(\omega) = \begin{cases} 2\Psi_1(\omega) & (\omega > 0) \\ 0 & (\omega < 0) \end{cases}. \quad (2.26)$$

where $\Psi_i(\omega)$ is the Fourier transform of $\psi_i(t)$.

2.4.2 Half-sample Delay Condition

It had been proven in [20], [23] ~ [27], [30] and [31] that two wavelet functions $\psi_i(t)$ are a Hilbert transform pair;

$$\psi_2(t) = H\{\psi_1(t)\}, \quad (2.27)$$

that is,

$$\Psi_2(\omega) = \begin{cases} -j\Psi_1(\omega) & (\omega > 0) \\ j\Psi_1(\omega) & (\omega < 0) \end{cases}, \quad (2.28)$$

if and only if the corresponding scaling lowpass filters $H_1(z)$ and $H_2(z)$ satisfy

$$H_2(e^{j\omega}) = H_1(e^{j\omega})e^{-j(2M+\frac{1}{2})\omega} \quad (|\omega| < \pi), \quad (2.29)$$

where M is an integer. Eq.(2.29) is the generalized half-sample delay condition, which is the necessary and sufficient condition for two wavelet bases to form a Hilbert transform pair. It should be noted that $M = 0$ is used in all design examples in this dissertation.

2.4.3 Error Function

It is obvious in Eq.(2.29) that $H_2(e^{j\omega})$ needs to be approximated to $H_1(e^{j\omega})e^{-j(2M+\frac{1}{2})\omega}$. Specifically, the scaling lowpass filters should be offset from another one by a half sample. Therefore, we define the error function $E(\omega)$ as

$$E(\omega) = H_2(e^{j\omega}) - H_1(e^{j\omega})e^{-j(2M+\frac{1}{2})\omega}. \quad (2.30)$$

In this dissertation, we will minimize the error function $E(\omega)$ to improve the analyticity.

2.5 Objective Measures of Analyticity

Practically, it is impossible to achieve the ideal Hilbert transform. Therefore, to evaluate the analyticity of complex wavelet, we use the p -norm of the spectrum $\Psi_c(\omega)$ to define an objective measure of quality as

$$E_p = \frac{\|\Psi_c(\omega)\|_{p,(-\infty,0)}}{\|\Psi_c(\omega)\|_{p,(0,\infty)}}, \quad (2.31)$$

where

$$\|\Psi_c(\omega)\|_{p,\Omega} = \left(\int_{\Omega} |\Psi_c(\omega)|^p d\omega \right)^{\frac{1}{p}}. \quad (2.32)$$

If $p = \infty$, $E_{\infty} = \lim_{p \rightarrow \infty} E_p$ evaluates the peak error in the negative frequency domain. If $p = 2$, E_2 evaluates the square root of the negative frequency energy. In this dissertation, we use E_{∞} and E_2 to evaluate the analyticity of the complex wavelets. It should be noted that the lower the values of E_{∞} and E_2 , the better the analyticity of complex wavelet.

2.6 Summary

In this chapter, we have introduced the Fourier transform and short-time Fourier transform at first and then reviewed the conventional wavelet theory and interpreted the discrete wavelet transform achieved by two-channel filter banks. Next, we discussed the orthonormality and the perfect reconstruction of two-channel filter banks. In addition, some important prop-

erties such as symmetry, vanishing moments of wavelets have been discussed. Next, DTCWT was introduced. The half-sample delay condition was given which is the necessary and sufficient condition for two wavelet bases to be a Hilbert transform pair. Finally, two objective measures were introduced to evaluate the performance of the complex wavelets.

Chapter 3 Orthogonal DTCWTs with Improved Analyticity and Frequency Selectivity

3.1 Introduction

Dual tree complex wavelet transforms (DTCWTs) have been proposed and found to be successful in many applications of signal and image processing [13], [16] ~ [22], [26]. Two wavelet bases are required to form to be a Hilbert transform pair. The corresponding scaling lowpass filters satisfy the half-sample delay condition. Several design procedures for Hilbert transform pairs of wavelet bases have been presented in [13], [16] ~ [22], [26], [30], [31] and [38] by using FIR filters, which are corresponding to the compactly supported wavelets. In [20], Selesnick had proposed the common-factor technique, where the scaling lowpass filters are constructed by using allpass filters to satisfy the half-sample delay condition. Selesnick had adopted the maximally flat allpass filter and given a class of FIR orthonormal and biorthogonal solutions, and IIR orthonormal solution. However, the maximally flat allpass filter has a large phase error as $|\omega|$ increases, resulting in a poor analyticity of complex wavelet. In addition, the scaling lowpass filters in [26] have as many zeros at $z = -1$ as possible, resulting a weak frequency selectivity. Moreover, the resulting IIR scaling lowpass filters have the numerator and denominator of the (almost) same

degree.

In [25], Kawada and Zhang had proposed a design method based on common-factor technique by using general IIR filters with numerator and denominator of different degree. We will review that method at first and then propose a new class of DTCWTs with improved analyticity and frequency selectivity. It is shown that the conventional FIR and IIR orthonormal solutions proposed in [20] are only the special cases of DTCWTs proposed in this dissertation. Finally, we investigate the performance on the proposed DTCWTs and indicate how to choose the approximation band properly.

3.2 The Common-Factor Technique

3.2.1 Hilbert Transform Pairs by Allpass Filter

It is known [6] that the transfer function of an allpass filter $A(z)$ with a delay of τ samples is defined by

$$A(z) = z^{-J} \frac{D(z^{-1})}{D(z)}, \quad (3.1)$$

where

$$D(z) = \sum_{n=0}^J a(n) z^{-n}. \quad (3.2)$$

with

$$a(n) = (-1)^n \binom{J}{n} \frac{(\tau - J)_n}{(\tau + 1)_n}, \quad (3.3)$$

where J is the degree of $A(z)$ and $a(n)$ are real filter coefficients, $a(0) = 1$ and $(x)_n$ represents the rising factorial, i.e., $(x)_n := (x)(x+1) \cdots (x+n-1)$. The allpass filter $A(z)$ has unit magnitude response at all frequencies and its phase response $\theta(\omega)$ is given by

$$\theta(\omega) = -J\omega + 2 \tan^{-1} \frac{\sum_{n=0}^J a_n \sin(n\omega)}{\sum_{n=0}^J a_n \cos(n\omega)}. \quad (3.4)$$

In [20], Selesnick had proposed the common factor technique where the scaling lowpass filters $H_1(z)$ and $H_2(z)$ are composed of the allpass filter by

$$\begin{cases} H_1(z) &= F(z)D(z) \\ H_2(z) &= F(z)z^{-J}D(z^{-1}) \end{cases}. \quad (3.5)$$

Since both of scaling lowpass filters have the same factor $F(z)$, we have

$$H_2(z) = H_1(z)z^{-J} \frac{D(z^{-1})}{D(z)} = H_1(z)A(z). \quad (3.6)$$

It is clear that $H_2(z)$ is expressed as the product of $H_1(z)$ and $A(z)$. The half-sample delay condition in Eq.(2.29) can be approximately achieved if the allpass filter is an approximate half-sample delay;

$$A(e^{j\omega}) \approx e^{-j(2M+\frac{1}{2})\omega} \quad (|\omega| < \pi). \quad (3.7)$$

Thus the half-sample delay condition is achieved approximately, and two wavelet bases form an approximate Hilbert transform pair. The advantage of this method is that the approximation accuracy of the half-sample delay is controlled only by the allpass filter.

3.2.2 FIR Orthonormal Solution

After $A(z)$ is determined, $F(z)$ needs to be constructed for $H_1(z)$ and $H_2(z)$. To obtain wavelet bases with K vanishing moments, $F(z)$ is chosen as

$$F(z) = Q(z)(1 + z^{-1})^K. \quad (3.8)$$

Thus,

$$\begin{cases} H_1(z) = Q(z)(1 + z^{-1})^K D(z) \\ H_2(z) = Q(z)(1 + z^{-1})^K z^{-J} D(z^{-1}) \end{cases}. \quad (3.9)$$

It is clear that $H_1(z)$ and $H_2(z)$ have the same product filter $P(z)$;

$$\begin{aligned} P(z) &= H_1(z)H_1(z^{-1}) = H_2(z)H_2(z^{-1}) \\ &= Q(z)Q(z^{-1})(1 + z)^K(1 + z^{-1})^K D(z)D(z^{-1}), \\ &= Q(z)Q(z^{-1})(z + 2 + z^{-1})^K D(z)D(z^{-1}) \end{aligned} \quad (3.10)$$

Let $Q(z)$ be a FIR filter and defining

$$R(z) = Q(z)Q(z^{-1}) = \sum_{n=-N_1}^{N_1} r(n)z^{-n}, \quad (3.11)$$

$$S(z) = (z + 2 + z^{-1})^K D(z)D(z^{-1}) = \sum_{n=-J-K}^{J+K} s(n)z^{-n}, \quad (3.12)$$

where $r(n) = r(-n)$ for $1 \leq n \leq N_1$ and $s(n) = s(-n)$ for $1 \leq n \leq J + K$, and Eq.(3.10) becomes

$$P(z) = R(z)S(z). \quad (3.13)$$

Therefore, the orthonormality condition in Eq.(2.17) becomes,

$$P(z) + P(-z) = 2, \quad (3.14)$$

or equivalently,

$$\sum_{k=I_{min}}^{I_{max}} s(2n-k)r(k) = \begin{cases} 1 & (n=0) \\ 0 & (1 \leq n \leq \frac{N_1+J+K}{2}) \end{cases}, \quad (3.15)$$

where $I_{min} = \max\{-N_1, 2n - J - K\}$ and $I_{max} = \min\{N_1, 2n + J + K\}$. Note that $P(z)$ is a halfband filter. The degree of $H_i(z)$ is $N = N_1 + J + K$. Since $r(n) = r(-n)$, there are totally $(N + 1)/2$ equations with respect to $(N_1 + 1)$ unknown coefficients of $r(n)$ in Eq.(3.15). Therefore, we can obtain the only solution if $(N + 1)/2 = N_1 + 1$.

In [20], Selesnick had chosen $N_1 = J + K - 1$ and obtained the filter of minimal degree for given J and K , which corresponds to the maximal K for given J and N_1 ,

$$K_{max} = N_1 - J + 1 = \frac{N + 1}{2} - J. \quad (3.16)$$

Thus the scaling lowpass filters have the maximally flat magnitude responses, resulting in the maximum number of vanishing moments. This is the FIR orthonormal solution proposed in [20].

3.2.3 IIR Orthonormal Solution

In general, IIR filters require a lower computational complexity than FIR filters to achieve a sharp frequency response. IIR filters can be also used

to construct DTCWT. In [20], Selesnick has chosen

$$F(z) = \frac{(1 + z^{-1})^K}{C(z^2)}, \quad (3.17)$$

then

$$\begin{cases} H_1(z) = \frac{(1 + z^{-1})^K D(z)}{C(z^2)} \\ H_2(z) = \frac{(1 + z^{-1})^K z^{-J} D(z^{-1})}{C(z^2)} \end{cases}. \quad (3.18)$$

$H_1(z)$ and $H_2(z)$ have the same product filter $P(z)$,

$$P(z) = \frac{(z + 2 + z^{-1})^K D(z) D(z^{-1})}{C(z^2) C(z^{-2})}. \quad (3.19)$$

Defining

$$B(z) = C(z) C(z^{-1}) = \sum_{n=-N_2}^{N_2} b(n) z^{-n}, \quad (3.20)$$

where $b(n) = b(-n)$ for $1 \leq n \leq N_2$. From the orthonormality condition in Eq.(2.16),

$$S(z) + S(-z) = 2B(z^2). \quad (3.21)$$

thus $N_2 = \lfloor \frac{J+K}{2} \rfloor$ and

$$b(n) = s(2n), \quad (3.22)$$

where $\lfloor x \rfloor$ means the largest integer not greater than x . This is the IIR orthonormal solution proposed in [20]. It is clear that the numerator and denominator of $H_i(z)$ are of degree $N = J + K$ and $2N_2 = 2\lfloor \frac{J+K}{2} \rfloor$ respectively, which are the almost same.

3.2.4 General IIR Orthonormal Solution

Now we consider the case of using general IIR filters with numerator and denominator of different degree [25]. We choose

$$F(z) = \frac{Q(z)(1+z^{-1})^K}{C(z^2)}, \quad (3.23)$$

then the corresponding scaling lowpass filters $H_i(z)$ become

$$\begin{cases} H_1(z) = \frac{Q(z)(1+z^{-1})^K D(z)}{C(z^2)} \\ H_2(z) = \frac{Q(z)(1+z^{-1})^K z^{-J} D(z^{-1})}{C(z^2)} \end{cases}, \quad (3.24)$$

where the degree of numerator is not less than the degree of denominator, that is, $N = J + K + N_1 \geq 2N_2$. If $N > 2N_2$, then N is an odd number, whereas if $N = 2N_2$, N is an even number.

Thus, the product filter $P(z)$ is

$$\begin{aligned} P(z) &= H_1(z)H_1(z^{-1}) = H_2(z)H_2(z^{-1}) \\ &= \frac{Q(z)Q(z^{-1})(1+z)^K(1+z^{-1})^K D(z)D(z^{-1})}{C(z^2)C(z^{-2})}. \\ &= \frac{R(z)S(z)}{B(z^2)} \end{aligned} \quad (3.25)$$

According to the orthonormality condition, we have

$$\sum_{k=I_{min}}^{I_{max}} s(2n-k)r(k) = \begin{cases} b(n) & (0 \leq n \leq N_2) \\ 0 & (N_2 < n \leq \frac{N}{2}) \end{cases}. \quad (3.26)$$

We rewrite Eq.(3.26) in the matrix form as

$$\mathbf{b} = \mathbf{S}_1 \mathbf{r}, \quad (3.27)$$

and

$$\mathbf{S}_2 \mathbf{r} = \mathbf{0}, \quad (3.28)$$

where $\mathbf{b} = [b(0), b(1), \dots, b(N_2)]^T$, $\mathbf{r} = [r(0), r(1), \dots, r(N_1)]^T$, $\mathbf{0} = [0, 0, \dots, 0]^T$, and the elements of the matrices \mathbf{S}_1 and \mathbf{S}_2 are given by

$$S_1(m, n) = \begin{cases} s(2m) & (n = 0) \\ s(2m - n) + s(2m + n) & (n = 1, 2, \dots, N_1) \end{cases} \quad (3.29)$$

where $0 \leq m \leq N_2$, and

$$S_2(m, n) = \begin{cases} s(2(N_2 + 1 + m)) & (n = 0) \\ s(2(N_2 + 1 + m) - n) + s(2(N_2 + 1 + m) + n) & (n = 1, 2, \dots, N_1) \end{cases} \quad (3.30)$$

where $0 \leq m \leq \lfloor \frac{N}{2} \rfloor - N_2 - 1$. Note that $s(-n) = s(n) = 0$ for $n > J + K$.

Assuming $r(0) = 1$ without any loss of generality, there are $(\lfloor \frac{N}{2} \rfloor - N_2)$ equations with respect to N_1 unknown coefficients $r(n)$ in Eq.(3.28). Therefore, it is clear that the only solution $r(n)$ exists if $\lfloor \frac{N}{2} \rfloor - N_2 = N_1$, and then $b(n)$ can be obtained by using Eq.(3.27). When $N > 2N_2$, $N_1 + 2N_2 = J + K - 1$, since N is odd. If we choose $N_2 = 0$, then $N_1 = J + K - 1$, which is correspondent to the FIR orthonormal solution in [20]. If we choose $N_1 = 0$, then $N = J + K$. When N is odd, $2N_2 = J + K - 1 = N - 1$, while if N is even, $2N_2 = J + K = N$. Thus $N_2 = \lfloor \frac{N}{2} \rfloor = \lfloor \frac{J+K}{2} \rfloor$, and it is the IIR orthonormal solution in [20]. Therefore, it is clear that the FIR

and IIR orthonormal solutions proposed in [20] are only the special cases of general IIR orthonormal solutions when $N_2 = 0$ or $N_1 = 0$. It should be noted that the minimum-phase spectral factor approach is applied to get $Q(z)$ from $R(z)$, $C(z)$ from $B(z)$ in this dissertation. TABLE.3.1 summarizes the FIR/IIR orthonormal solutions using general IIR filters with numerator and denominator of different degree.

TABLE 3.1 FIR/IIR Orthonormal Solutions

N_1, N_2	N	Number of equation	Filter Type
$N_1 \neq 0, N_2 = 0$	ODD	$N_1 = J + K - 1$	FIR [20]
$N_1 \neq 0, N_2 \neq 0$	ODD	$N_1 + N_2 = \lfloor \frac{N}{2} \rfloor$	IIR
$N_1 = 0, N_2 \neq 0$	EVEN or ODD	$N_2 = \lfloor \frac{N}{2} \rfloor = \lfloor \frac{J+K}{2} \rfloor$	IIR [20]

3.2.5 Design Examples

In this section, two examples will be presented. In the first example, we consider a class of DTCWTs using general IIR filters. In the second example, K and J will be varied to construct a new class of DTCWTs.

Example 3.1

We consider a class of DTCWTs using IIR filters with numerator and denominator of different degree. As proposed in [20], we have used the maximally flat allpass filter with $J = 2$ and $K = 4$. To obtain the filters of minimal degree, we can choose $\{N_1, N_2\} = \{5, 0\}, \{3, 1\}, \{1, 2\}, \{0, 3\}$, where the degree of numerators are $N = 11, 9, 7, 6$, respectively. Note that the filter with $\{N_1, N_2\} = \{5, 0\}$ is FIR filter. We have designed these four filters, and the resulting magnitude responses of $H_i(z)$ are shown in Fig.3.1. It is seen that IIR filters have more sharp magnitude responses than FIR filter. To get stable filters, the numerator and denominator are obtained by using the minimum-phase spectral factor [20]. Their group delay responses are given in Fig.3.2. It is seen that the group delay becomes more flat as a decreasing N_2 , and the half-sample delay condition is approximately achieved. Moreover, the magnitude responses of $E(\omega)$ are shown in Fig.3.3. The maximum error of IIR filters are smaller than the conventional FIR filter. The scaling and wavelet functions $\phi_i(t), \psi_i(t)$ are also shown in Fig.3.4. Furthermore, the spectrum $\Psi_i(\omega)$ and the spectrum $\Psi_c(\omega)$ are shown in Fig.3.5, Fig.3.6 and Fig.3.7 respectively. In Fig.3.7, the complex wavelet constructed by FIR filter has a bigger spectrum in

the negative frequency domain than that by IIR filters. Finally, the analyticity measures of E_∞ and E_2 are summarized in Table 3.2 and both of E_∞ and E_2 decrease as an increasing N_2 .

TABLE 3.2 Analyticity Measures E_∞ and E_2 .

N_1	N_2	$E_\infty(\%)$	$E_2(\%)$
5	0	1.627	1.894
3	1	1.064	1.173
1	2	1.017	1.061
0	3	1.014	1.048

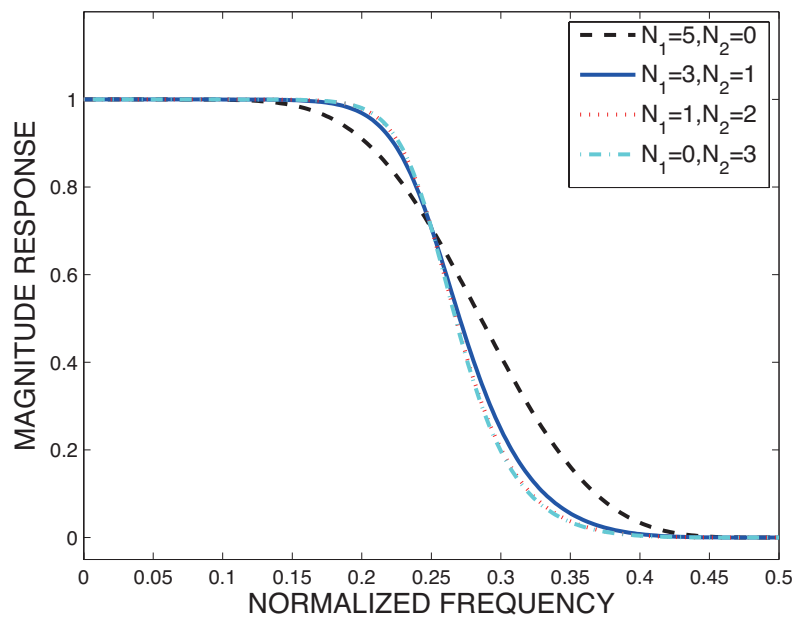


Fig.3.1 Magnitude responses of scaling lowpass filters $H_i(z)$.

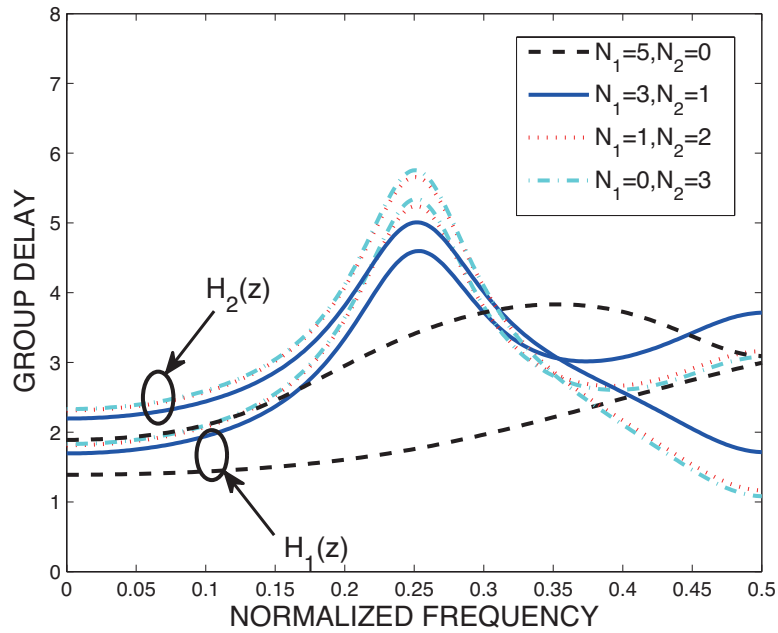


Fig.3.2 Group delay responses of scaling lowpass filters $H_i(z)$.

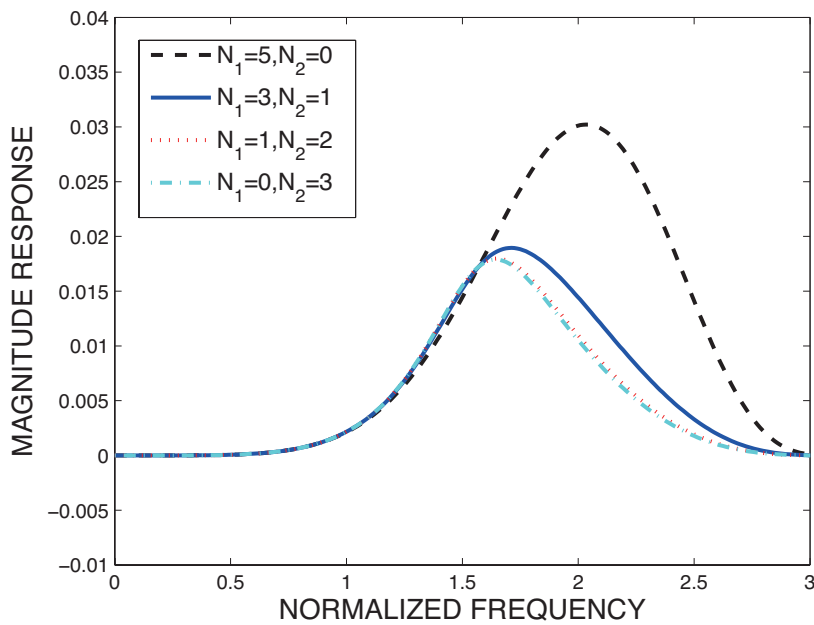
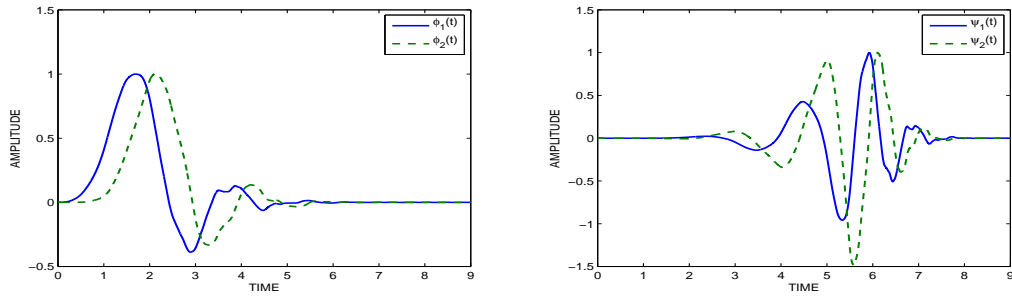
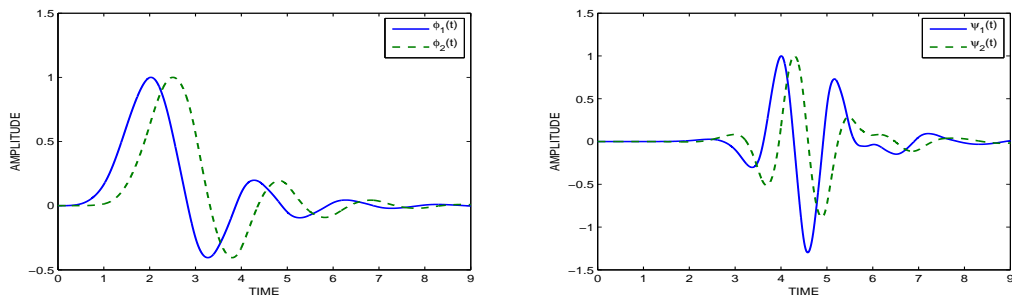
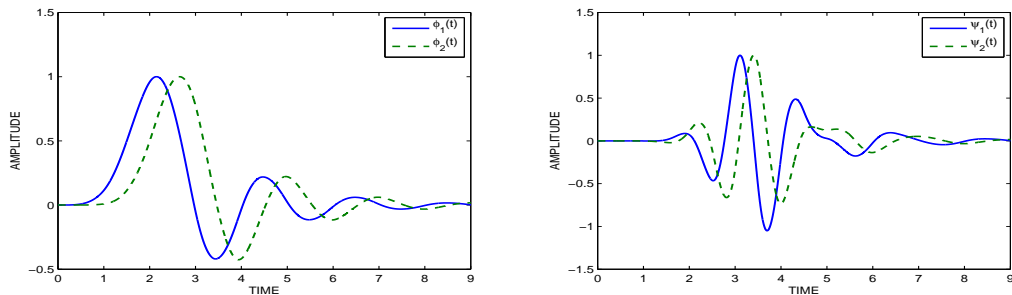
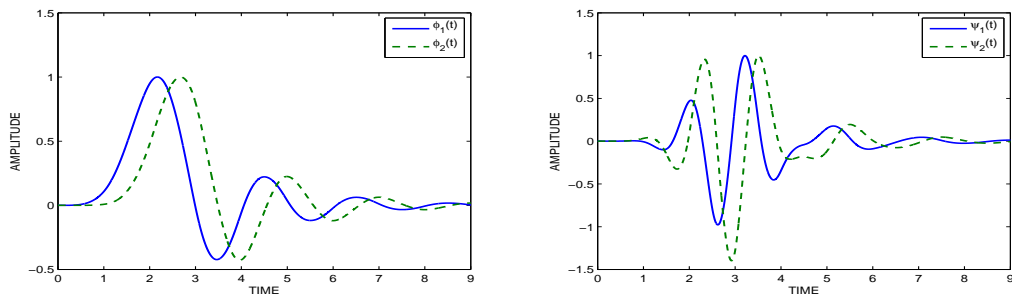


Fig.3.3 Magnitude responses of $E(\omega)$.

(a) $N_1 = 5, N_2 = 0$.(b) $N_1 = 3, N_2 = 1$.(c) $N_1 = 1, N_2 = 2$.(d) $N_1 = 0, N_2 = 3$.Fig.3.4 Scaling and wavelet functions $\phi_i(t), \psi_i(t)$.

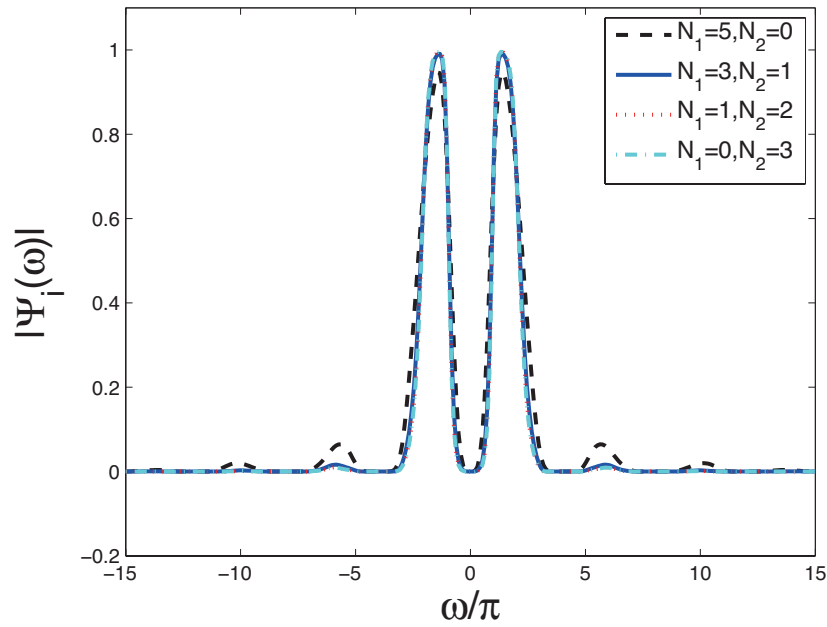


Fig.3.5 Magnitude responses of $\Psi_i(\omega)$.

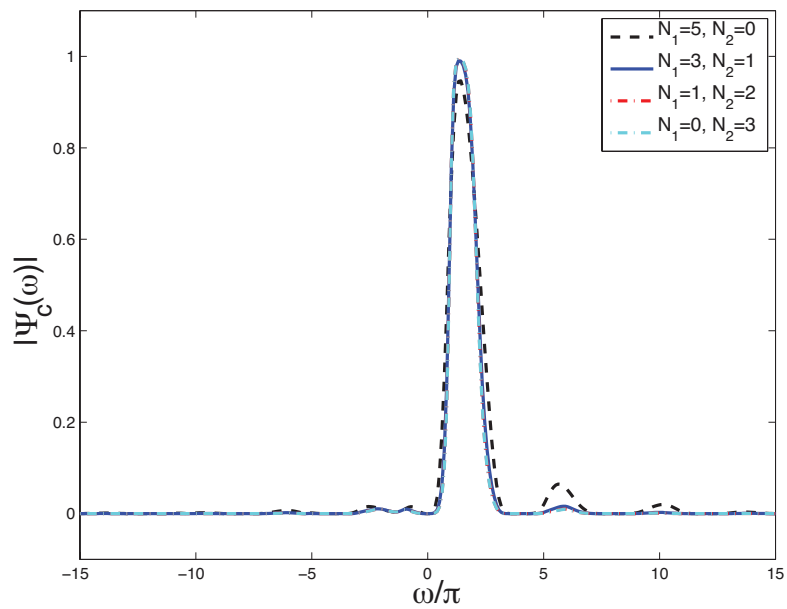
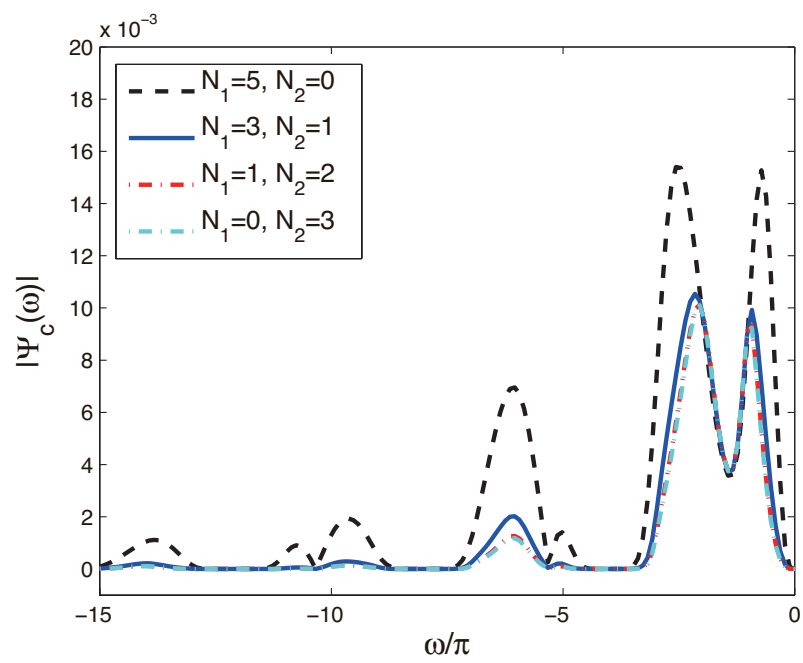


Fig.3.6 Magnitude responses of $\Psi_c(\omega)$.

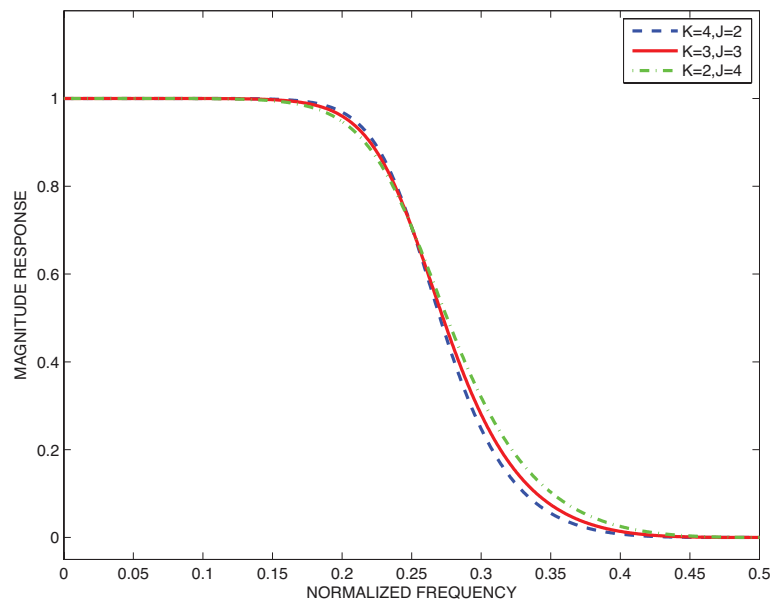
Fig.3.7 Magnitude responses of $\Psi_c(\omega)$.

Example 3.2

We consider a class of DTCWTs using IIR Filters with $N = 9, N_1 = 3$. We can choose different K and J , where $K + J = 6$. Therefore, K and J are selected as $\{K, J\} = \{4, 2\}, \{3, 3\}, \{2, 4\}$, respectively. The resulting magnitude response of $H_i(z)$ are shown in Fig.3.8. It is obvious that with the increasing of K , the transition band of the scaling lowpass filters becomes sharp. Their group delay responses are given in Fig.3.9, where the half-sample delay condition is approximately achieved. Moreover, the magnitude responses of $E(\omega)$ are given in Fig.3.10. It is maximum when $\{K = 4, J = 2\}$ while minimum when $\{K = 2, J = 4\}$. Next, the scaling functions $\phi_i(t)$ and wavelet functions $\psi_i(t)$ are shown in Fig.3.11. Furthermore, the spectrum of wavelet function $\Psi_i(\omega)$ and complex wavelet $\Psi_c(\omega)$ are given in Fig.3.12, Fig.3.13, and Fig.3.14, respectively. When $\{K = 2, J = 4\}$, the negative spectrum of DTCWT is small, i.e., better analyticity of DTCWT. Finally, the objective measures of quality are summarized in Table 3.3.

TABLE 3.3 Analyticity Measures E_∞ and E_2 .

K	J	$E_\infty(\%)$	$E_2(\%)$
4	2	1.064	1.173
3	3	0.254	0.293
2	4	0.147	0.265

Fig.3.8 Magnitude responses of scaling lowpass filters $H_i(z)$.

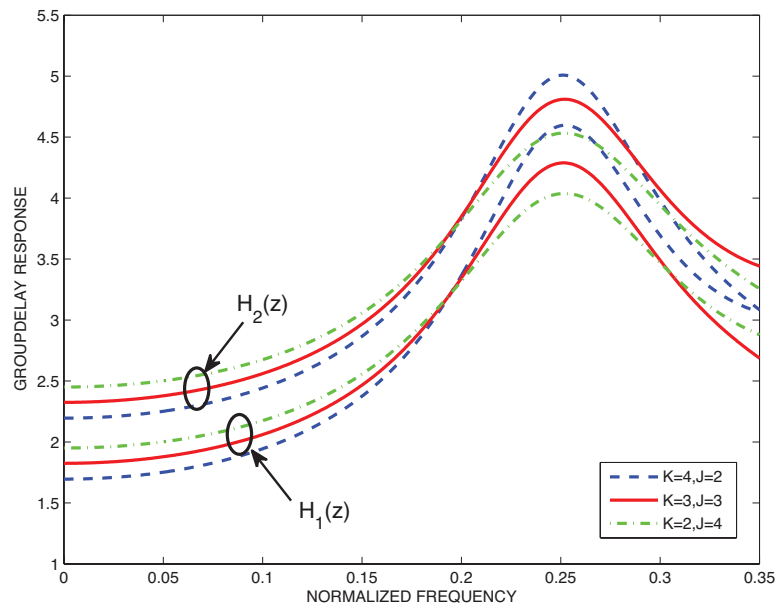


Fig.3.9 Group delay responses of scaling lowpass filters $H_i(z)$.

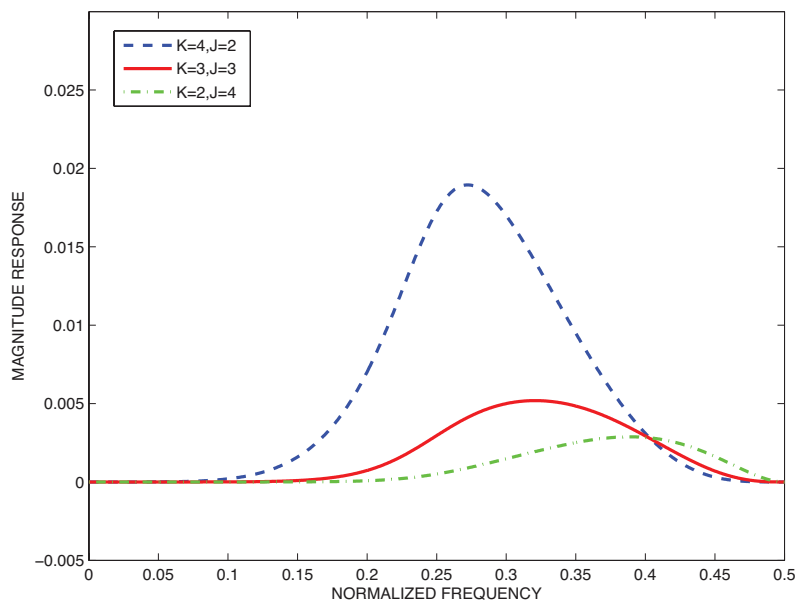
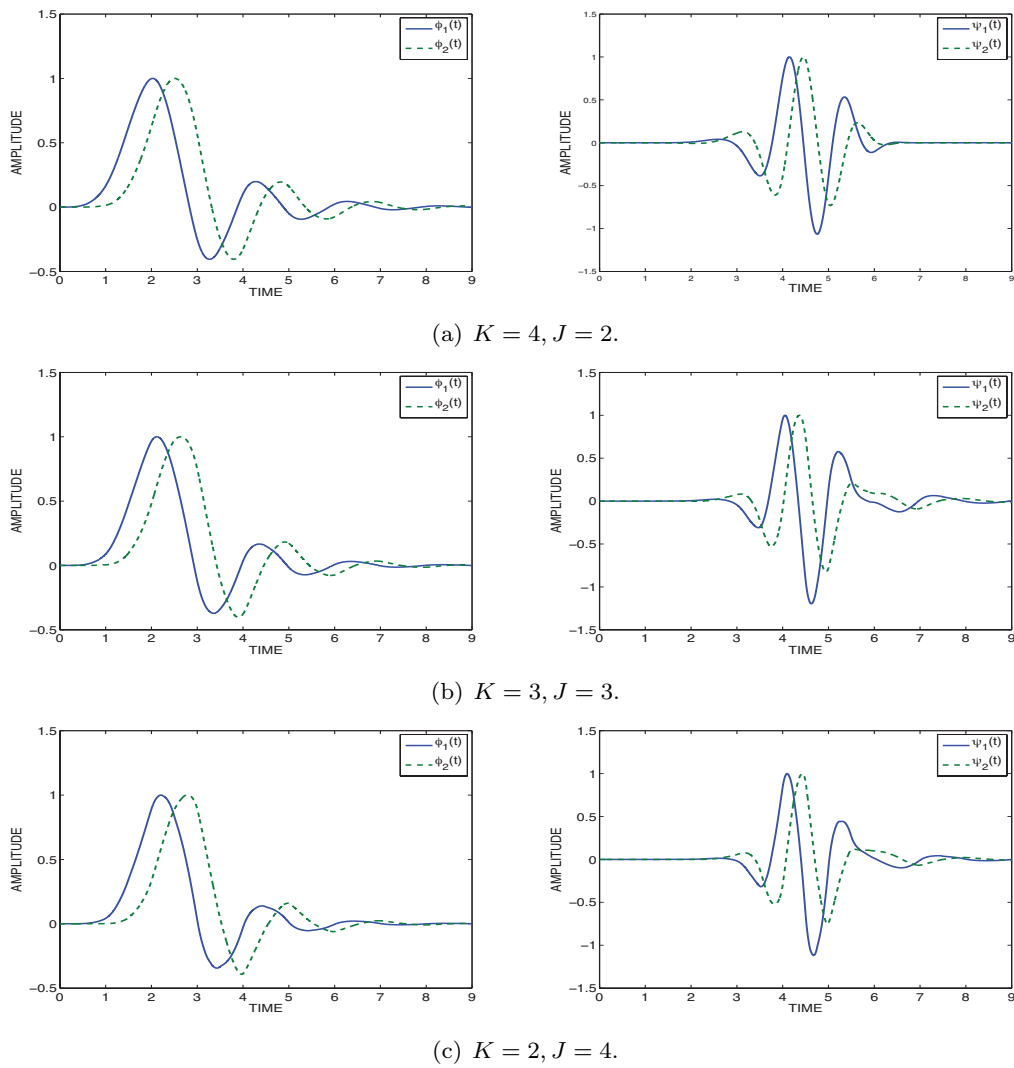


Fig.3.10 Magnitude responses of $E(\omega)$.

Fig.3.11 Scaling and wavelet functions $\phi_i(t), \psi_i(t)$.

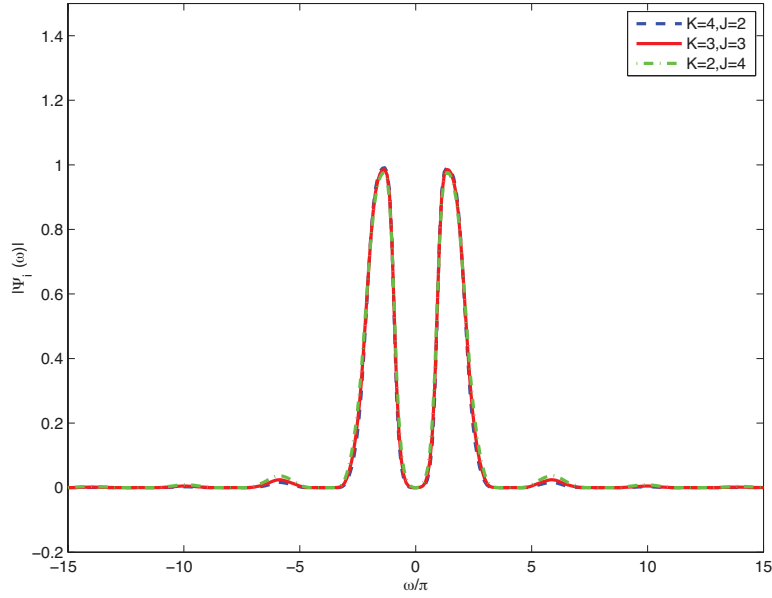


Fig.3.12 Magnitude responses of $\Psi_i(\omega)$.

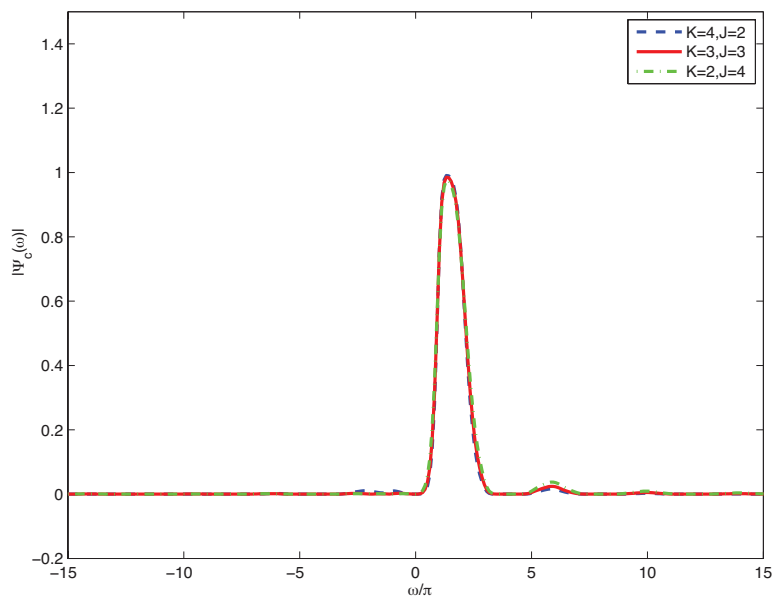
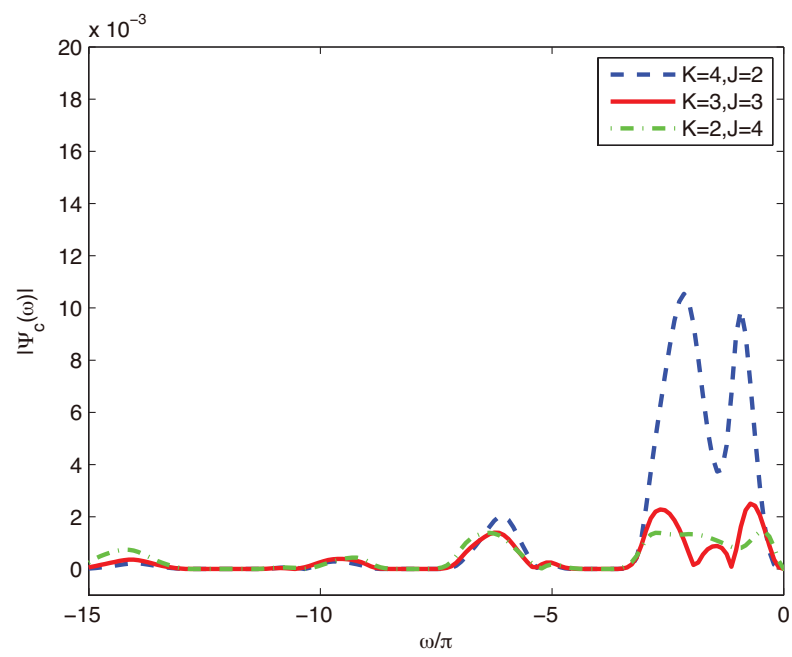


Fig.3.13 Magnitude responses of $\Psi_c(\omega)$.

Fig.3.14 Magnitude responses of $\Psi_c(\omega)$.

3.3 DTCWTs with Improved Analyticity

In the previous section, we had introduced the common-factor technique, where the maximally flat allpass filters $A(z)$ had been adopted for constructing the scaling lowpass filters. Since $\omega = 0$ is chosen as the point of approximation, the phase error will increase as $|\omega|$ increases. Therefore, $E(\omega)$ has a large error in transition band, resulting in a poor analyticity of complex wavelet. In the following, we will discuss how to improve the analyticity of complex wavelet.

3.3.1 Flatness Condition

From Eqs.(2.30) and (3.5), we have

$$\begin{aligned} E(\omega) &= H_2(e^{j\omega}) - H_1(e^{j\omega})e^{-j(2M+\frac{1}{2})\omega} \\ &= H_1(e^{j\omega})[A(e^{j\omega}) - e^{-j(2M+\frac{1}{2})\omega}], \end{aligned} \quad (3.31)$$

thus

$$|E(\omega)| = 2|H_1(e^{j\omega})| \left| \sin \frac{\theta(\omega) + (2M + \frac{1}{2})\omega}{2} \right|. \quad (3.32)$$

where $\theta(\omega)$ is the phase response of $A(z)$. It is clear that $|E(\omega)|$ is dependent on both the magnitude response $|H_1(e^{j\omega})|$ and the phase error of $A(z)$. Since $H_1(z)$ is a lowpass filter, we must minimize the phase error not only in passband but also in transition band to improve the analyticity of complex wavelet. There are many design methods for allpass filters to approximate a fractional delay response, for example, the maximally flat [6], equiripple approximations [8], and so on. It will be better if the

minimax (Chebyshev) phase approximation of allpass filters is used.

It is known that the wavelet function is defined by the infinite product formula. Thus, it is necessary that $A(z)$ has a certain degree of flatness at $\omega = 0$ to improve the analyticity. In the following, we present a design method of allpass filters with the specified degree of flatness at $\omega = 0$ and equiripple phase response in the approximation band.

The desired phase response is $\theta_d(\omega) = -(2M + \frac{1}{2})\omega$. The difference $\theta_e(\omega)$ between $\theta(\omega)$ and $\theta_d(\omega)$ is given by

$$\theta_e(\omega) = \theta(\omega) - \theta_d(\omega) = 2 \tan^{-1} \frac{N_J(\omega)}{D_J(\omega)}, \quad (3.33)$$

where

$$\begin{cases} N_J(\omega) = \sum_{n=0}^J a(n) \sin\{(n - \frac{J}{2} + M + \frac{1}{4})\omega\} \\ D_J(\omega) = \sum_{n=0}^J a(n) \cos\{(n - \frac{J}{2} + M + \frac{1}{4})\omega\} \end{cases}. \quad (3.34)$$

Firstly, we consider the flatness condition of the phase response at $\omega = 0$. It is required that the derivatives of $\theta(\omega)$ are equal to that of $\theta_d(\omega)$ at $\omega = 0$;

$$\left. \frac{\partial^{2r+1}\theta(\omega)}{\partial\omega^{2r+1}} \right|_{\omega=0} = \left. \frac{\partial^{2r+1}\theta_d(\omega)}{\partial\omega^{2r+1}} \right|_{\omega=0} \quad (r = 0, 1, \dots, L-1), \quad (3.35)$$

where L is a parameter that controls the degree of flatness, and $0 \leq L \leq J$.

Eq.(3.35) is equivalent to

$$\left. \frac{\partial^{2r+1}\theta_e(\omega)}{\partial\omega^{2r+1}} \right|_{\omega=0} = 0 \quad (r = 0, 1, \dots, L-1). \quad (3.36)$$

From Eq.(3.33), Eq.(3.36) can be reduced to

$$\left. \frac{\partial^{2r+1} N_J(\omega)}{\partial \omega^{2r+1}} \right|_{\omega=0} = 0 \quad (r = 0, 1, \dots, L-1). \quad (3.37)$$

By substituting $N_J(\omega)$ in Eq.(3.34) into Eq.(3.37), we can derive a system of linear equations as follows;

$$\sum_{n=0}^J \left(n - \frac{J}{2} + M + \frac{1}{4} \right)^{2r+1} a(n) = 0 \quad (r = 0, 1, \dots, L-1). \quad (3.38)$$

It should be noted that if $L = J$, we can solve the linear equations in Eq.(3.38) to obtain the maximally flat allpass filters, due to $a(0) = 1$.

3.3.2 Phase Error Minimization

In the following, we consider the case of $L < J$. We want to obtain an equiripple phase response in the approximation band $[0, \omega_c]$ by using the remaining degree of freedom $J - L$. Let ω_i ($0 < \omega_0 < \omega_1 < \dots < \omega_{J-L} = \omega_c$) be the extremal frequencies in the approximation band. We apply **Remez exchange algorithm** [4] and formulate $\theta_e(\omega)$ as

$$\tan \frac{\theta_e(\omega_i)}{2} = \frac{\sum_{n=0}^J a(n) \sin\left\{\left(n - \frac{J}{2} + M + \frac{1}{4}\right)\omega_i\right\}}{\sum_{n=0}^J a(n) \cos\left\{\left(n - \frac{J}{2} + M + \frac{1}{4}\right)\omega_i\right\}} = (-1)^i \delta, \quad (3.39)$$

where δ is an error. We then rewrite Eqs.(3.38) and (3.39) in the matrix form as

$$\mathbf{Pa} = \delta \mathbf{Qa}, \quad (3.40)$$

where $\mathbf{a} = [a(0), a(1), \dots, a(J)]^T$, and the elements of the matrices \mathbf{P} and \mathbf{Q} are given by

$$P(m, n) = \begin{cases} (n - \frac{J}{2} + M + \frac{1}{4})^{(2m+1)} & (m = 0, 1, \dots, L-1) \\ \sin\{(n - \frac{J}{2} + M + \frac{1}{4})\omega_{(m-L)}\} & (m = L, L+1, \dots, J) \end{cases} \quad (3.41)$$

$$Q(m, n) = \begin{cases} 0 & (m = 0, 1, \dots, L-1) \\ (-1)^{m-L} \cos\{(n - \frac{J}{2} + M + \frac{1}{4})\omega_{(m-L)}\} & (m = L, L+1, \dots, J) \end{cases} \quad (3.42)$$

It should be noted that Eq.(3.40) corresponds to a generalized eigenvalue problem, i.e., δ is an eigenvalue, and \mathbf{a} is the corresponding eigenvector. To minimize δ , we should choose the absolute minimum eigenvalue by solving the eigenvalue problem, thus the corresponding eigenvector give a set of filter coefficients $a(n)$. To be an equiripple phase response in the approximation band, we make use of an iteration procedure to obtain the optimal filter coefficients $a(n)$ [8],[39].

3.3.3 Design Algorithm

In this section, we summarize the algorithm for designing allpass filters with specified degree of flatness at $\omega = 0$ and equiripple phase response in the approximation band.

Design Algorithm

Begin

- (1) Read J , L and ω_c .
- (2) Select initial extremal frequencies Ω_i ($0 < \Omega_0 < \Omega_1 < \dots < \Omega_{J-L} = \omega_c$) equally spaced in $[0, \omega_c]$.

Repeat

- (3) Set $\omega_i = \Omega_i$ for ($i = 0, 1, \dots, J - L$).
- (4) Compute \mathbf{P} and \mathbf{Q} then find the absolute minimum eigenvalue δ to obtain a set of filter coefficients $a(n)$.
- (5) Search the peak frequencies Ω_i ($0 < \Omega_0 < \Omega_1 < \dots < \Omega_{J-L} = \omega_c$) of $\theta_e(\omega)$ in the approximation band $[0, \omega_c]$.

Until

Satisfy the following condition for a prescribed small constant ε (e.g., $\varepsilon = 10^{-12}$);

$$\sum_{i=0}^{J-L} |\omega_i - \Omega_i| < \varepsilon$$

End.

3.3.4 Design Examples

In this section, we present two design examples to demonstrate the efficiency of our proposed algorithm. First of all, we design a class of DTCWTs with improved analyticity by using FIR scaling lowpass filters. Next, we pick different ω_c to investigate the influence on the analyticity of complex wavelet.

Example 3.3

First of all, we consider a class of DTCWTs with improved analyticity by using FIR filters. We have designed an allpass filter with $J = 2$, $\omega_c = \frac{5}{8}\pi$ and $L = 1$. The resulting phase error $\theta_e(\omega)$ and phase response of allpass filter $A(z)$ are shown in Fig.3.15 and Fig.3.16, respectively. For the comparison, the phase response and phase error with $\{L = 0, L = 2\}$ are also plotted. Note that $L = 0$ means the allpass filter without the flatness condition, while $L = 2$ means the maximally flat allpass filter has been adopted. We then have used the method proposed in [20] to construct the scaling lowpass filters $H_i(z)$ with $N_1 = 5$, $K = 4$. The magnitude response and group delay of $H_i(z)$ are shown in Fig.3.17 and Fig.3.18, respectively. The scaling lowpass filters have the same degree ($N = 11$) and the magnitude responses are the almost same. However, $E(\omega)$ are different, as shown in Fig.3.19. When $L = 0$, the maximum error of $E(\omega)$ is minimum, while it is maximum when $L = 2$. Moreover, the scaling function and wavelet functions $\phi_i(t)$ and wavelet function $\psi_i(t)$ with different L are shown in Fig.3.20. Furthermore, the spectrum of

$\Psi_i(\omega)$ are shown in Fig.3.21, which are the almost same. The spectrum of complex wavelet $\Psi_c(\omega)$ are shown in Fig.3.22 and Fig.3.23, respectively. In Fig.3.23, the negative spectrum is small when $L = 1$. Finally the objective measures of quality are summarized in TABLE.3.4. When $L = 1$, the analyticity of complex wavelets is better. It is necessary to let allpass filter have certain flatness degree while minimizing the phase error.

TABLE 3.4 Analyticity Measures E_∞ and E_2 .

L	$E_\infty(\%)$	$E_2(\%)$
0	1.077	1.0
1	0.689	0.830
2	1.627	1.894

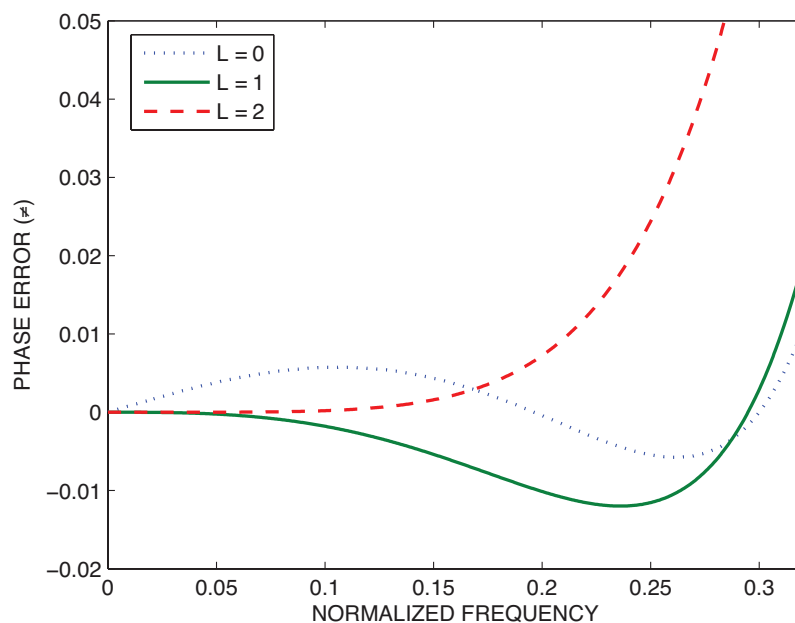
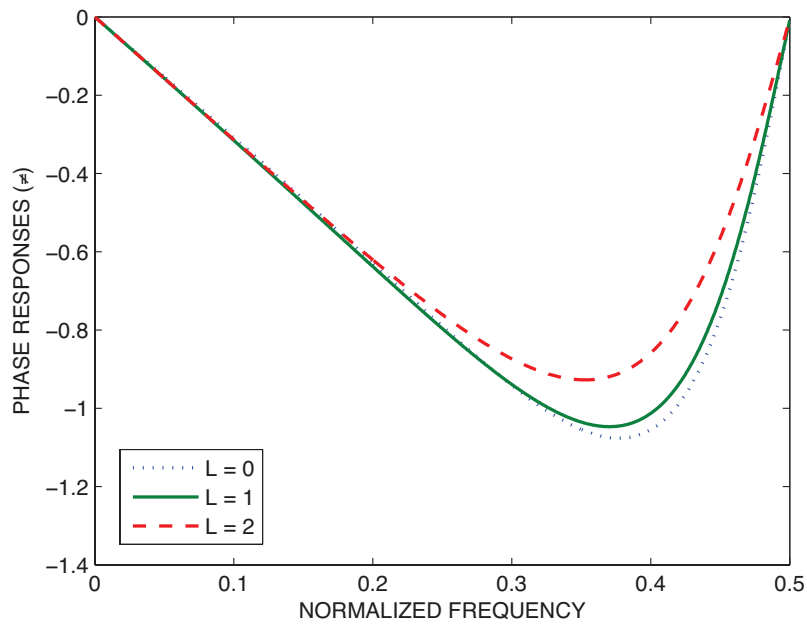
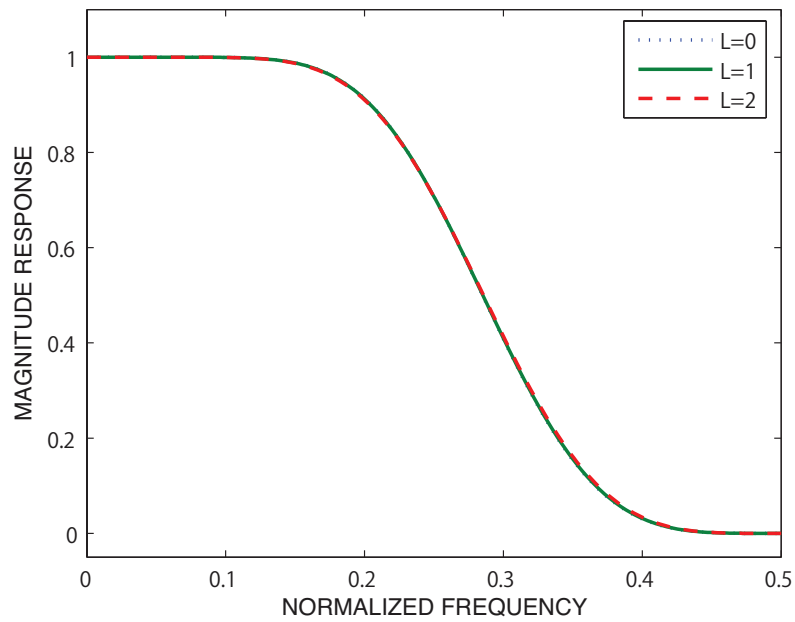


Fig.3.15 Phase errors of allpass filters $A(z)$.

Fig.3.16 Phase responses of allpass filters $A(z)$.Fig.3.17 Magnitude responses of scaling lowpass filters $H_i(z)$.

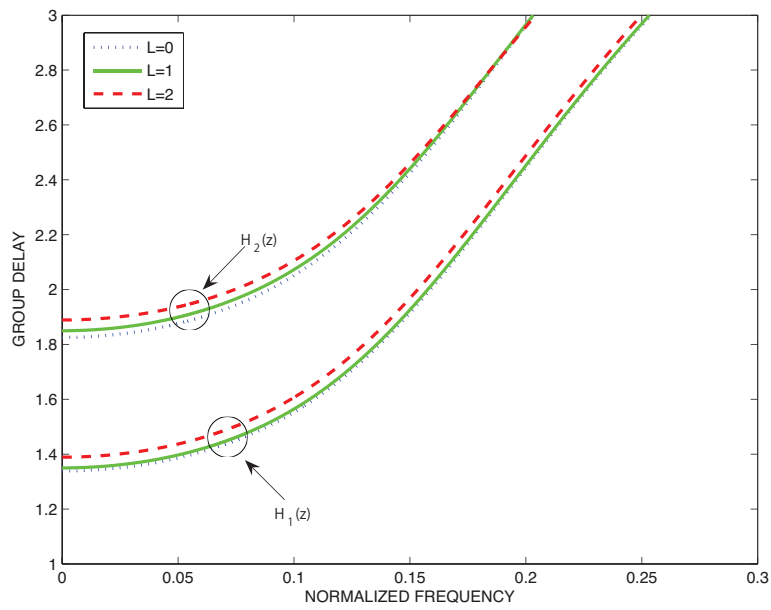


Fig.3.18 Group delay responses of scaling lowpass filters $H_i(z)$.

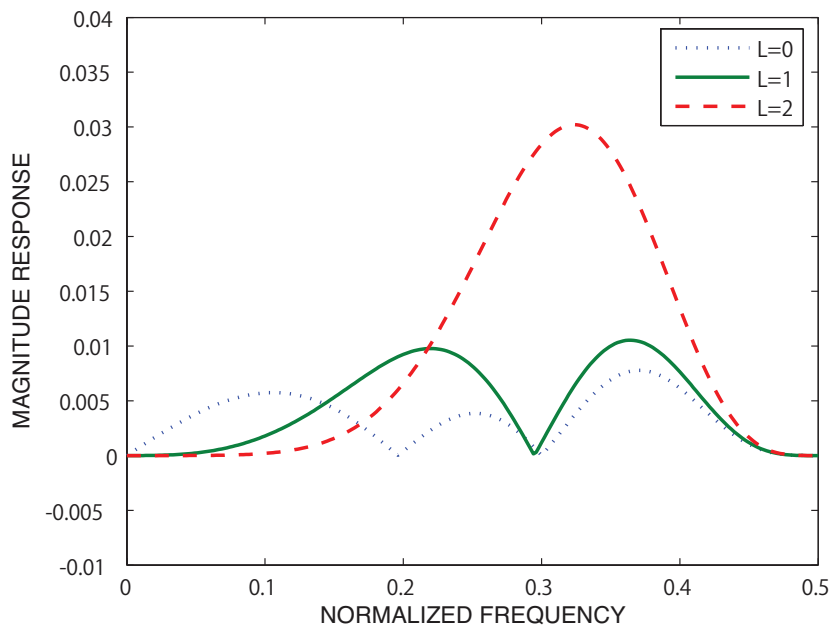
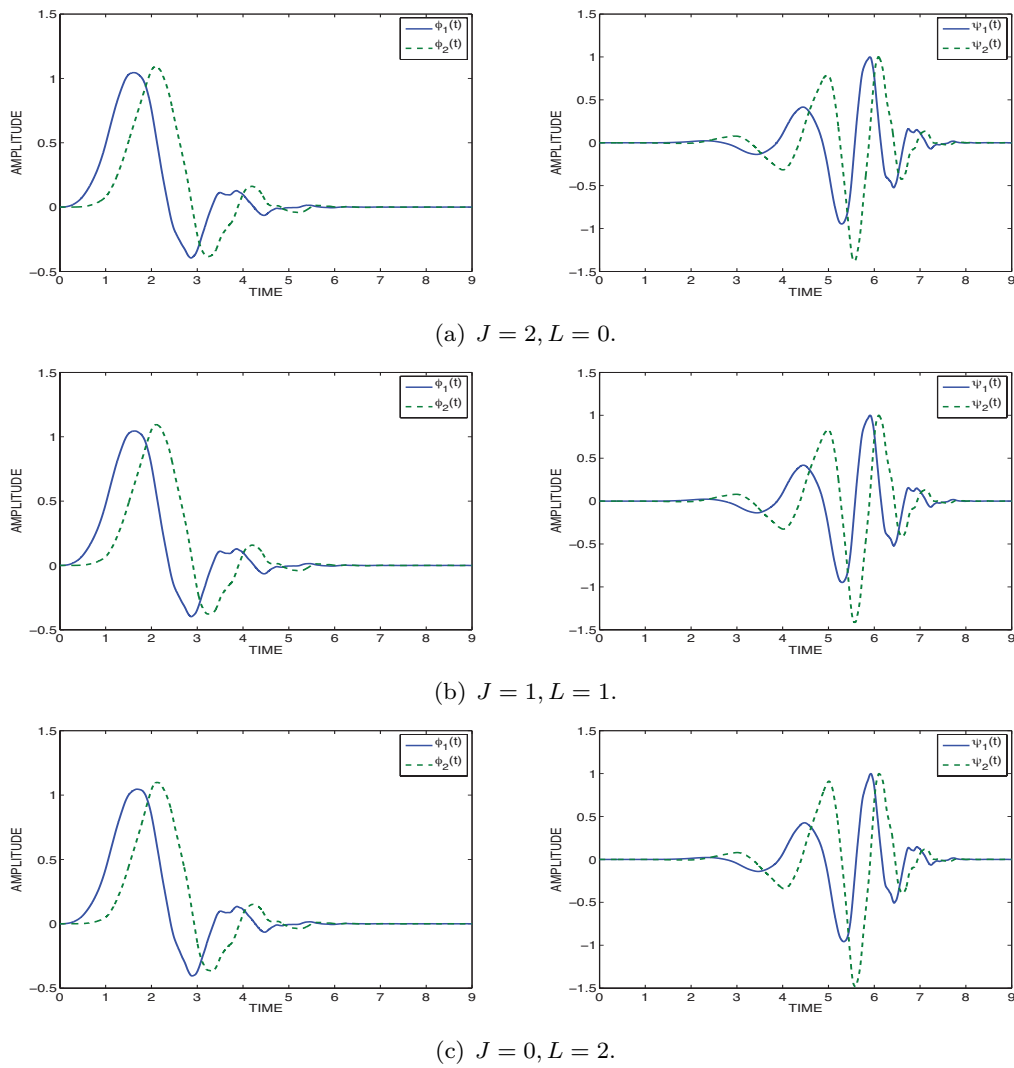


Fig.3.19 Magnitude responses of $E(\omega)$.

Fig.3.20 Scaling and wavelet functions $\phi_i(t), \psi_i(t)$.

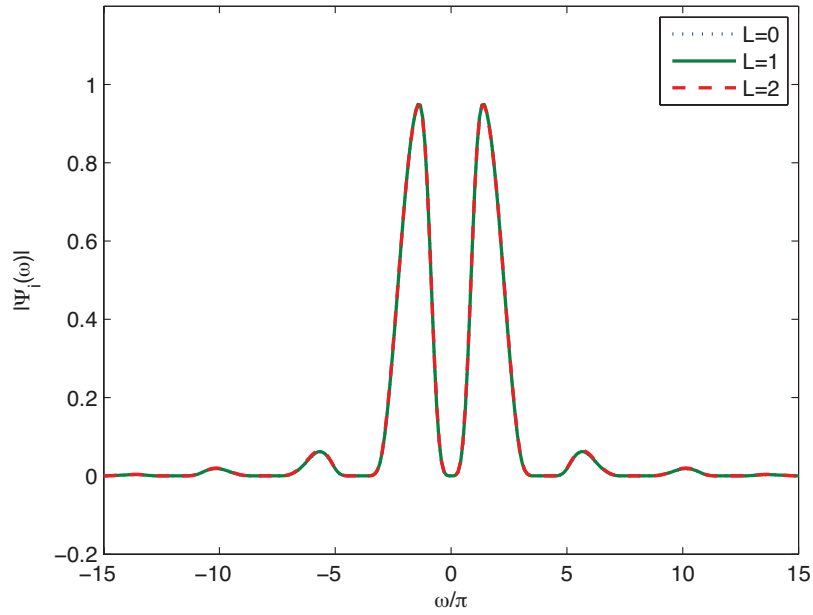


Fig.3.21 Magnitude responses of $\Psi_i(\omega)$.

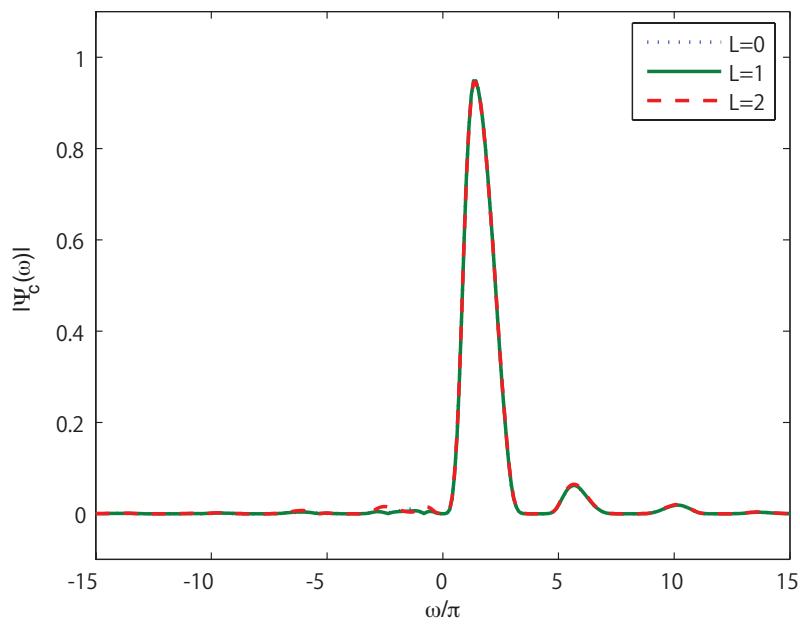
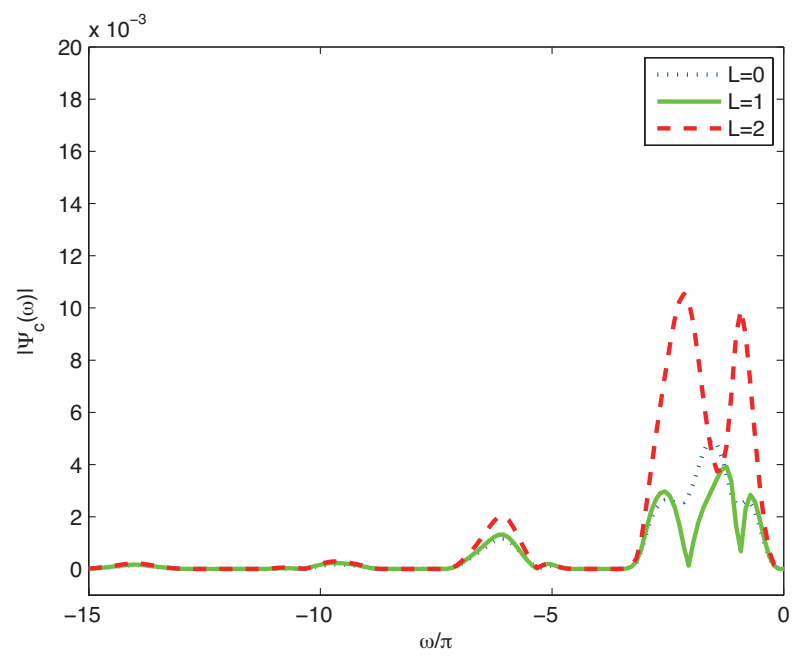


Fig.3.22 Magnitude responses of $\Psi_c(\omega)$.

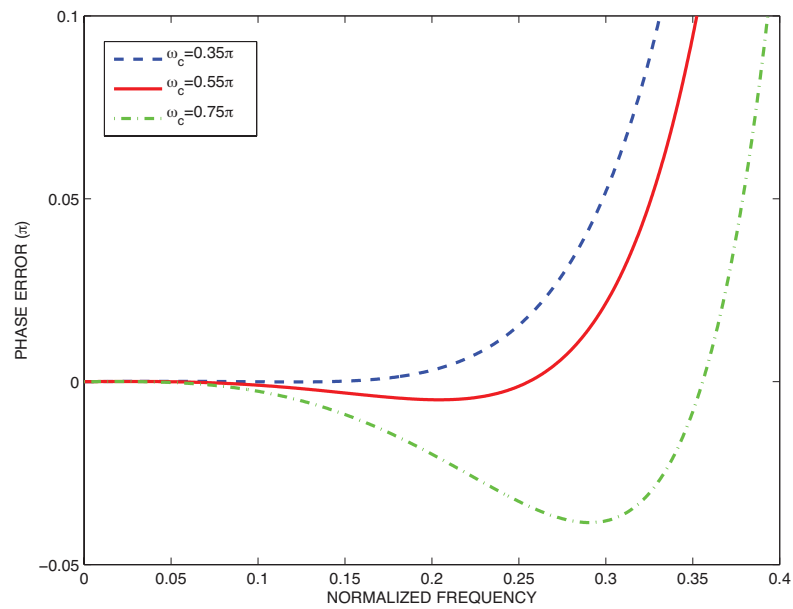
Fig.3.23 Magnitude responses of $\Psi_c(\omega)$.

Example 3.4

We consider a class of DTCWTs with improved analyticity by using IIR filters. We have designed three allpass filters with $J = 2$, $L = 1$. The approximation band is selected as $\omega_c = \{0.35\pi, 0.55\pi, 0.75\pi\}$. First of all, the phase error $\theta_e(\omega)$ are shown in Fig.3.24. It is obvious that with the increasing of ω_c , the phase error also increase. The phase responses of allpass filters $A(z)$ are shown in Fig.3.25. Next, we have constructed the scaling lowpass filters $H_i(z)$ with $K = 4$, $N_1 = 5$ and $N_2 = 1$. Their magnitude responses are shown in Fig.3.26, which are almost the same. Their group delay responses are shown in Fig.3.27, respectively. Moreover, the magnitude responses of error function $E(\omega)$ are shown in Fig.3.28. It is obvious that $E(\omega)$ is minimum when $\omega_c = 0.55\pi$, while it is maximum when $\omega_c = 0.75\pi$. If ω_c is too small or too big, the maximum error $E(\omega)$ will increase, resulting in a poor analyticity, as shown in Table 3.5. That is to say, how to determine the approximation band will effect $E(\omega)$, as well as the analyticity of complex wavelet. In addition, the scaling functions $\phi_i(t)$ and wavelet functions $\psi_i(t)$ are shown in Fig.3.29. Furthermore, the spectrum of $\Psi_i(\omega)$ and complex wavelet are shown in Fig.3.30, Fig.3.31 and Fig.3.32, respectively. In Fig.3.32, it is clear that the negative spectrum of DTCWT is minimum when $\omega_c = 0.55\pi$. Finally, E_∞ and E_2 are summarized in Table 3.5.

TABLE 3.5 Analyticity Measures E_∞ and E_2 .

ω_c	$E_\infty(\%)$	$E_2(\%)$
0.35π	0.718	0.782
0.55π	0.395	0.417
0.75π	1.523	1.527



s

Fig.3.24 Phase errors of allpass filters $A(z)$.

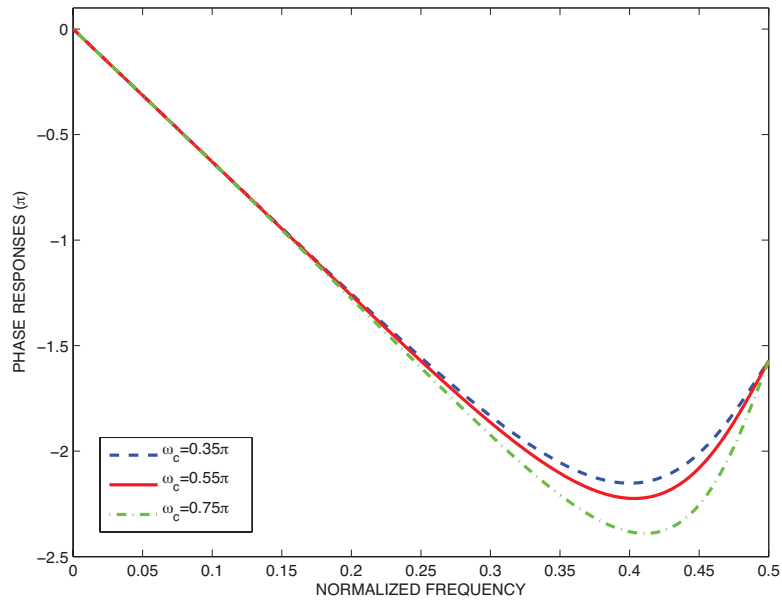


Fig.3.25 Phase responses of allpass filters $A(z)$.

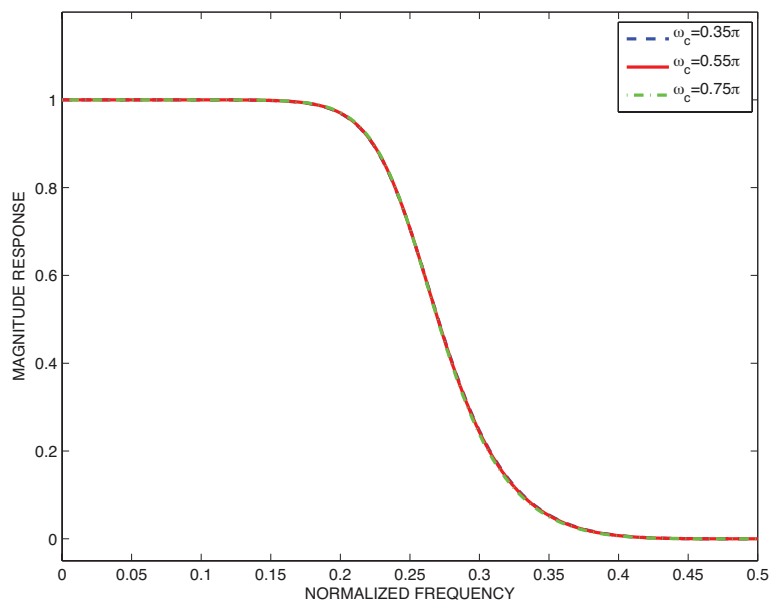


Fig.3.26 Magnitude responses of scaling lowpass filters $H_i(z)$.

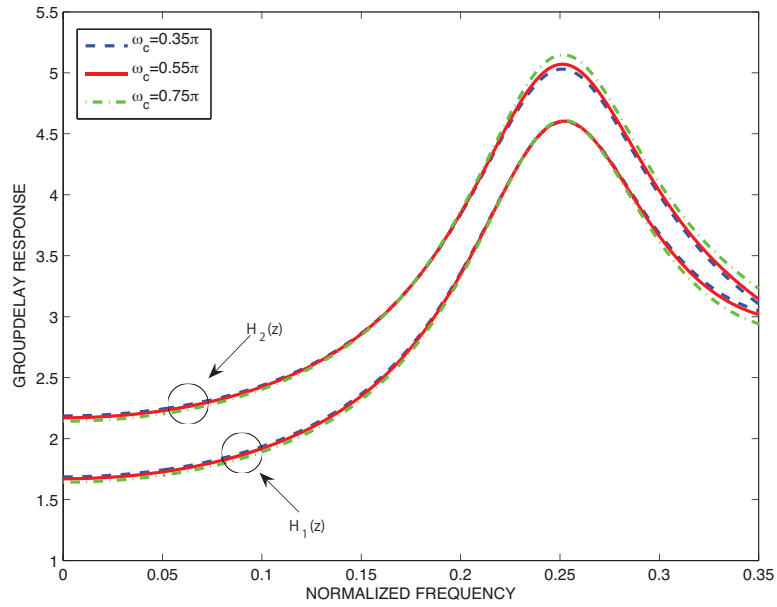


Fig.3.27 Group delay responses of scaling lowpass filters $H_i(z)$.

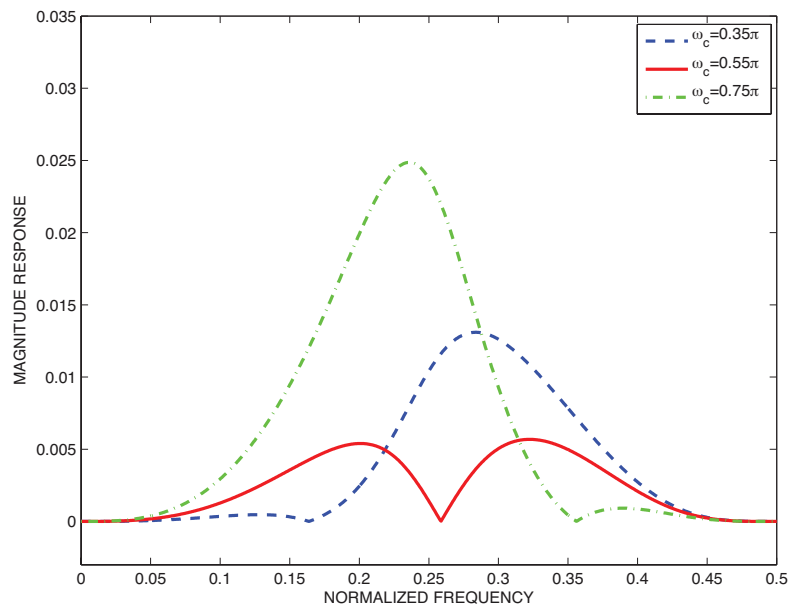


Fig.3.28 Magnitude responses of $E(\omega)$.

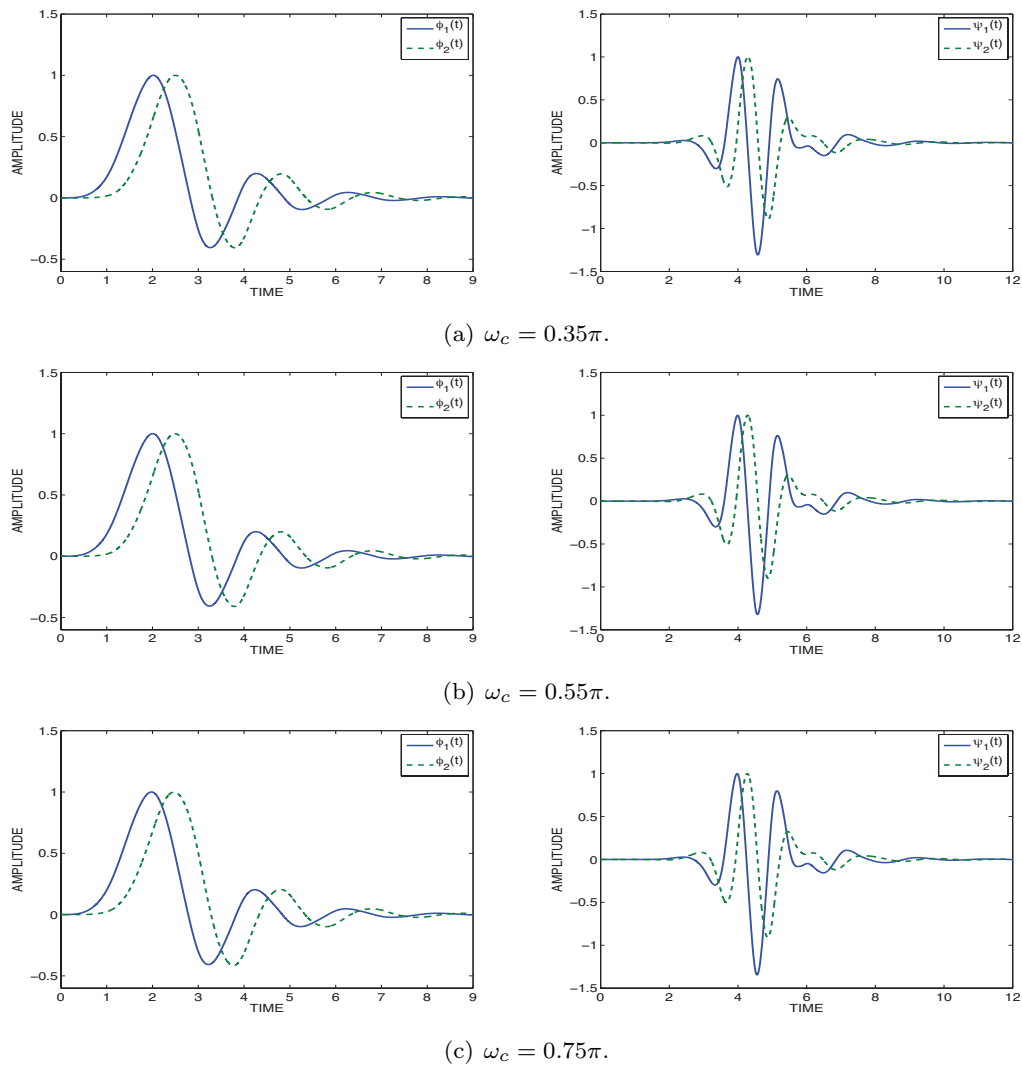
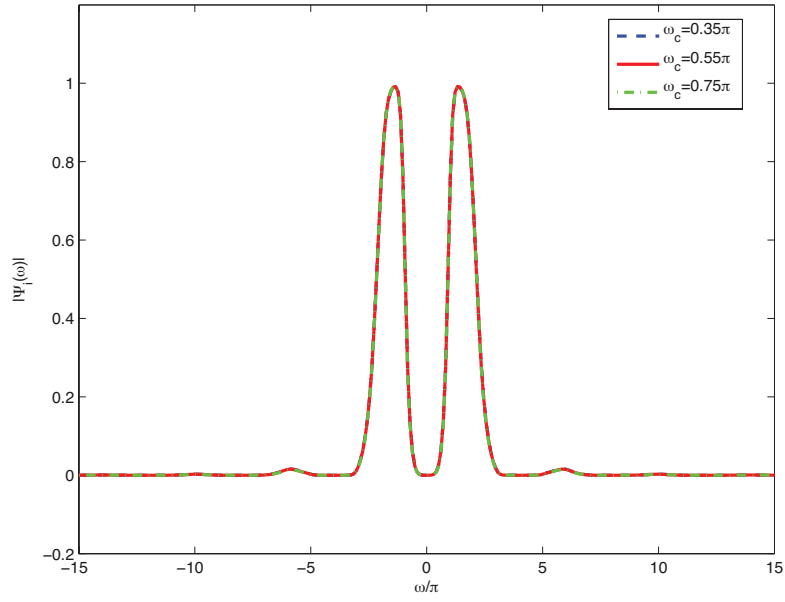
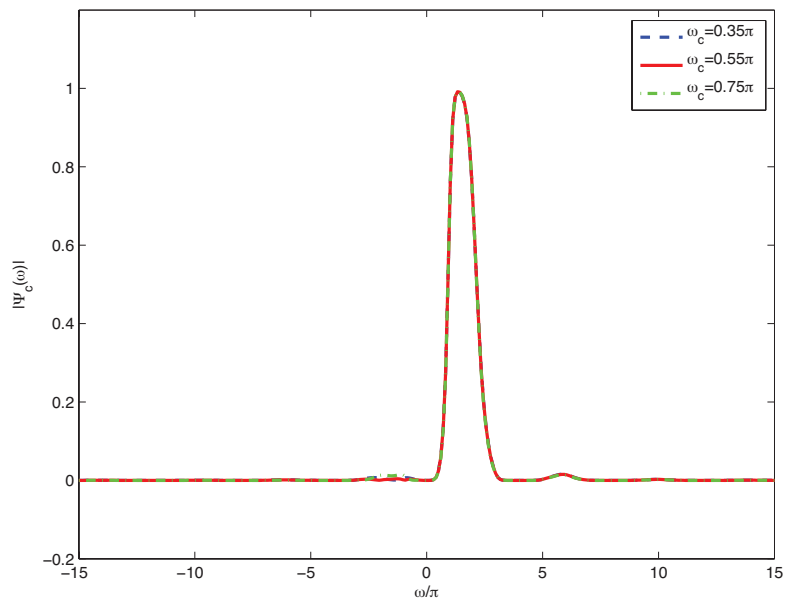


Fig.3.29 Scaling and wavelet functions $\phi_i(t), \psi_i(t)$.

Fig.3.30 Magnitude responses of $\Psi_i(\omega)$.Fig.3.31 Magnitude responses of $\Psi_c(\omega)$.

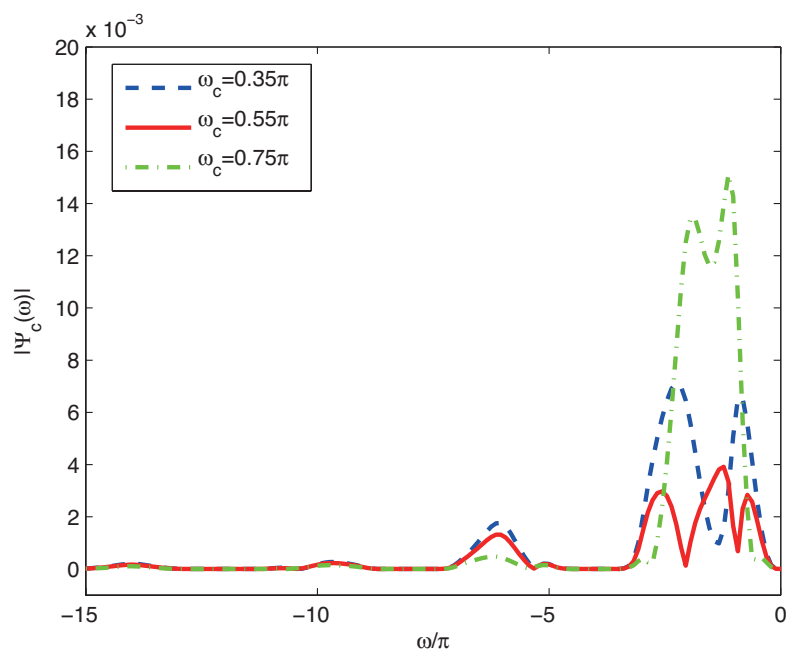


Fig.3.32 Magnitude responses of $\Psi_c(\omega)$.

3.4 DTCWTs with Improved Frequency Selectivity

It is well-known in [3] that frequency selectivity is a useful property for many applications of signal and image processing. However, the maximally flat filters have poor frequency selectivity. In the above-mentioned sections, the orthogonal scaling lowpass filters have as many zeros at $z = -1$ as possible to obtain the maximum number of vanishing moments, resulting in the maximally flat magnitude responses. In the following, in order to improve the frequency selectivity of the scaling lowpass filters, we specify the number of zeros at $z = -1$ from the viewpoint of vanishing moments and then minimize the stopband error by using the remaining degree of freedom. The filter coefficients can be obtained easily by solving an eigenvalue problem.

3.4.1 Formulation using Remez exchange algorithm

We first specify the number of zeros at $z = -1$ from the viewpoint of regularity. We assume $K < K_{max}$ where $K_{max} = \lfloor \frac{N+1}{2} \rfloor + N_2 - J$. Then the remaining degree of freedom is $K_{max} - K$, which can be used for obtaining the optimal possible frequency selectivity. Since zeros on the unit circle are complex-conjugate pair except $z = \pm 1$, $K_{max} - K$ should be even, i.e., $K_{max} - K = 2I$.

Next, we apply the Remez exchange algorithm to get an equiripple magnitude response in the stopband $[\omega_s, \pi]$, where ω_s is the cutoff frequency

of scaling lowpass filters. Assuming ω_i ($\omega_s = \omega_0 < \omega_1 < \dots < \omega_I < \pi$) to be a set of extremal frequencies, we formulate $P(e^{j\omega})$ as

$$P(e^{j\omega_i}) = \frac{R(e^{j\omega_i})S(e^{j\omega_i})}{B(e^{j2\omega_i})} = \frac{1 + (-1)^i}{2}\delta, \quad (3.43)$$

where $\delta(> 0)$ is an error. Note that we force $P(e^{j\omega_i}) \geq 0$ to permit spectral factorization of $R(z)$. From Eq.(3.43), we have

$$S(e^{j\omega_i})R(e^{j\omega_i}) = \frac{1 + (-1)^i}{2}\delta B(e^{j2\omega_i}), \quad (3.44)$$

where

$$\begin{cases} R(e^{j\omega}) = r(0) + 2 \sum_{n=1}^{N_1} r(n) \cos(n\omega) \\ B(e^{j\omega}) = b(0) + 2 \sum_{n=1}^{N_2} b(n) \cos(n\omega) \end{cases}. \quad (3.45)$$

Thus, we rewrite Eq.(3.44) in the matrix form as

$$\mathbf{P}_1 \mathbf{r} = \delta \mathbf{Q}_1 \mathbf{b}, \quad (3.46)$$

where the elements of the matrices \mathbf{P}_1 and \mathbf{Q}_1 are given by

$$\begin{aligned} P_1(m, n) &= \begin{cases} S(e^{j\omega_m}) & (n = 0) \\ 2S(e^{j\omega_m}) \cos(n\omega_m) & (n = 1, 2, \dots, N_1) \end{cases} \\ Q_1(m, n) &= \begin{cases} (1 + (-1)^m)/2 & (n = 0) \\ (1 + (-1)^m) \cos(2n\omega_m) & (n = 1, 2, \dots, N_2) \end{cases} \end{aligned} \quad (3.47)$$

It should be noted that the orthonormality condition has been given in Eqs.(3.27) and (3.28). Hence, we use Eq.(3.27) to obtain

$$\mathbf{P}_1 \mathbf{r} = \delta \mathbf{Q}_1 \mathbf{b} = \delta \mathbf{Q}_1 \mathbf{S}_1 \mathbf{r}. \quad (3.48)$$

We rewrite Eq.(3.48) in the matrix form as

$$\begin{bmatrix} \mathbf{S}_2 \\ \mathbf{P}_1 \end{bmatrix} \mathbf{r} = \delta \begin{bmatrix} \mathbf{0} \\ \mathbf{Q}_1 \mathbf{S}_1 \end{bmatrix} \mathbf{r}, \quad (3.49)$$

which is correspondent to a generalized eigenvalue problem, i.e., δ is the eigenvalue and \mathbf{r} is the corresponding eigenvector. Since there exist more than one eigenvalue, we choose the minimum positive eigenvalue δ and the corresponding eigenvector gives a set of filter coefficients $r(n)$. The initial extremal frequencies may not be the optimal peak frequencies so that we make use of an iteration procedure to obtain the optimal coefficients $r(n)$. We then compute $b(n)$ by Eq.(3.27).

3.4.2 Design Algorithm

Design Algorithm

Begin

- (1) Read K, J, L and the cutoff frequency ω_s .
- (2) Design $A(z)$ to get $a(n)$, and use Eq.(3.12) to compute $s(n)$.
- (3) Select initial extremal frequencies Ω_i ($\omega_s = \Omega_0 < \Omega_1 < \dots < \Omega_I < \pi$) equally spaced in the stopband.

Repeat

- (4) Set $\omega_i = \Omega_i$ for $i = 0, 1, \dots, I$.
- (5) Compute \mathbf{S}_1 and \mathbf{S}_2 in Eq.(3.29) and Eq.(3.30), respectively.
- (6) Compute \mathbf{P}_1 and \mathbf{Q}_1 in Eq.(3.47).
- (7) Choose the minimum positive eigenvalue δ and corresponding eigenvector \mathbf{r} in Eq.(3.49) to obtain a set of filter coefficients $r(n)$.
- (8) Obtain the coefficients $b(n)$ by Eq.(3.28).
- (9) Search the peak frequencies Ω_i ($\omega_s = \Omega_0 < \Omega_1 < \dots < \Omega_I < \pi$) of $P(e^{j\omega})$ in the stopband.

Until

Satisfy the following condition for a prescribed small constant ε (e.g., $\varepsilon = 10^{-12}$);

$$\sum_{i=1}^I |\omega_i - \Omega_i| < \varepsilon$$

End.

3.4.3 Design Examples

In the following, two examples will be presented to demonstrate our proposed procedure. We construct a class of DTCWTs with improved analyticity and frequency selectivity by using general IIR filters at first. Next, we investigate the influence of the stopband on the analyticity of complex wavelet.

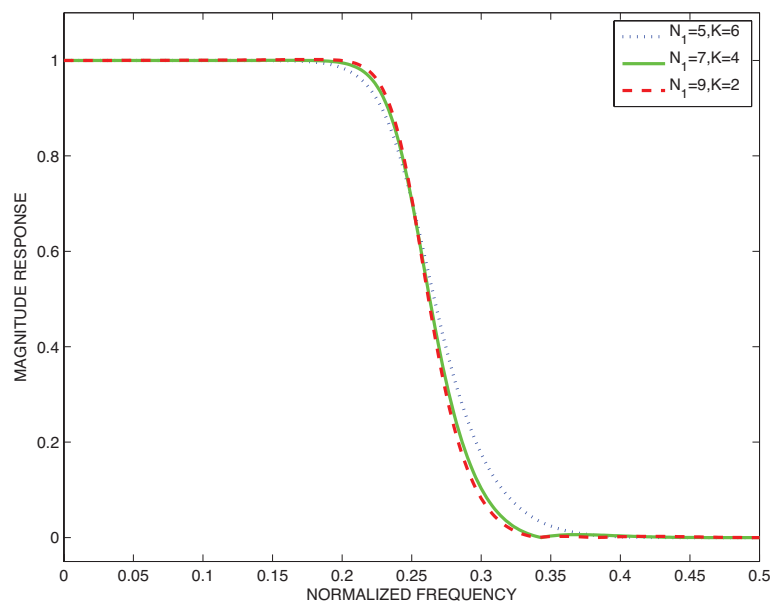
Example 3.5

We consider a class of DTCWTs with improved analyticity and frequency selectivity. Firstly, we have used the allpass filter with $J = 2$, $L = 1$, $\omega_c = 0.51\pi$, and then designed the scaling lowpass filters $H_i(z)$ with $N = 13$, $N_2 = 1$, $\omega_s = 0.67\pi$. We set $K = 4$ and $N_1 = 7$. The resulting magnitude response of $H_i(z)$ are shown in Fig.3.33 and Fig.3.34, respectively. For comparison, the scaling lowpass filter with the maximally flat magnitude response ($K = 6$, $N_1 = 5$), and the filter with two equiripples in the stopband ($K = 2$, $N_1 = 9$) are also designed and their magnitude responses are shown in Fig.3.33. It is clear that the magnitude responses of $H_i(z)$ with improved frequency selectivity are more sharp than the maximally flat filter. Their group delay responses are shown in Fig.3.35. In addition, the magnitude responses of $E(\omega)$ are shown in Fig.3.36, where the error decreases at the expense of decreasing vanishing moments. Besides, the scaling functions $\phi_i(t)$ and wavelet functions $\psi_i(t)$ are shown in Fig.3.37. The wavelet spectrum $\Psi_i(\omega)$ are shown in Fig.3.38, which are almost same. Furthermore, the spectrum $\Psi_c(\omega)$ are

shown in Fig.3.39 and Fig.3.40, where the negative spectrum of proposed DTCWTs are smaller than that constructed by the maximally flat scaling lowpass filter. Finally, Table 3.6 summarizes the analyticity measures of E_∞ and E_2 . It is seen that the analyticity can be also improved slightly by improving the frequency selectivity of $H_i(z)$.

TABLE 3.6 Analyticity Measures E_∞ and E_2 .

K	N_1	$E_\infty(\%)$	$E_2(\%)$
6	5	0.268	0.299
4	7	0.262	0.236
2	9	0.258	0.232

Fig.3.33 Magnitude responses of scaling lowpass filters $H_i(z)$.

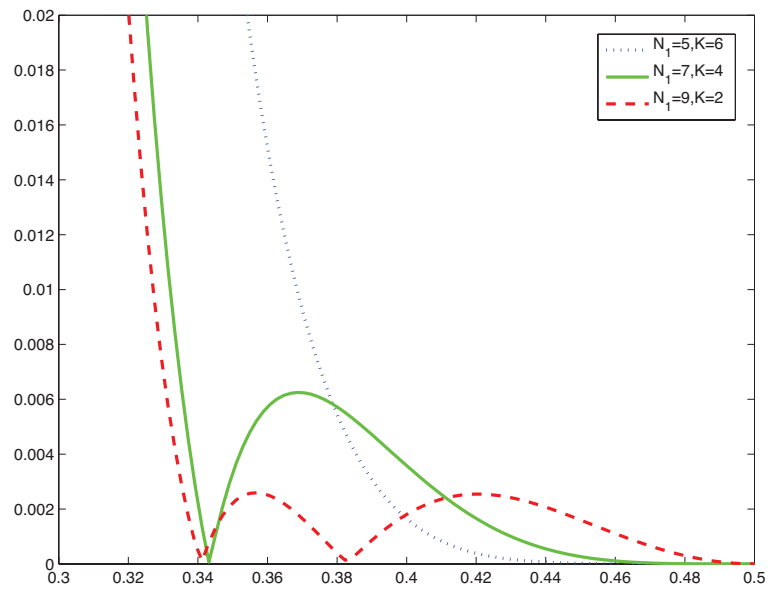


Fig.3.34 Magnitude responses of scaling lowpass filters $H_i(z)$.

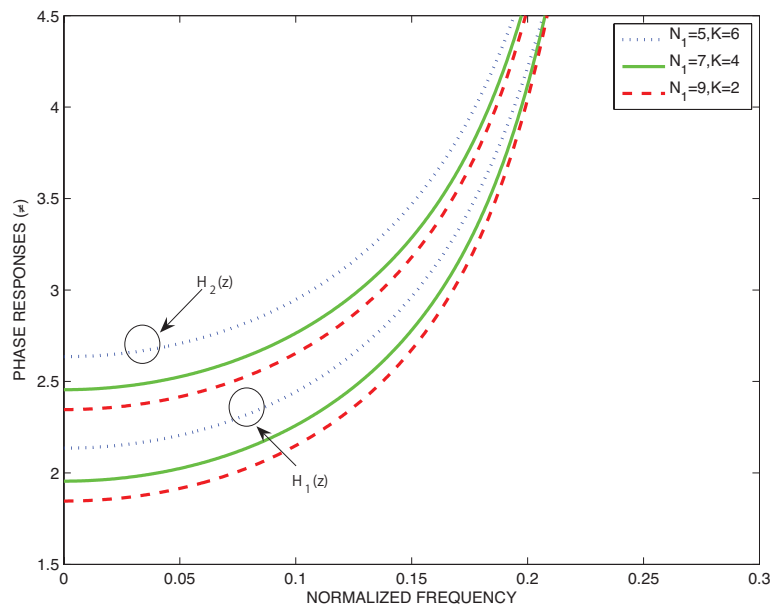


Fig.3.35 Group delay responses of scaling lowpass filters $H_i(z)$.

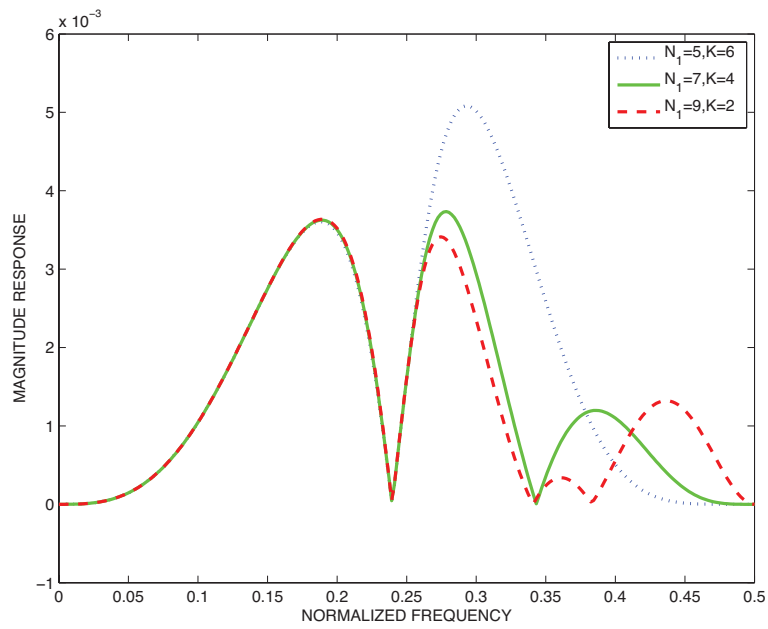
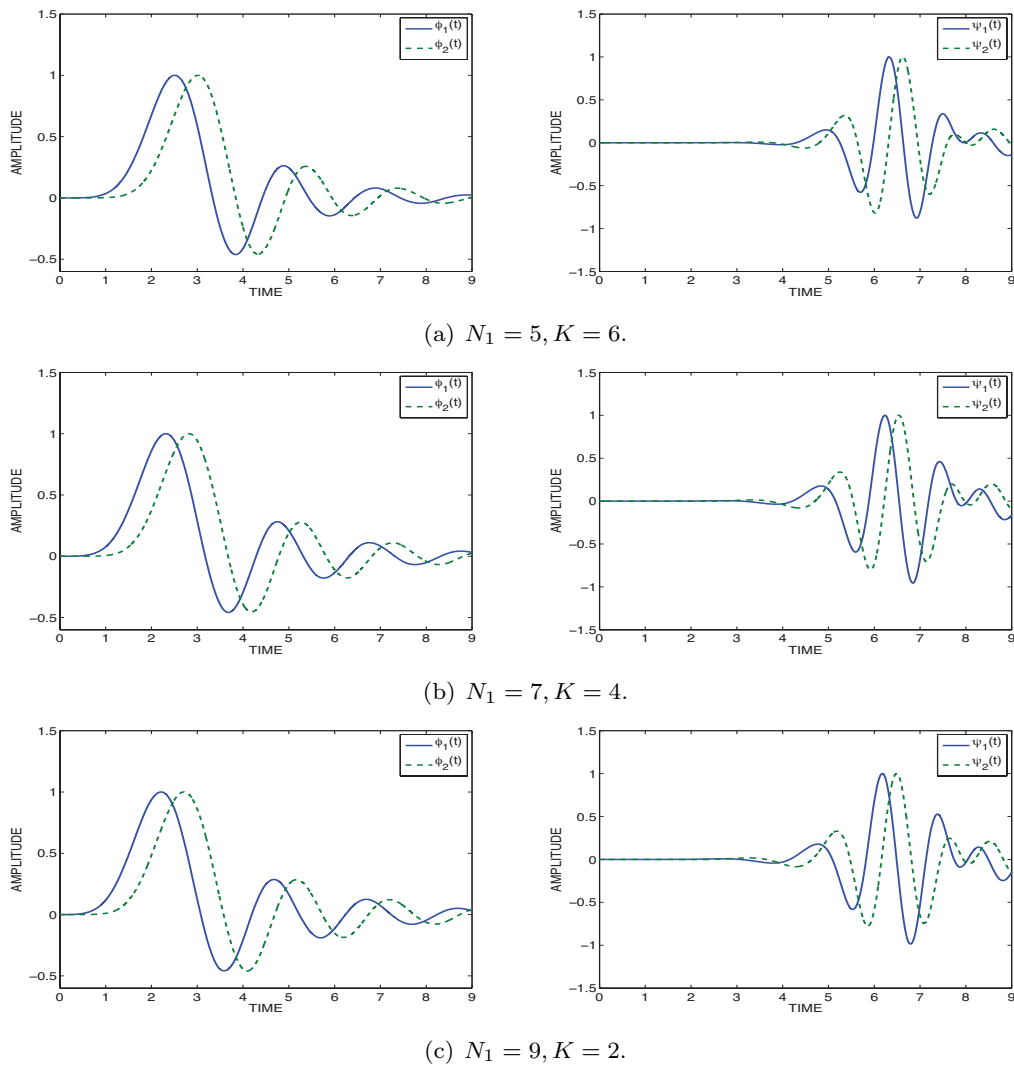


Fig.3.36 Magnitude responses of $E(\omega)$.

Fig.3.37 Scaling and wavelet functions $\phi_i(t), \psi_i(t)$.

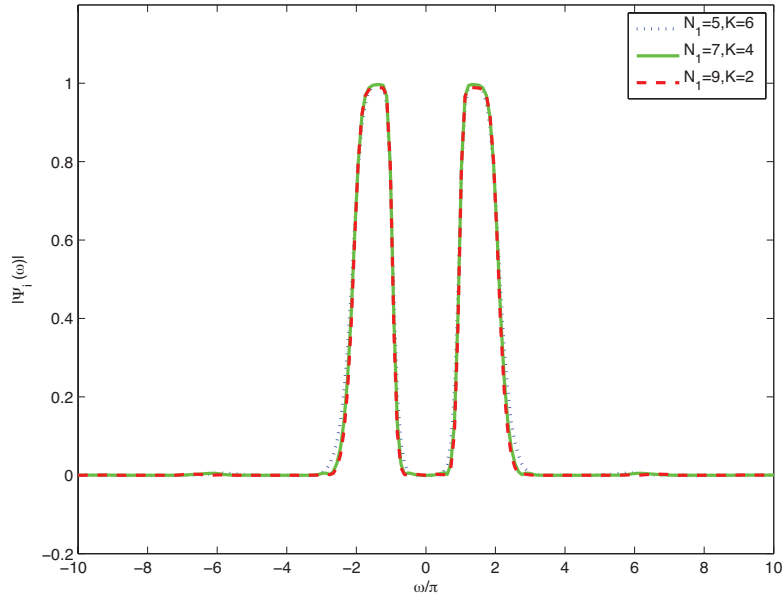


Fig.3.38 Magnitude responses of $\Psi_i(\omega)$.

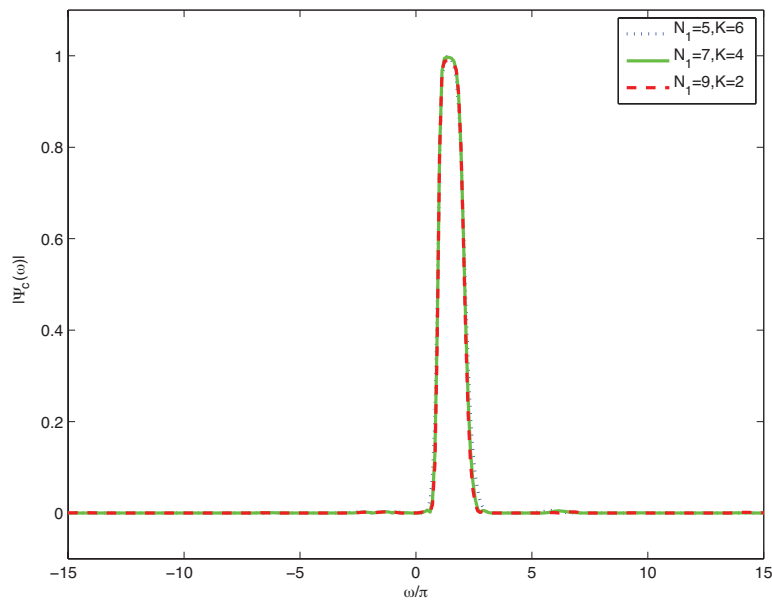
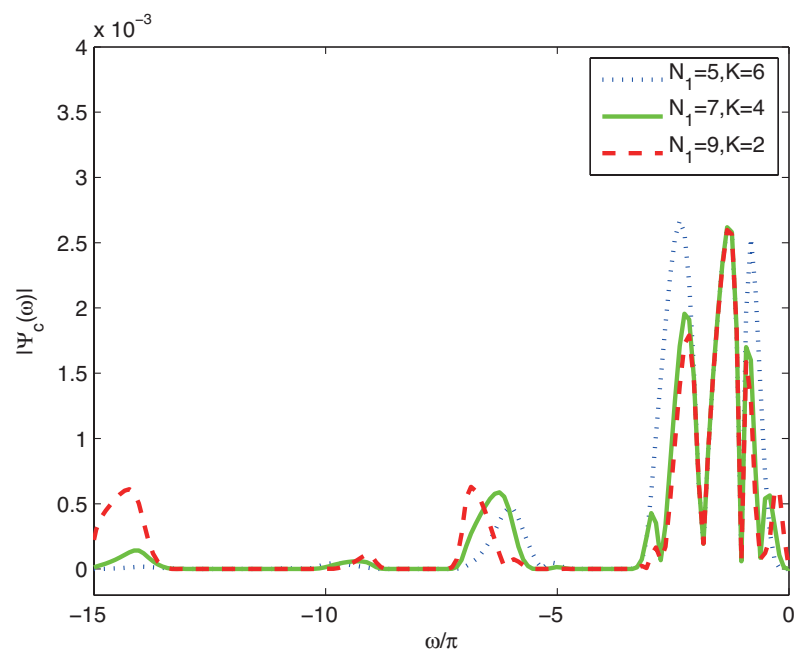


Fig.3.39 Magnitude responses of $\Psi_c(\omega)$.

Fig.3.40 Magnitude responses of $\Psi_c(\omega)$.

Example 3.6

We consider a class of DTCWTs with improved analyticity and frequency selectivity. Firstly, we have used the allpass filter with $J = 2$, $L = 1$, $\omega_c = 0.51\pi$, and then designed scaling lowpass filters $H_i(z)$ with $K = 4$, $N_1 = 7$, and $N_2 = 1$. The cutoff frequency ω_s is chosen as $\omega_s = \{0.56\pi, 0.61\pi, 0.88\pi\}$, respectively. The magnitude responses of resulting lowpass filters are shown in Fig.3.41 and Fig.3.42, respectively. It is obvious that the scaling lowpass filters become sharp as ω_s decreases. Their group delay responses are shown in Fig.3.43, where the half-sample delay condition are almost achieved. Next, the magnitude responses of $E(\omega)$ are shown in Fig.3.44. It is seen in Fig.3.44 that cutoff frequency ω_s influence the magnitude responses of $E(\omega)$. If ω_s is too small or too big, the maximum error $E(\omega)$ increase, resulting in a poor analyticity of complex wavelet, as shown in Table 3.7. Moreover, the scaling functions $\phi_i(t)$ and wavelet functions $\psi_i(t)$ are shown in Fig.3.45. The wavelet spectrum $\Psi_i(\omega)$ are given in Fig.3.46. Furthermore, the spectrum of DTCWTs are shown in Fig.3.47 and Fig.3.48, respectively. In Fig.3.48, the negative spectrum is minimum when $\omega_s = 0.61\pi$. Finally, we summarize the objective measures of quality E_∞ and E_2 in Table 3.7.

TABLE 3.7 Analyticity Measures E_∞ and E_2 .

ω_s	$E_\infty(\%)$	$E_2(\%)$
0.56 π	0.298	0.366
0.61 π	0.262	0.254
0.88 π	0.263	0.290

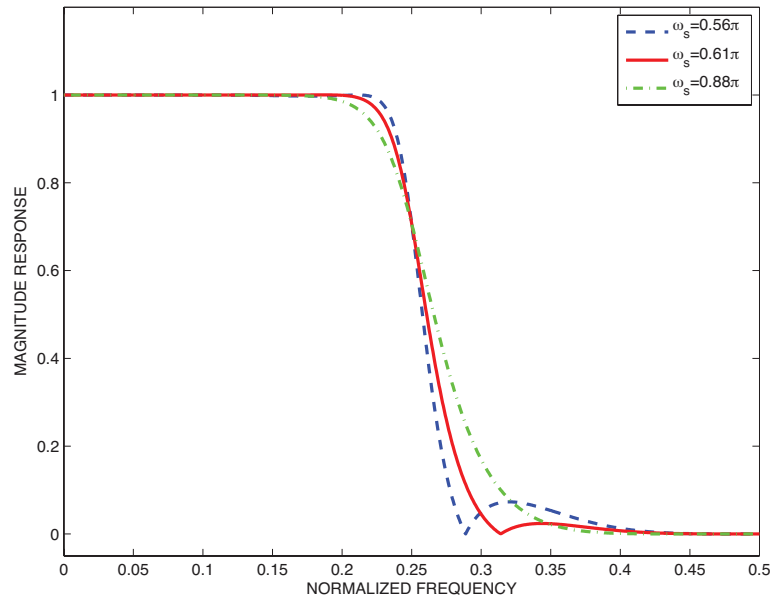


Fig.3.41 Magnitude responses of scaling lowpass filters $H_i(z)$.

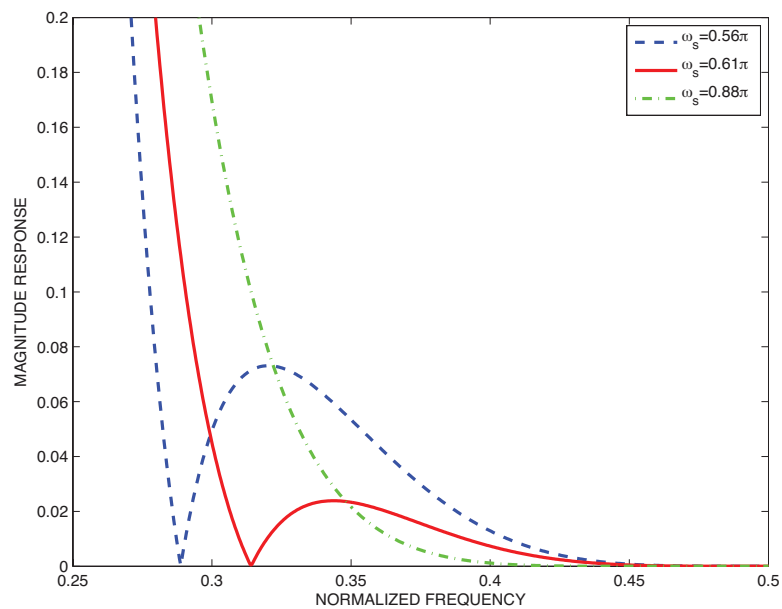


Fig.3.42 Magnitude responses of scaling lowpass filters $H_i(z)$.

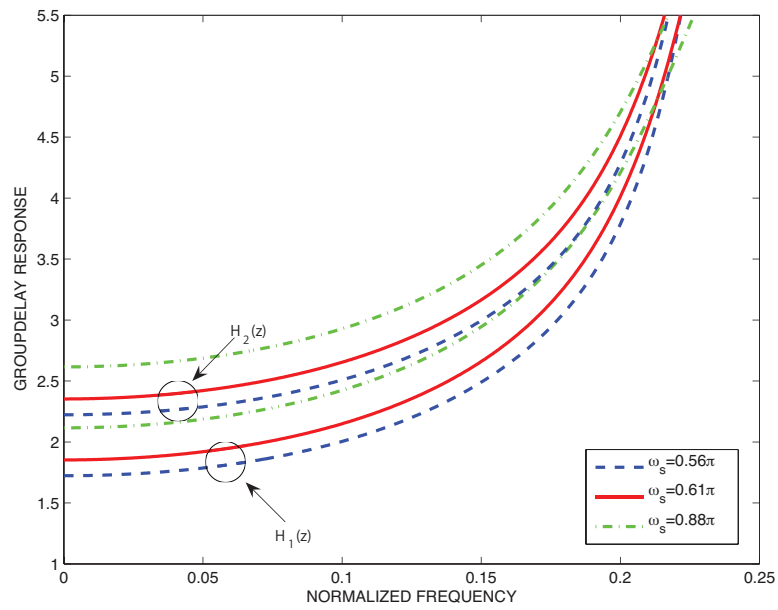


Fig.3.43 Group delay responses of scaling lowpass filters $H_i(z)$.

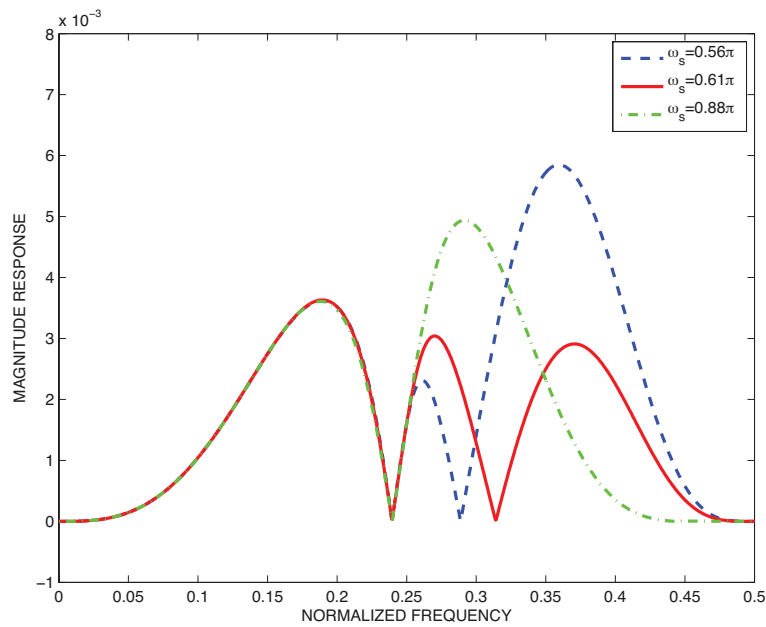
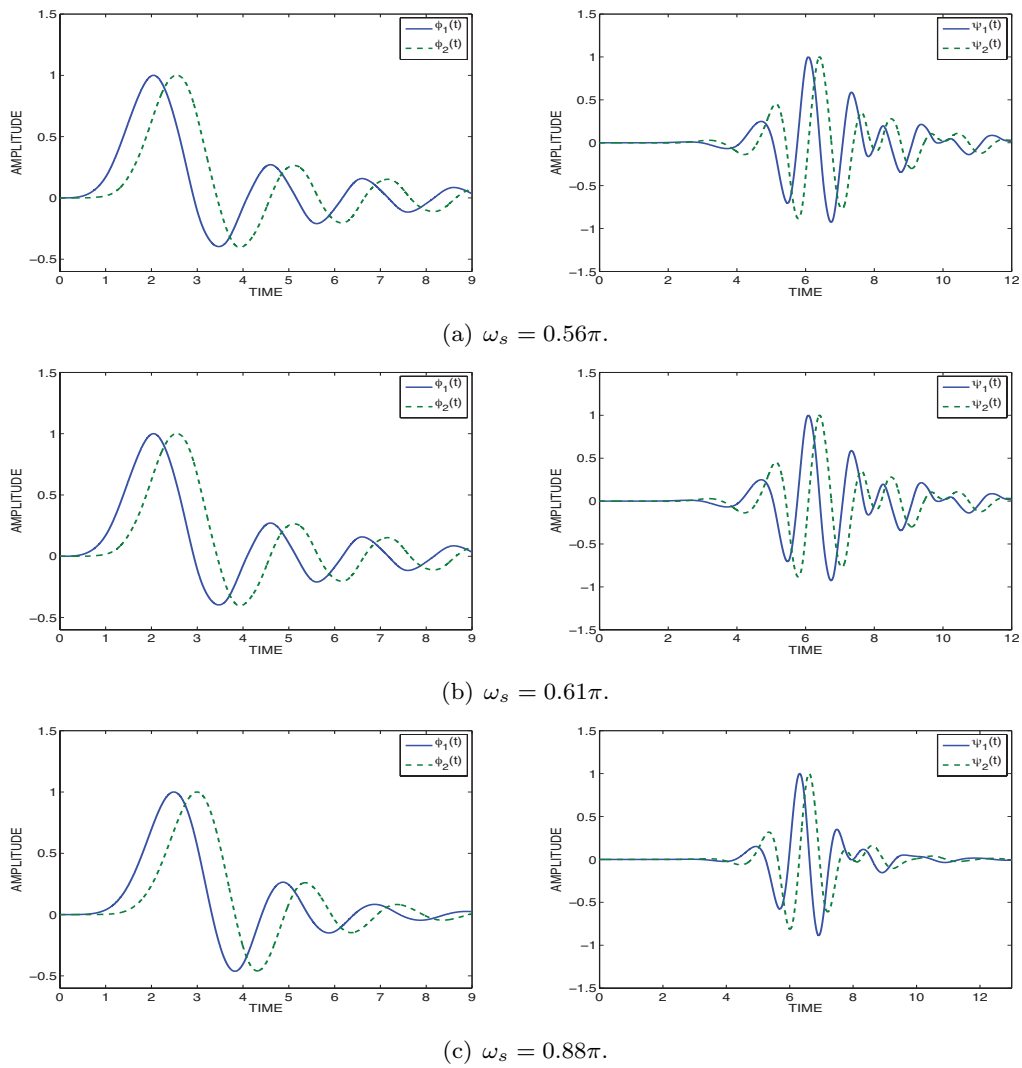


Fig.3.44 Magnitude responses of $E(\omega)$.

Fig.3.45 Scaling and wavelet functions $\phi_i(t), \psi_i(t)$.

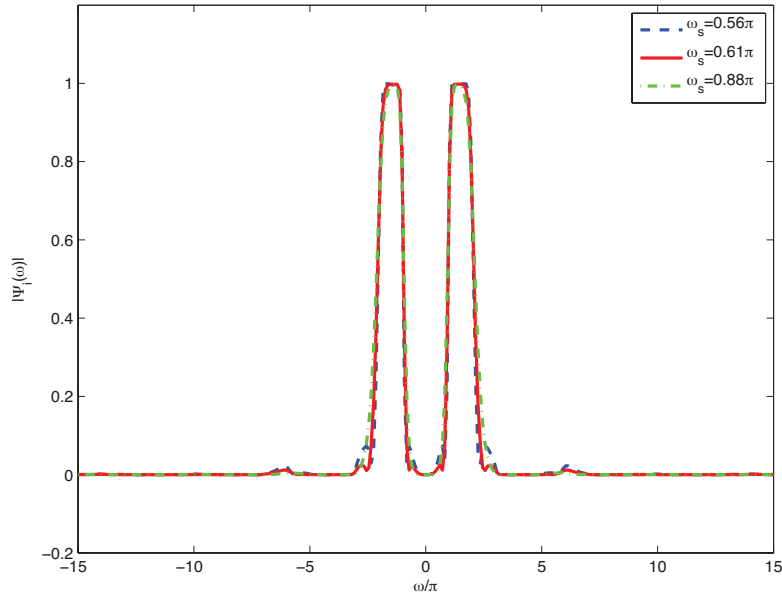


Fig.3.46 Magnitude responses of $\Psi_i(\omega)$.

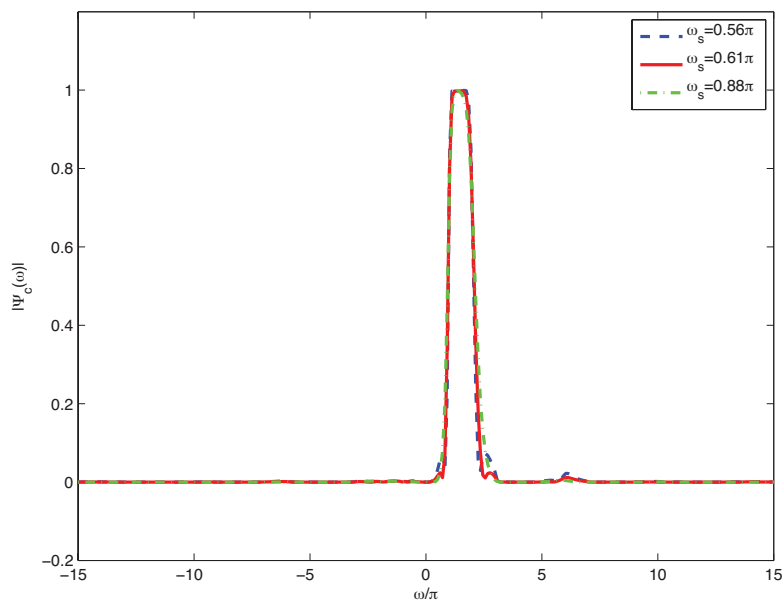
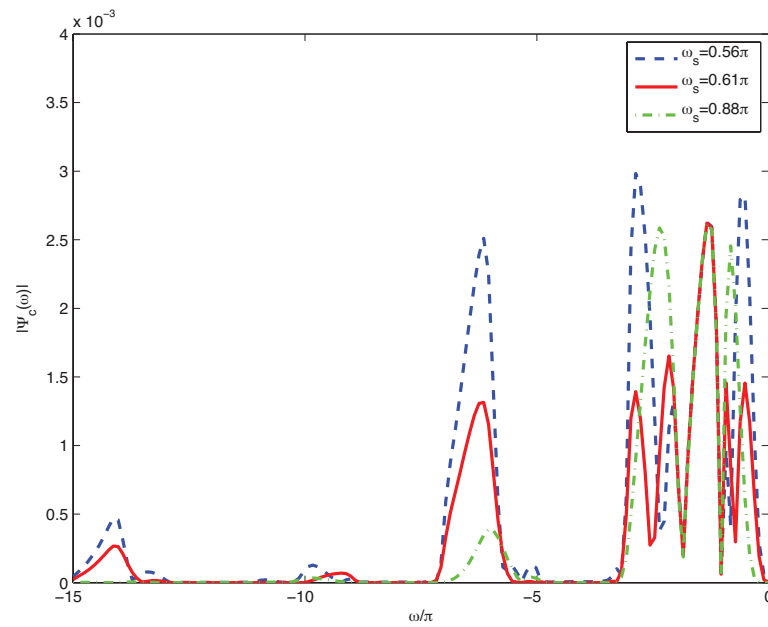


Fig.3.47 Magnitude responses of $\Psi_c(\omega)$.

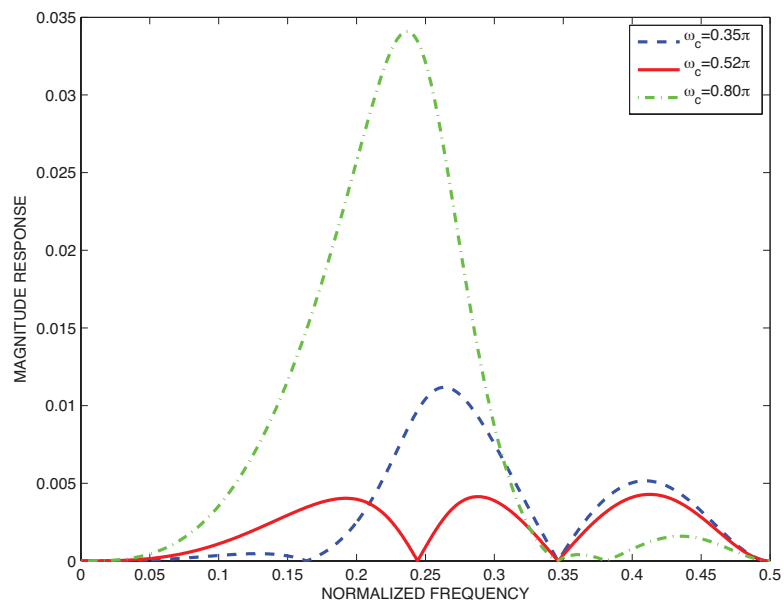
Fig.3.48 Magnitude responses of $\Psi_c(\omega)$.

3.5 Performance Investigation

In this section, we investigate the performance on the proposed DTCWTs with improved analyticity and frequency selectivity. First of all, we have designed the allpass filters with $J = 2$, $L = 1$ and the cutoff frequency is chosen as $\omega_c = \{0.35\pi, 0.52\pi, 0.80\pi\}$. Then we have designed the scaling lowpass filters $H_i(z)$ with $K = 2$, $N_1 = 5$, $N_2 = 1$ and $\omega_s = 0.67\pi$. The resulting magnitude responses of $E(\omega)$ are shown in Fig.3.49, and it is seen that the maximum error of $E(\omega)$ is the minimum when $\omega_c = 0.52\pi$. If ω_c is too small or too big, the maximum error of $E(\omega)$ will increase, resulting in a poor analyticity as shown in Table 3.8. That is to say, how to determine the cutoff frequency ω_c influences $E(\omega)$ as well as the analyticity of complex wavelets. Next, we have varied ω_c from 0.3π to 0.8π to investigate the relationship between the analyticity measures of E_∞ , E_2 and the cutoff frequency ω_c . It is seen in Fig.3.50 when ω_c is too small or too big, the analyticity measures of E_∞ , E_2 become larger. Furthermore, we have also varied cutoff frequency ω_s from 0.55π to 0.95π to investigate the relationship between the optimal frequency ω_c^{opt} and ω_s . It is clear in Fig.3.51 that if the stopband is too wide, i.e., ω_s is closer to 0.5π , the optimal cutoff frequency ω_c^{opt} is larger, that is, the approximation band of allpass filter become wider. It is because the stopband error of lowpass scaling filter is larger in this case, requiring the allpass filter to improve the error $E(\omega)$ also in stopband. On other hand, the optimal frequency ω_c^{opt} is almost constant when the stopband is not too wide, since the stopband error of lowpass scaling filter is small and has little effect on the analyticity. Finally, the objective measures of quality are summarized in Table 3.8.

TABLE 3.8 Analyticity Measures E_∞ and E_2 .

ω_c	$E_\infty(\%)$	$E_2(\%)$
0.35π	0.626	0.653
0.52π	0.292	0.378
0.80π	2.013	1.977

Fig.3.49 Magnitude responses of $E(\omega)$.

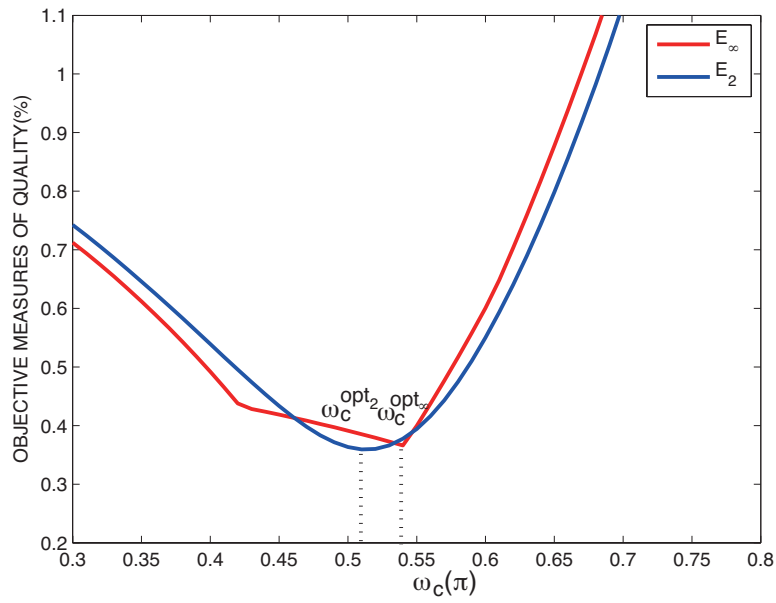
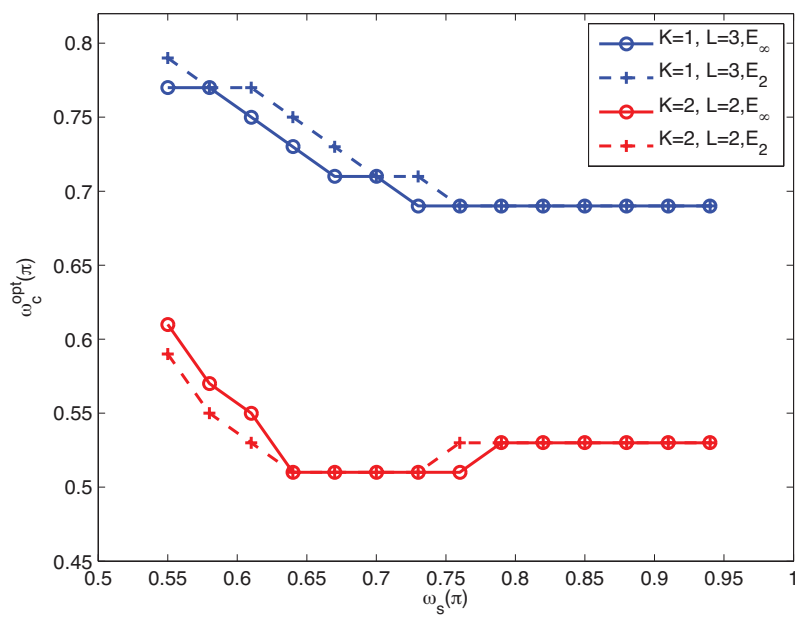


Fig.3.50 Relationship between E_∞ , E_2 and ω_c .



Z

Fig.3.51 Relationship between ω_c^{opt} and ω_s .

3.6 Summary

In this chapter, we have firstly reviewed the common-factor technique proposed by Selesnick [20]. Next, the common-factor technique by using general IIR filters with numerator and denominator of different degree was introduced [25]. It has been proved that the FIR and IIR orthonormal solutions proposed in [20] are only the special cases of general IIR orthonormal solutions. Moreover, in order to improve the analyticity of complex wavelet, we have proposed a design procedure of allpass filter with the specified degree of flatness at $\omega = 0$ and an equiripple phase response in the approximation band. Furthermore, to improve the frequency selectivity of scaling lowpass filters, we have specified the number of vanishing moments at $z = -1$ and used the remaining degree of freedom to approximate an equiripple magnitude response in the stopband. Some design examples are presented to demonstrate the efficiency of our proposed algorithm. Finally, the performance on the proposed DTCWTs has been investigated, where a properly chosen approximation band can improve the analyticity of complex wavelets.

Chapter 4 Almost Symmetric DTCWTs with Arbitrary Center of Symmetry

4.1 Introduction

In the previous chapter, the common-factor method has been generalized by using IIR filters with numerator and denominator of different degree to obtain a class of general IIR orthogonal solutions. However, the wavelet filters obtained by the common-factor method have nonlinear phase responses, resulting in asymmetric wavelet bases. Therefore, the purpose of this chapter is to design the symmetric orthogonal DTCWTs. Q-shift filter is one of the representative filters used for obtaining the symmetric wavelet bases, which was proposed by Kingsbury in [16], [17], [22]. The group delay responses of Q-shift filters are required to be $1/4$ or $3/4$ sample from the half-sample delay condition. However, digital filters with the specified (fractional or integer) group delay are often needed in many applications of signal and image processing [3], [6].

Thus, in this chapter, we review the design of Q-shift filters at first and then propose a method for designing two scaling lowpass filters with the arbitrarily specified flat group delay responses, which satisfy the half-sample delay condition. Moreover, two scaling lowpass filters are designed simultaneously to satisfy the specified degree of flatness of group delays,

vanishing moments and orthogonality condition. Furthermore, the difference of the frequency responses between two scaling lowpass filters can be effectively minimized to improve the analyticity of complex wavelet. It will be shown that the proposed DTCWTs can have arbitrary center of symmetry with improved analyticity. Finally, several experiments of signal denoising are carried out to demonstrate the efficiency of the proposed DTCWTs.

4.2 Q-Shift Filters

In [16] and [17] and [22], Kingsbury had proposed Q-shift filters in order to provide the improved symmetry property. One scaling lowpass filter is chosen to be the time reverse of another filter;

$$H_2(z) = z^{-N} H_1(z^{-1}), \quad (4.1)$$

where $H_i(z)$ is FIR filter of degree N for $i = 1, 2$. The transfer function of $H_i(z)$ are given by

$$H_i(z) = \sum_{n=0}^N h_i(n) z^{-n}, \quad (4.2)$$

where $h_i(n)$ are real filter coefficients and N is an odd number.

Q-shift filters are required to have linear phase responses. That is, the desired phase response of $H_1(z)$ is

$$\theta_1^d(\omega) = -\left(\frac{N}{2} - \frac{1}{4}\right)\omega. \quad (4.3)$$

Therefore, the phase response of $H_2(z)$ will be $-\left(\frac{N}{2} + \frac{1}{4}\right)\omega$, and then two scaling lowpass filters $H_1(z)$ and $H_2(z)$ satisfy the half-sample delay con-

dition.

In addition to the phase condition given in Eq.(4.3), $H_i(z)$ is also required to satisfy the conditions of regularity and orthonormality of wavelets. From the viewpoint of regularity, $H_i(z)$ must have K zeros at $z = -1$;

$$H_i(z) = Q_i(z)(1 + z^{-1})^K. \quad (4.4)$$

When the maximum K is chosen, the maximum number of vanishing moments can be obtained.

Moreover the condition of orthonormality for $H_i(z)$ is given by

$$H_i(z)H_i(z^{-1}) + H_i(-z)H_i(-z^{-1}) = 2, \quad (4.5)$$

which means the product filter $P_i(z) = H_i(z)H_i(z^{-1})$ must satisfy

$$p_i(2n) = \begin{cases} 1 & (n = 0) \\ 0 & (n > 0) \end{cases}, \quad (4.6)$$

where $p_i(n) = p_i(-n)$ is the impulse response of $P_i(z)$.

To achieve the approximate group delay of $\frac{1}{4}$, Kingsbury had proposed a method in [22] for designing a linear-phase lowpass filter $H_{L2}(z)$ of degree $2N + 1$.

$$\begin{aligned} H_{L2}(z) &= H_1(z^2) + z^{-1}H_1(z^{-2}) \\ &= H_1(z^2) + z^{-1}H_2(z^2) \end{aligned}, \quad (4.7)$$

which has a group delay of $\frac{1}{2}$. By subsampling $H_{L2}(z)$, the scaling lowpass filter $H_1(z)$ can be obtained with half of its delay and twice its bandwidth.

To avoid unwanted passbands appear from subsampled filters, it is rea-

sonable to ensure that the stopband of $H_1(z)$ reduces as much energy as possible. It is sufficient to consider the combined frequency responses between $H_1(z)$ and $H_1(z^2)$, which is

$$H_1(z)H_1(z^2)|_{z=e^{j\omega}} = H_1(e^{j\omega})H_1(e^{j2\omega}). \quad (4.8)$$

Assuming the stopband cutoff frequency of $H_1(z)$ is ω_s , then the transition band and passband of $H_1(z^2)$ should extend from $\pi - \frac{\omega_s}{2}$ to π . Therefore, to avoid the overlapping from $H_1(z^2)$,

$$\omega_s \leq \pi - \frac{\omega_s}{2} \quad \Rightarrow \quad \omega_s \leq \frac{2\pi}{3}. \quad (4.9)$$

Thus, the Q-shift filter can be designed from $H_{L2}(z)$ of degree $2N + 1$ with zero amplitude for the stopband, i.e., $\frac{\pi}{3} \leq \omega_s \leq \pi$.

4.3 DTCWTs with Arbitrary Center of Symmetry

The Q-shift filters can construct the symmetric wavelet bases with the fixed center of symmetry. To obtain the wavelet functions with arbitrary center of symmetry, we propose a new design method of scaling lowpass filters with arbitrarily specified flat group delay responses at $\omega = 0$, which satisfy the half-sample delay condition.

4.3.1 Approximation of Flat Group Delay

To obtain symmetric wavelet bases, the desired linear phase response $\theta_i^d(\omega)$ of $H_i(z)$ is

$$\theta_i^d(\omega) = -\tau_i\omega. \quad (4.10)$$

From the half-sample delay condition in Eq.(2.29),

$$\tau_2 = \tau_1 + 2M + \frac{1}{2}. \quad (4.11)$$

Therefore, the scaling functions have the arbitrary center of symmetry since the group delay τ_1 can be arbitrarily specified.

We now consider the flatness condition of group delay response. Many criteria can be used to approximate the group delay, e.g., the maximally flat, weighted least square, equiripple approximation, and so on. To obtain a number of vanishing moments on scaling functions [1], [12], we use the flat approximation in this dissertation. From Eq.(4.2), the phase response of $H_i(z)$ is given by

$$\theta_i(\omega) = -\tan^{-1} \frac{\sum_{n=0}^N h_i(n) \sin(n\omega)}{\sum_{n=0}^N h_i(n) \cos(n\omega)}. \quad (4.12)$$

Thus, the difference $\theta_i^e(\omega)$ between $\theta_i(\omega)$ and $\theta_i^d(\omega)$ is

$$\theta_i^e(\omega) = \theta_i(\omega) - \theta_i^d(\omega) = \tan^{-1} \frac{N_i(\omega)}{D_i(\omega)}, \quad (4.13)$$

where

$$\begin{cases} N_i(\omega) = \sum_{n=0}^N h_i(n) \sin\{(\tau_i - n)\omega\} \\ D_i(\omega) = \sum_{n=0}^N h_i(n) \cos\{(\tau_i - n)\omega\} \end{cases}. \quad (4.14)$$

The group delay response is required to be flat with the specified degree of flatness at $\omega = 0$;

$$\begin{cases} \tau_i(0) = \tau_i \\ \left. \frac{\partial^{2r} \tau_i(\omega)}{\partial \omega^{2r}} \right|_{\omega=0} = 0 \quad (r = 1, 2, \dots, L-1) \end{cases}, \quad (4.15)$$

where $L (> 0)$ is a parameter that controls the degree of flatness. Since $\tau_i(\omega) = -\frac{\partial \theta_i(\omega)}{\partial \omega}$, Eq.(4.15) is equivalent to

$$\left. \frac{\partial^{2r+1} \theta_e^i(\omega)}{\partial \omega^{2r+1}} \right|_{\omega=0} = 0 \quad (r = 0, 1, \dots, L-1). \quad (4.16)$$

By using Eq.(4.13), Eq.(4.16) can be reduced to

$$\left. \frac{\partial^{2r+1} N_i(\omega)}{\partial \omega^{2r+1}} \right|_{\omega=0} = 0 \quad (r = 0, 1, \dots, L-1). \quad (4.17)$$

We substitute $N_i(\omega)$ in Eq.(4.14) into Eq.(4.17), then derive a set of linear equations;

$$\sum_{n=0}^N (\tau_i - n)^{2r+1} h_i(n) = 0 \quad (r = 0, 1, \dots, L-1). \quad (4.18)$$

It is clear that there are L equations in Eq.(4.18) with respect to $(N+1)$ unknown coefficients $h_i(n)$.

4.3.2 Orthonormality and Vanishing Moments

In addition to the group delay condition, the wavelets are also required to have the specified number of vanishing moments and satisfy the condition of orthogonality. Thus, to obtain K zeros at $z = -1$, Eq.(4.4) is equivalent to

$$\left. \frac{\partial^r H_i(e^{j\omega})}{\partial \omega^r} \right|_{\omega=\pi} = 0 \quad (r = 0, 1, \dots, K - 1). \quad (4.19)$$

By substituting $H_i(e^{j\omega})$ in Eq.(4.2) into Eq.(4.19), we obtain a set of linear equations as follow;

$$\sum_{n=0}^N (-1)^n n^r h_i(n) = 0 \quad (r = 0, 1, \dots, K - 1), \quad (4.20)$$

where there are K equations with respect to $h_i(n)$.

Moreover, we rewrite the orthonormality condition in Eq.(4.6) as

$$\sum_{k=0}^{N-2n} h_i(2n+k)h_i(k) = \begin{cases} 1 & (n = 0) \\ 0 & (n > 0) \end{cases}, \quad (4.21)$$

where there exist $(N + 1)/2$ equations with respect to $h_i(n)$. If $K + L = (N + 1)/2$, the number of equations becomes $K + L + (N + 1)/2 = N + 1$ in Eqs.(4.18), (4.20) and (4.21) with respect to $(N + 1)$ unknown filter coefficients $h_i(n)$. By solving Eqs.(4.18), (4.20) and (4.21), the scaling lowpass filters $h_i(n)$ can be obtained for $i = 1, 2$.

It is seen that Eq.(4.21) is a set of quadratic constraints on the filter coefficients $h_i(n)$. Generally, it is difficult to solve this nonlinear problem, particularly if the filter is of higher degree, although some nonlinear

optimization tools are available, such as Matlab optimization toolbox.

4.3.3 Linearization of the Design Problem

In the following, we first linearize the nonlinear equation in Eq.(4.21), and then use an iterative procedure to obtain a set of filter coefficients, as proposed in [22].

Let $h_i^{(l)}(n)$ be the filter coefficients at l th iteration, which is given by

$$h_i^{(l)}(n) = h_i^{(l-1)}(n) + \Delta h_i^{(l)}(n). \quad (4.22)$$

Then, Eq.(4.21) becomes

$$\begin{aligned} \sum_{k=0}^{N-2n} [h_i^{(l-1)}(k+2n)h_i^{(l-1)}(k) + h_i^{(l-1)}(k+2n)\Delta h_i^{(l)}(k) \\ + h_i^{(l-1)}(k)\Delta h_i^{(l)}(k+2n) + \Delta h_i^{(l)}(k)\Delta h_i^{(l)}(k+2n)] = \delta(n). \end{aligned} \quad (4.23)$$

Assuming $\Delta h_i^{(l)}(k)$ becomes small enough as l increases, then the term $\Delta h_i^{(l)}(k)\Delta h_i^{(l)}(k+2n)$ can be neglected. Therefore, we have

$$\begin{aligned} \sum_{k=0}^N [h_i^{(l-1)}(k+2n) + h_i^{(l-1)}(k+2n)]\Delta h_i^{(l)}(k) \\ = \delta(n) - \sum_{k=0}^{N-2n} h_i^{(l-1)}(k+2n)h_i^{(l-1)}(k), \end{aligned} \quad (4.24)$$

where $h_i^{(l-1)}(k) = 0$ for $k < 0$ and $k > N$. Similarly, Eq.(4.18) and Eq.(4.20) become

$$\sum_{n=0}^N (\tau_i - n)^{2r+1} \Delta h_i^{(l)}(n) = \sum_{n=0}^N (n - \tau_i)^{2r+1} h_i^{(l-1)}(n). \quad (4.25)$$

$$\sum_{n=0}^N (-1)^n n^r \Delta h_i^{(l)}(n) = \sum_{n=0}^N (-1)^{n+1} n^r h_i^{(l-1)}(n), \quad (4.26)$$

Therefore, we can obtain $\Delta h_i^{(l)}(n)$ by solving the set of linear equations in Eq.(4.24), Eq.(4.25) and Eq.(4.26), if coefficients $h_i^{(l-1)}(n)$ have already known. The filter coefficients are subsequently updated by $\Delta h_i^{(l)}(n)$ in Eq.(4.22).

To converge to the optimal solution, a set of good initial coefficients $h_i^{(0)}(n)$ are needed. It is known that $P_i(z) = H_i(z)H_i(z^{-1})$ is a linear phase half band filter. We firstly design $P_i(z)$ as the maximally flat half-band filter, and choose the magnitude responses of $H_i(z)$ as $|H_i(e^{j\omega})| = |P_i(e^{j\omega})|^{\frac{1}{2}}$. Then we set its phase response as τ_i , that is

$$H_i(e^{j\omega}) = |P_i(e^{j\omega})|^{\frac{1}{2}} e^{-j\tau_i\omega}. \quad (4.27)$$

Therefore, a set of initial coefficients $h_i^{(0)}(n)$ are computed by taking $N+1$ point inverse discrete Fourier transform (IDFT).

4.3.4 Design Algorithm

Design Algorithm

Begin

- 1) Read N , K , L and τ_i .
- 2) Set $l = 0$.
- 3) Obtain the filter coefficients $h_i^{(l)}(n)$ by taking $N + 1$ point IDFT of $H_i(e^{j\omega})$ in Eq.(4.27).

Repeat

- 3) $l = l + 1$;
- 4) Solve Eqs.(4.24), Eq.(4.25) and Eq.(4.26) to obtain a set of coefficients $\Delta h_i^{(l)}(n)$.
- 5) Update the filter coefficients with $h_i^{(l)}(n) = h_i^{(l-1)}(n) + \Delta h_i^{(l)}(n)$.

Until

Satisfy the following condition for a prescribed small constant ϵ (e.g., $\epsilon = 10^{-12}$);

$$\sum_{n=0}^N |\Delta h_i^{(l)}(n)| < \epsilon.$$

End.

4.3.5 Design Examples

In this section, two examples will be given to demonstrate the proposed algorithm. First of all, we consider a class of DTCWTs with different degree of flatness and number of vanishing moments. Next, we consider a class of DTCWTs with different center of symmetry.

Example 4.1

We consider a class of DTCWTs with $N = 15$, $K = \{3, 5, 7\}$ and $L = (N + 1)/2 - K = \{5, 3, 1\}$ with group delay $\{\tau_1 = 8.5, \tau_2 = 9.0\}$. We have designed these three scaling lowpass filters, and the resulting magnitude responses of $H_i(z)$ are shown in Fig.4.1, Fig.4.2, respectively. With the increasing of the number of vanishing moments K , the transition band becomes sharp. The group delay responses become flat as an increasing L , as shown in Fig.4.3. It is clear that the half-sample delay condition are approximately achieved. In addition, the magnitude responses of $E(\omega)$ has been shown in Fig.4.4. It is maximum when $\{K = 5, L = 3\}$, while it is minimum when $\{K = 3, L = 5\}$. Since two scaling lowpass filters are designed independently, it is difficult to minimize the error function. Moreover, the scaling function $\phi_i(t)$ and wavelet functions $\psi_i(t)$ are shown in Fig.4.5. Furthermore, the spectrum of the wavelet functions $\Psi_i(\omega)$ and the spectrum of the complex wavelet $\Psi_c(\omega)$ are given in Fig.4.6 and Fig.4.7, respectively. It is obvious that the negative spectrum is maximum when $K = 5, L = 3$ while it is minimum when $K = 3, L = 5$. Finally, the analyticity measures of E_∞ and E_2 are summarized in Table 4.1.

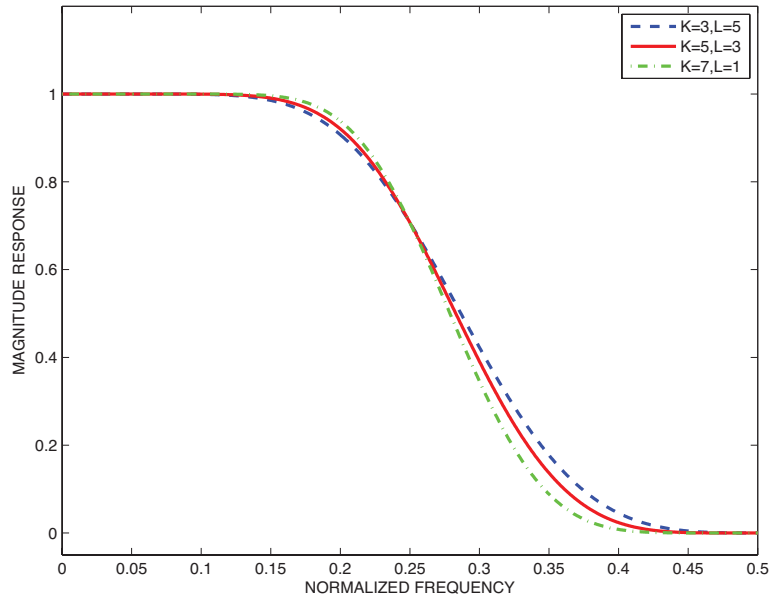


Fig.4.1 Magnitude responses of scaling lowpass filters $H_1(z)$.

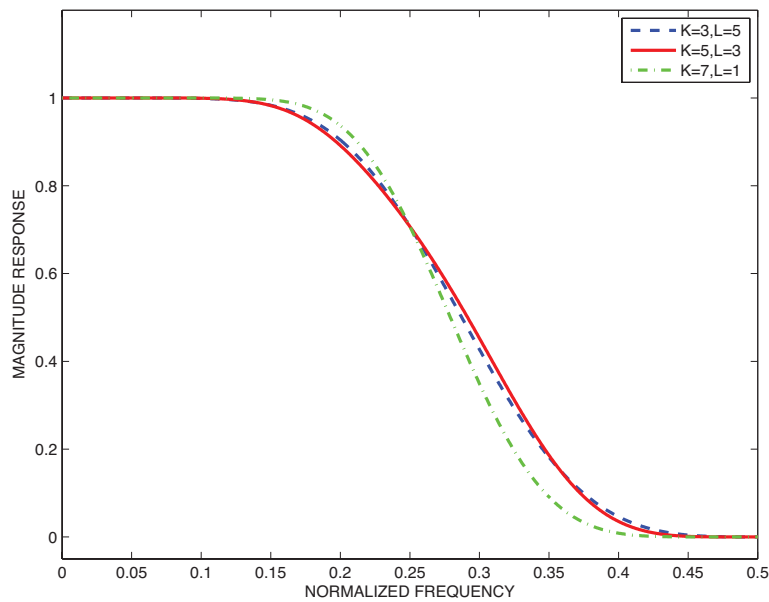
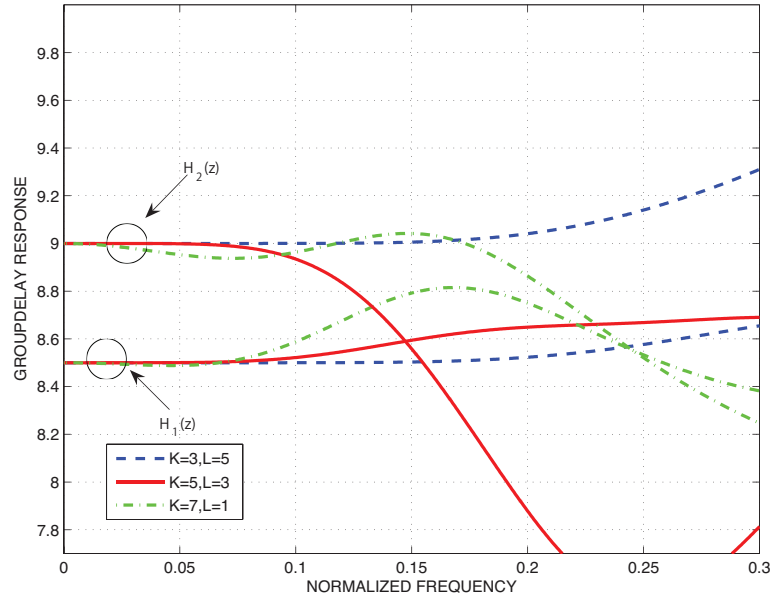
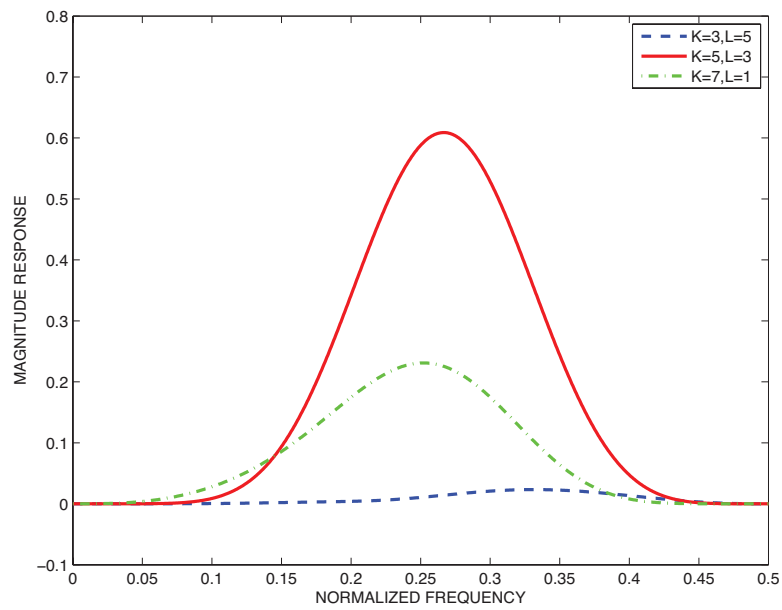
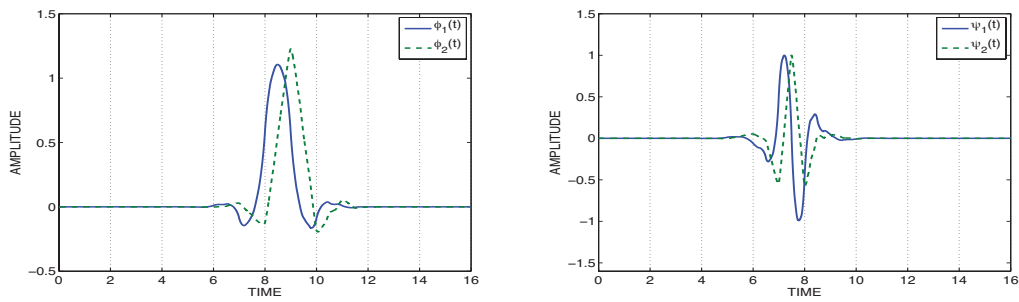
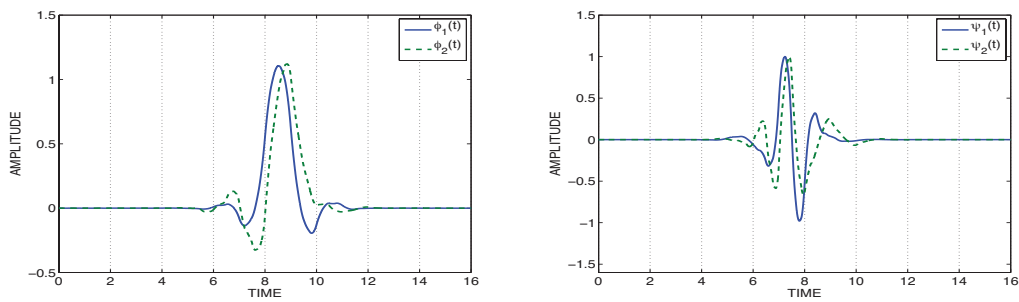


Fig.4.2 Magnitude responses of scaling lowpass filters $H_2(z)$.

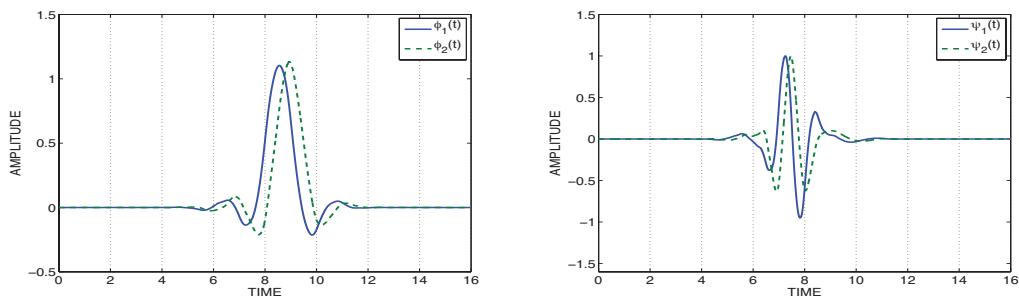
Fig.4.3 Group delay responses of scaling lowpass filters $H_i(z)$.Fig.4.4 Magnitude responses of $E(\omega)$.



(a) $K = 3, L = 5$.



(b) $K = 5, L = 3$.



(c) $K = 7, L = 1$.

Fig.4.5 Scaling and wavelet functions $\phi_i(t), \psi_i(t)$.

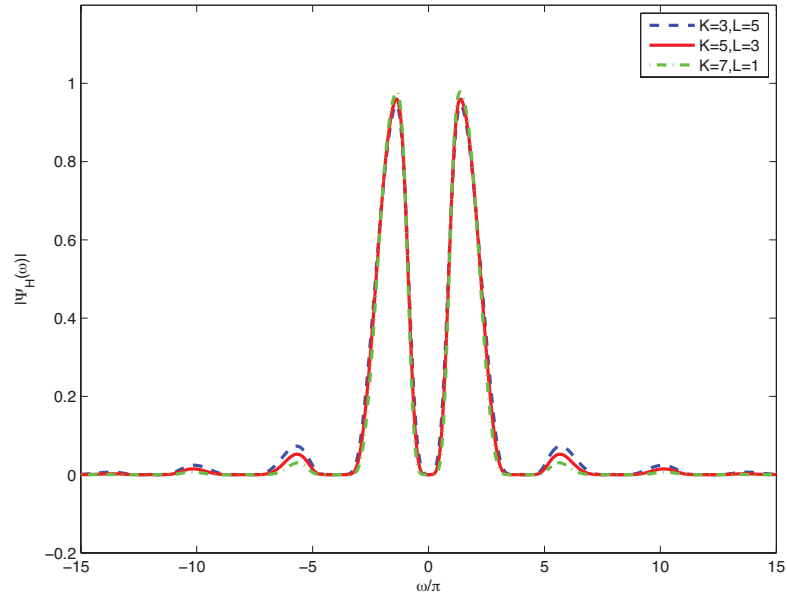
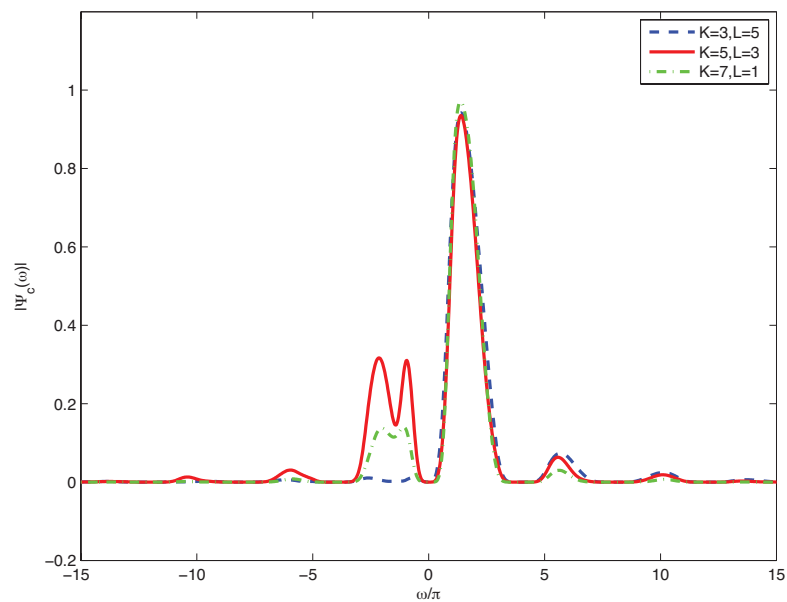
Fig.4.6 Magnitude responses of $\Psi_i(\omega)$.Fig.4.7 Magnitude responses of $\Psi_c(\omega)$.

TABLE 4.1 Analyticity Measures E_∞ and E_2 .

N	K	L	$E_\infty(\%)$	$E_2(\%)$
15	3	5	1.221	1.334
15	5	3	33.882	39.031
15	7	1	14.484	17.021

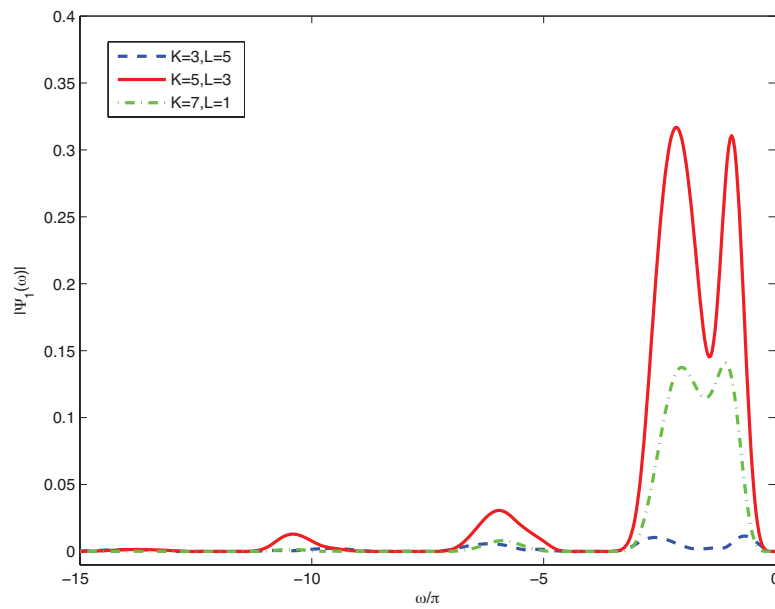


Fig.4.8 Magnitude responses of $\Psi_c(\omega)$.

Example 4.2

We consider a class of DTCWTs with $N = 17$, $K = 4$, $L = 5$. Since the group delay can be arbitrarily specified, the group delay τ_i is selected as $\tau_1 = \{7.6, 8.3, 9.0\}$. From the half-sample delay condition, $\tau_2 = \{8.1, 8.8, 9.5\}$. The magnitude responses of $H_i(z)$ are shown in Fig.4.9 and Fig.4.10 respectively, which are almost the same. Next, the group delay responses are displayed in Fig.4.11. From Fig.4.11, it is clear that the half-sample delay has been approximately achieved and the scaling lowpass filters have flat group delay response at $\omega = 0$. The magnitude responses of $E(\omega)$ are shown in Fig.4.12. It is obvious in Fig.4.12 that choosing different τ_i can influence the error function $E(\omega)$. It is minimum when $\{\tau_1 = 8.3, \tau_2 = 8.8\}$. Moreover, the scaling functions $\phi_i(t)$ and wavelet functions $\psi_i(t)$ are shown in Fig.4.13. It is obvious that the scaling functions have different center of symmetry, while the center of symmetry of wavelet functions remain unchanged. Furthermore, the spectrums of wavelet function $\Psi_i(\omega)$ and complex wavelet $\Psi_c(\omega)$ are given in Fig.4.14, Fig.4.15, respectively. When $\{\tau_1 = 8.3, \tau_2 = 8.8\}$, the negative spectrum of $\Psi_c(\omega)$ is minimum, as shown in Fig.4.16. Finally, we summarize the analyticity measures of E_∞ and E_2 in Table 4.2.

TABLE 4.2 Analyticity Measures E_∞ and E_2 .

N	K	L	τ_1	$E_\infty(\%)$	$E_2(\%)$
15	4	5	7.6	6.829	7.264
15	4	5	8.3	1.275	1.322
15	4	5	9.0	9.486	10.004

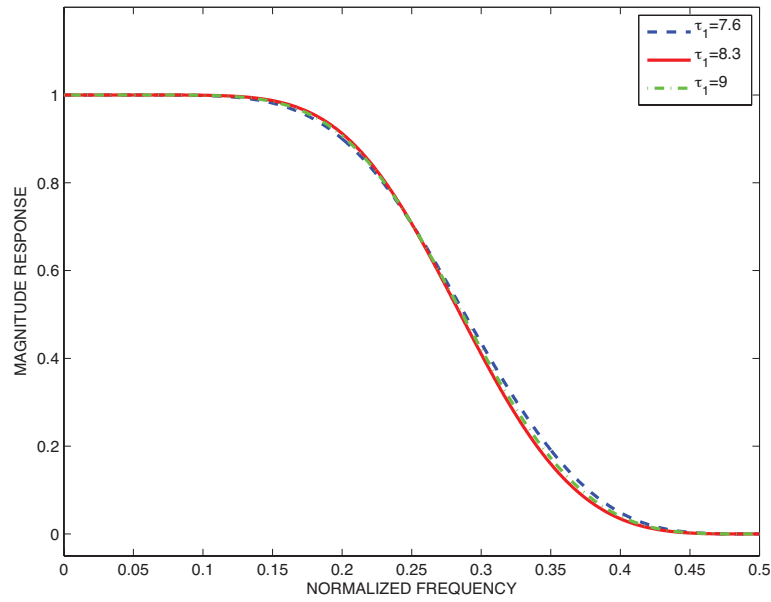


Fig.4.9 Magnitude responses of scaling lowpass filters $H_1(z)$.

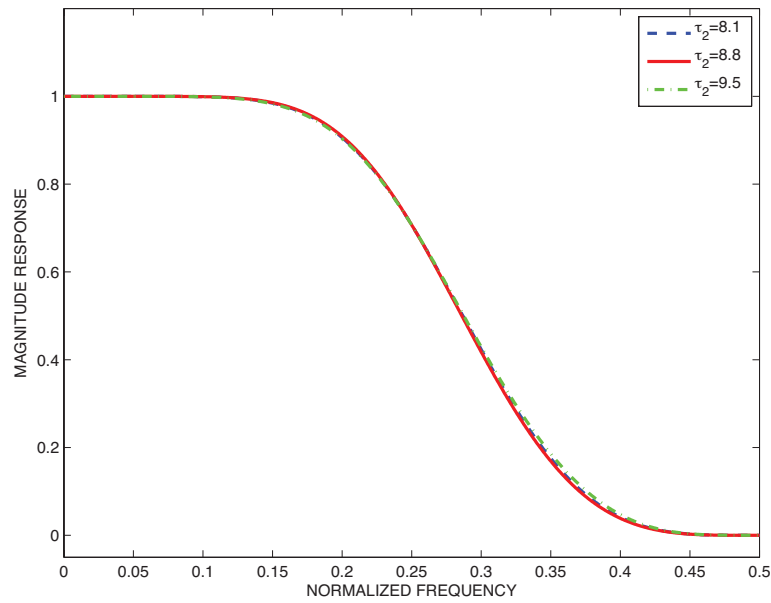


Fig.4.10 Magnitude responses of scaling lowpass filters $H_2(z)$.

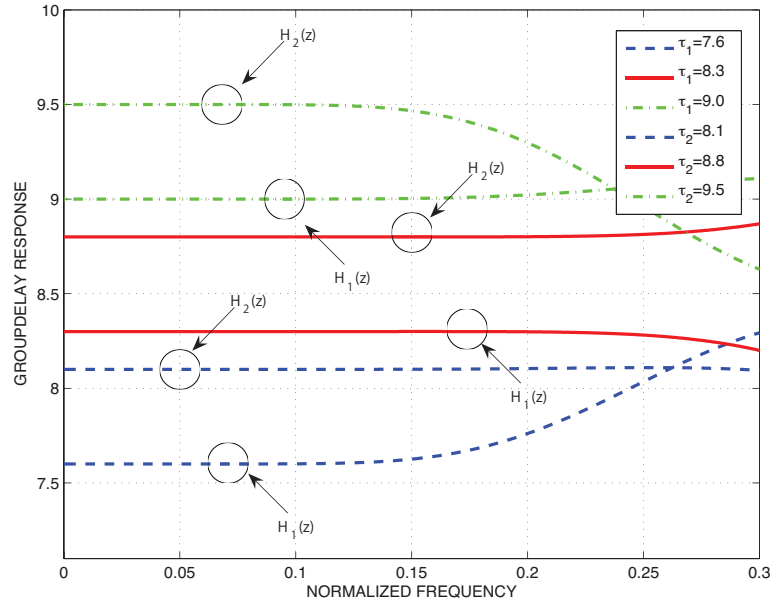


Fig.4.11 Group delay responses of scaling lowpass filters $H_i(z)$.

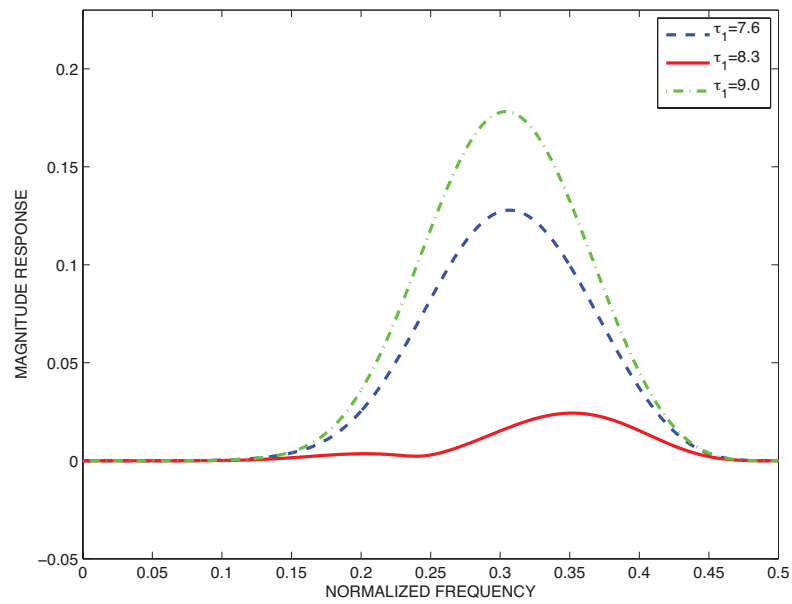
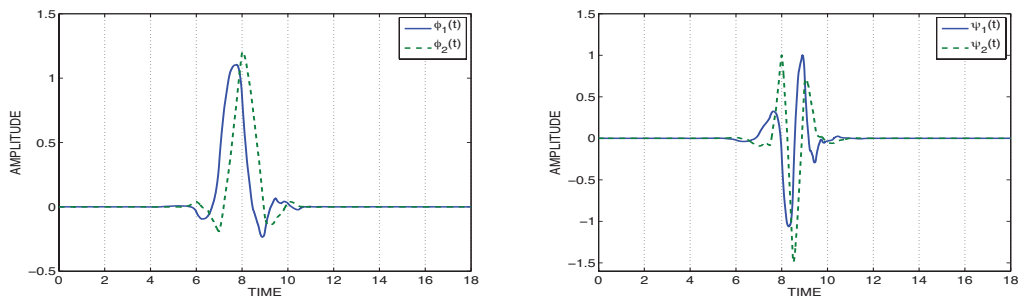
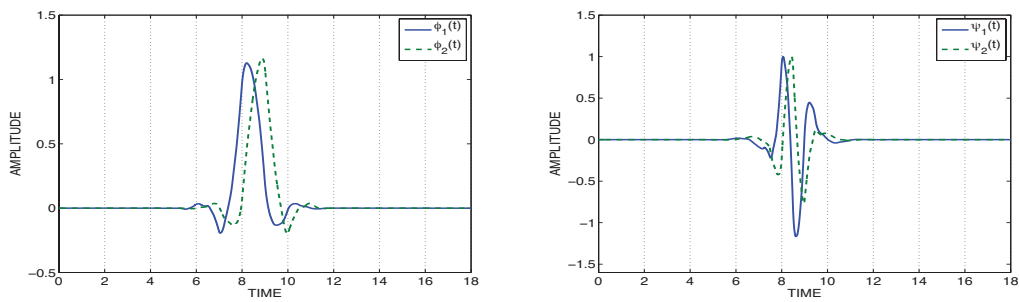


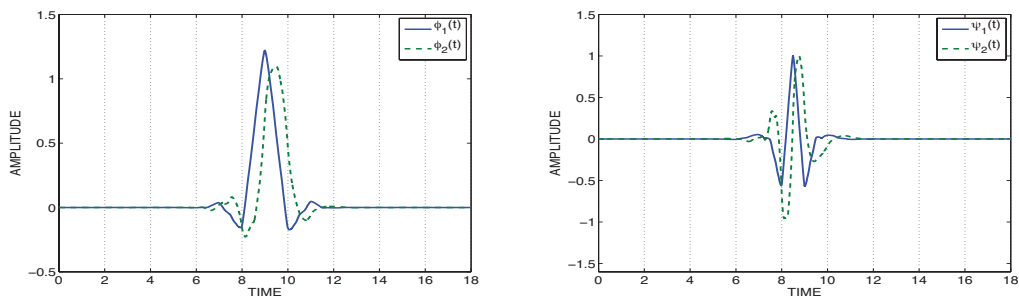
Fig.4.12 Magnitude responses of $E(\omega)$.



(a) $\tau_1 = 7.6, \tau_2 = 8.1$.

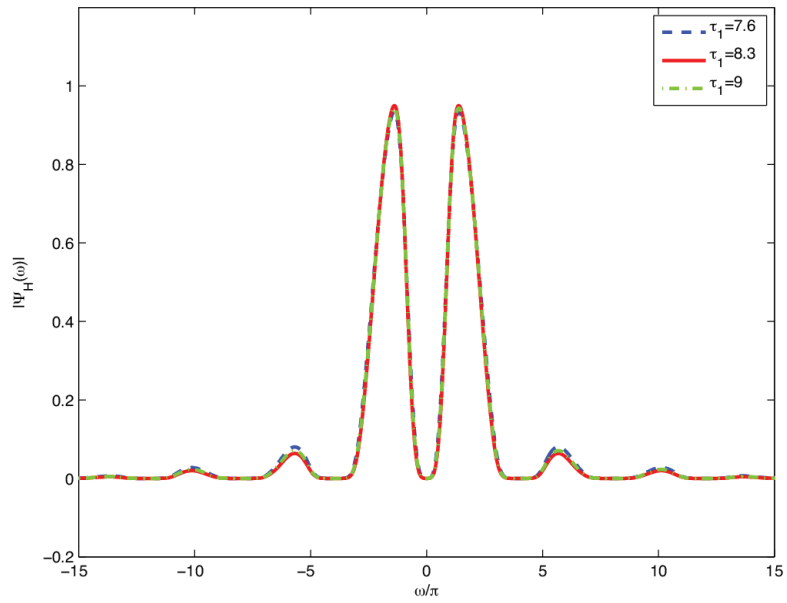
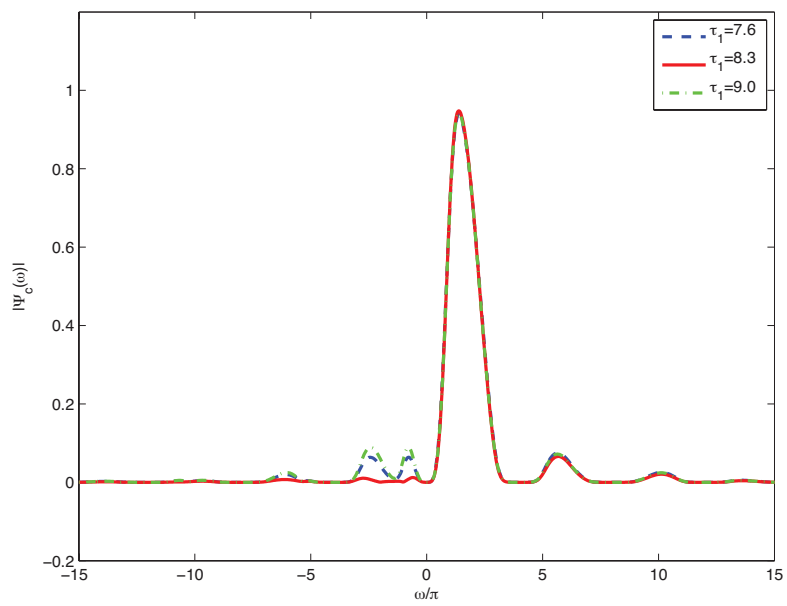


(b) $\tau_1 = 8.3, \tau_2 = 8.8$.



(c) $\tau_1 = 9.0, \tau_2 = 9.5$.

Fig.4.13 Scaling and wavelet functions $\phi_i(t), \psi_i(t)$.

Fig.4.14 Magnitude responses of $\Psi_i(\omega)$.Fig.4.15 Magnitude responses of $\Psi_c(\omega)$.

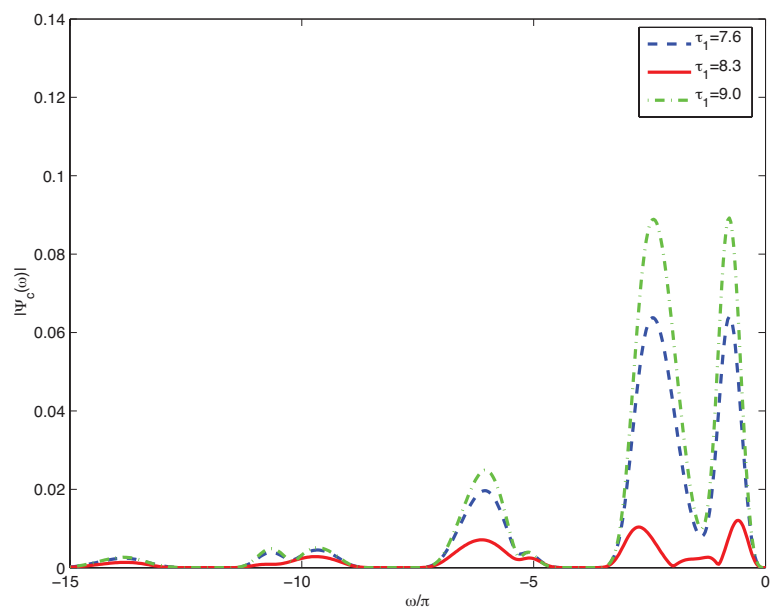


Fig.4.16 Magnitude responses of $\Psi_c(\omega)$.

4.4 DTCWTs with Improved Analyticity

In the previous section, the scaling lowpass filters with the specified flat group delay have been designed. However, the scaling lowpass filters are designed independently, so that the difference of frequency responses between two scaling lowpass filters has not been taken into consideration, which results in poor analyticity of complex wavelet. In the following, we design two scaling lowpass filters simultaneously to improve the analyticity of complex wavelet. Furthermore, the Remez exchange algorithm will be applied to obtain an equiripple behaviour of the error function. It will be shown that the resulting complex wavelets are orthogonal and almost symmetric, and have the improved analyticity.

4.4.1 Initial Solution

To minimize the difference of frequency responses between two scaling lowpass filters, we consider the case of $L + K < (N + 1)/2$. The remaining degree of freedom is $I = (N + 1)/2 - K - L$. We will use the remaining degree of freedom to improve the analyticity of complex wavelets. Let $\tilde{\omega}_k (0 < \tilde{\omega}_0 < \tilde{\omega}_1 < \dots < \tilde{\omega}_{I-1} < \pi)$ be the frequency points at which makes the error between two scaling lowpass filters equal to zero;

$$E(\tilde{\omega}_k) = H_2(e^{j\tilde{\omega}_k}) - H_1(e^{j\tilde{\omega}_k})e^{-j(2M+\frac{1}{2})\tilde{\omega}_k} = 0. \quad (4.28)$$

Eq.(4.28) is separated into real and imaginary parts to obtain a set of linear equations as follows;

$$\left\{ \begin{array}{l} \sum_{n=0}^N \{h_2(n) \cos(n\tilde{\omega}_k) - h_1(n) \cos[(n + 2M + \frac{1}{2})\tilde{\omega}_k]\} = 0 \\ \sum_{n=0}^N \{h_2(n) \sin(n\tilde{\omega}_k) - h_1(n) \sin[(n + 2M + \frac{1}{2})\tilde{\omega}_k]\} = 0 \end{array} \right., \quad (4.29)$$

for $k = 0, 1, \dots, I - 1$. Similarly, Eq.(4.18), Eq.(4.20) and Eq.(4.21) become

$$\left\{ \begin{array}{l} \sum_{n=0}^N (\tau_1 - n)^{2r+1} h_1(n) = 0 \\ \sum_{n=0}^N (\tau_2 - n)^{2r+1} h_2(n) = 0 \end{array} \right. \quad (r = 0, 1, \dots, L - 1), \quad (4.30)$$

$$\left\{ \begin{array}{l} \sum_{n=0}^N (-1)^n n^r h_1(n) = 0 \\ \sum_{n=0}^N (-1)^n n^r h_2(n) = 0 \end{array} \right. \quad (r = 0, 1, \dots, K - 1), \quad (4.31)$$

$$\left\{ \begin{array}{l} \sum_{k=0}^{N-2n} h_1(2n+k) h_1(k) = \delta(n) \\ \sum_{k=0}^{N-2n} h_2(2n+k) h_2(k) = \delta(n) \end{array} \right. . \quad (4.32)$$

There are totally $2K + 2L + N + 1 + 2I = 2(N + 1)$ equations in Eqs.(4.29), (4.30), (4.31) and (4.32) with respect to $2N + 2$ unknown filter coefficients $h_1(n)$, $h_2(n)$. Thus, we can obtain the filter coefficients $h_1(n)$ and $h_2(n)$

simultaneously by solving this set of equations.

4.4.2 Formulation using Remez exchange algorithm

In the previous section, we use the remaining degree of freedom to let the frequency points equal to zero. However, the frequency points ω_k are equally spaced in $[0, \pi]$. In the following, we apply the Remez exchange algorithm to obtain an equiripple magnitude behaviours of the error function $E(\omega)$ in order to improve the analyticity of complex wavelet.

It is obvious that if the scaling lowpass filters have no remaining degree of freedom ($I = 0$), the error function $E(\omega)$ has only one peak point, while there are $I + 1$ peak points if $I > 0$. We want to make it to be equiripple when $I > 0$. Therefore, we apply Remez exchange algorithm to obtain the equiripple behavior of $E(\omega)$. Let $\omega_i (0 < \omega_0 < \omega_1 < \dots < \omega_I < \pi)$ be the frequencies of the peak points of $E(\omega)$, which are computed by using the filter coefficients obtained in the preceding section. Then we formulate the error function $E(\omega)$ as follows;

$$E(\omega_i) = H_2(e^{j\omega_i}) - H_1(e^{j\omega_i})e^{-j(2M+\frac{1}{2})\omega_i} = \delta e^{j(\theta_e(\omega_i)+\Delta\theta)}, \quad (4.33)$$

where δ is a magnitude error and $\Delta\theta$ is a phase error. $\theta_e(\omega_i)$ is the phase of $E(\omega_i)$ computed by using the filter coefficients in the preceding section. Since $\delta e^{j\Delta\theta} = \delta \cos(\Delta\theta) + j\delta \sin(\Delta\theta) = \delta_c + j\delta_s$, Eq.(4.33) becomes

$$H_2(e^{j\omega_i}) - H_1(e^{j\omega_i})e^{-j(2M+\frac{1}{2})\omega_i} - (\delta_c + j\delta_s)e^{j\theta_e(\omega_i)} = 0. \quad (4.34)$$

Therefore, Eq.(4.34) is separated into real and imaginary parts as,

$$\left\{ \begin{array}{l} \sum_{n=0}^N \{h_2(n) \cos(n\omega_i) - h_1(n) \cos[(n + 2M + \frac{1}{2})\omega_i]\} \\ \qquad \qquad \qquad -\delta_c \cos(\theta_e(\omega_i)) + \delta_s \sin(\theta_e(\omega_i)) = 0 \\ \sum_{n=0}^N \{h_2(n) \sin(n\omega_i) - h_1(n) \sin[(n + 2M + \frac{1}{2})\omega_i]\} \\ \qquad \qquad \qquad -\delta_c \sin(\theta_e(\omega_i)) - \delta_s \cos(\theta_e(\omega_i)) = 0 \end{array} \right. , \quad (4.35)$$

for $i = 0, 1, \dots, I$.

It should be noted that Eqs.(4.30), (4.31), (4.32) and (4.35) have $2K + 2L + N + 1 + 2(I + 1) = 2N + 4$ equations with respect to $2N + 2$ filter coefficients $h_i(n)$ plus δ_c and δ_s . Therefore, we can solve this set of equations to obtain a set of coefficients $h_1(n)$ and $h_2(n)$, respectively. Furthermore, we make use of an iterative procedure to obtain the equiripple magnitude response of $E(\omega)$. Thus, the optimal filter coefficients can be easily obtained through a few iterations. The design algorithm is given in the following.

4.4.3 Design Algorithm

Design Algorithm

Begin

1. Read N, K, L and τ_1, τ_2 .
2. Select initial frequency points $\tilde{\omega}_k$ ($0 < \tilde{\omega}_0 < \tilde{\omega}_1 < \dots < \tilde{\omega}_{I-1} < \pi$) equally spaced in $[0, \pi]$.
3. Solve Eqs.(4.29), (4.30), (4.31) and (4.32) to obtain a set of initial coefficients $h_1(n), h_2(n)$.
4. Compute $E(\omega)$ to find the peak frequency points Ω_i ($0 < \Omega_0 < \Omega_1 < \dots < \Omega_I < \pi$).

Repeat

- 5) Set $\omega_i = \Omega_i$ ($i = 0, 1, \dots, I$).
- 6) Solve Eqs.(4.30), (4.31), (4.32) and (4.35) to obtain a set of filter coefficients $h_1(n), h_2(n)$.
- 7) Compute $E(\omega)$ to find the peak frequency points Ω_i ($0 < \Omega_0 < \Omega_1 < \dots < \Omega_I < \pi$).

Until

Satisfy the following condition for a prescribed small constant ϵ (e.g., $\epsilon = 10^{-12}$);

$$\sum_{i=0}^I |\omega_i - \Omega_i| < \epsilon$$

End.

4.4.4 Design Examples

In this section, several examples are presented to demonstrate the effectiveness of our proposed algorithm. In the first design example, we consider a class of DTCWTs with different flatness degree of group delay. In the second example, we consider a class of DTCWTs with different center of symmetry. Finally, we consider a class of DTCWTs and compare with the Q-shift filter designed by Kingsbury in [22] to show the priority of our proposed algorithm.

Example 4.3

We have used the proposed method to design $H_1(z)$ and $H_2(z)$ with $N = 15$, $K = 4$, $L = \{3, 2, 1\}$ and $\tau_1 = 9.0$, $\tau_2 = 9.5$. The remaining degree of freedom is $I = \{1, 2, 3\}$, respectively. The magnitude responses of scaling lowpass filters are given in Fig.4.17 and Fig.4.18, which are almost the same. Their group delay responses are shown in Fig.4.19, where the half-sample delay condition is approximately achieved. Moreover, the magnitude responses of $E(\omega)$ with different I are shown in Fig.4.20. It is clear that the equiripple magnitude responses of $E(\omega)$ have been obtained and the maximum error of $|E(\omega)|$ has been effectively minimized by applying the Remez exchange algorithm. In addition, the scaling functions $\phi_i(t)$ and wavelet functions are presented in Fig.4.21, which are almost the same. Furthermore, Fig.4.22 displays the wavelet spectrum $\Psi_i(\omega)$ and the complex wavelet spectrum $\Psi_c(\omega)$ are given in Fig.4.23. The negative spectrum of DTCWTs are shown in Fig.4.24. It is minimum when $I = 2$,

while it is maximum when $I = 1$, i.e., poor analyticity of DTCWT. Finally, the analyticity measures of E_∞ and E_2 are summarized in Table 4.3. It is obvious that the analyticity of complex wavelet has been improved by minimizing the magnitude responses of $E(\omega)$.

TABLE 4.3 Analyticity Measures E_∞ and E_2 .

N	K	L	I	$E_\infty(\%)$	$E_2(\%)$
15	4	3	1	1.146	1.360
15	4	2	2	0.513	0.578
15	4	1	3	0.638	0.665

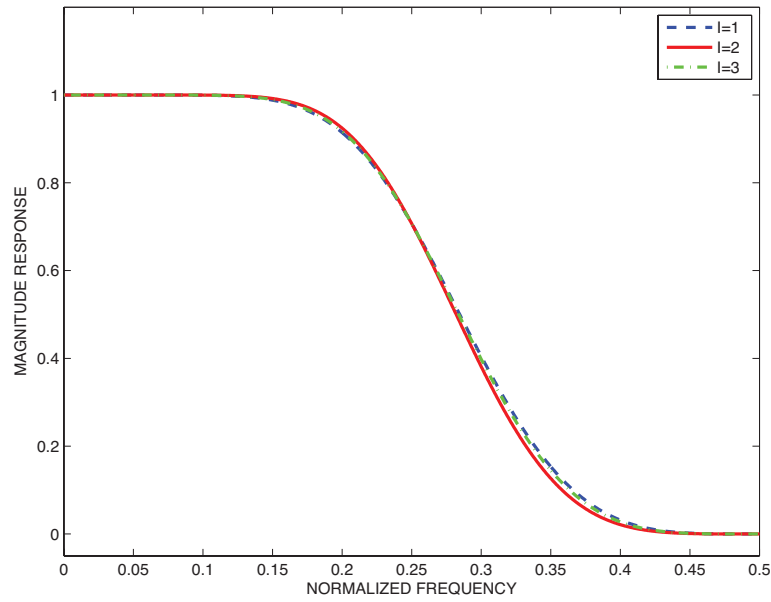


Fig.4.17 Magnitude responses of scaling lowpass filters $H_1(z)$.

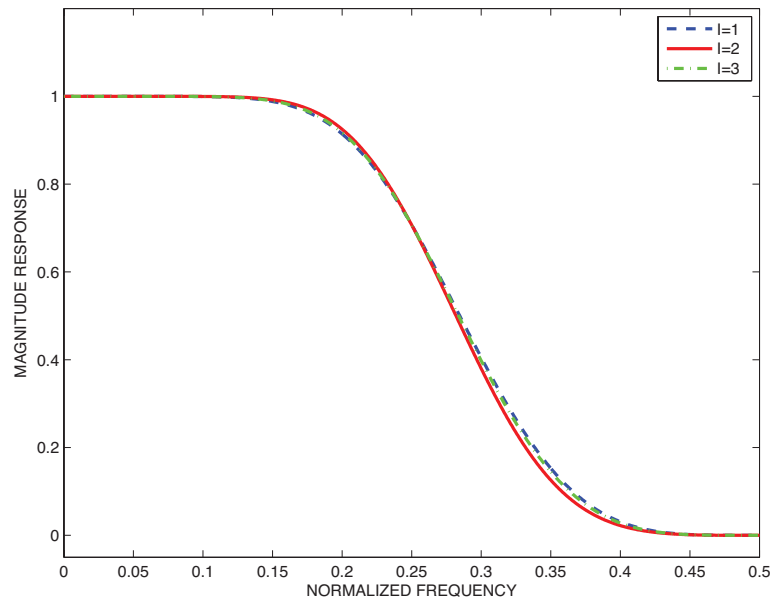


Fig.4.18 Magnitude responses of scaling lowpass filters $H_2(z)$.

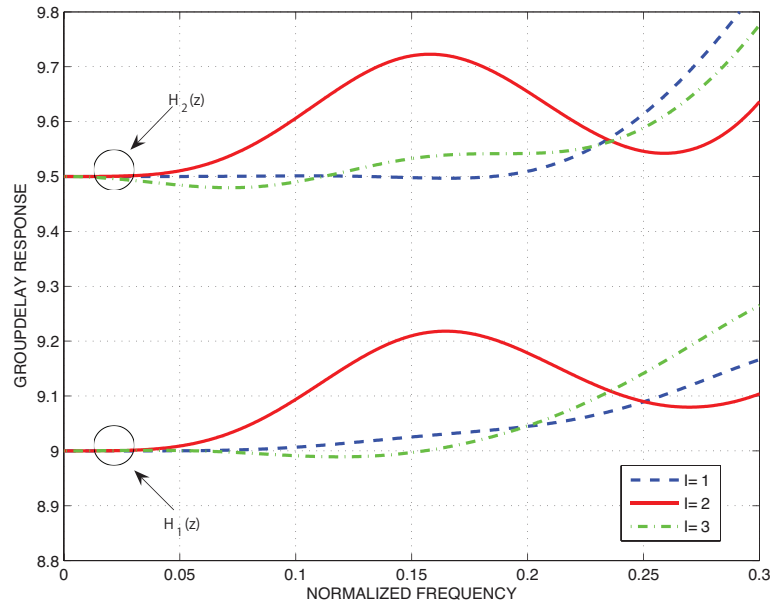


Fig.4.19 Group delay responses of scaling lowpass filters $H_i(z)$.

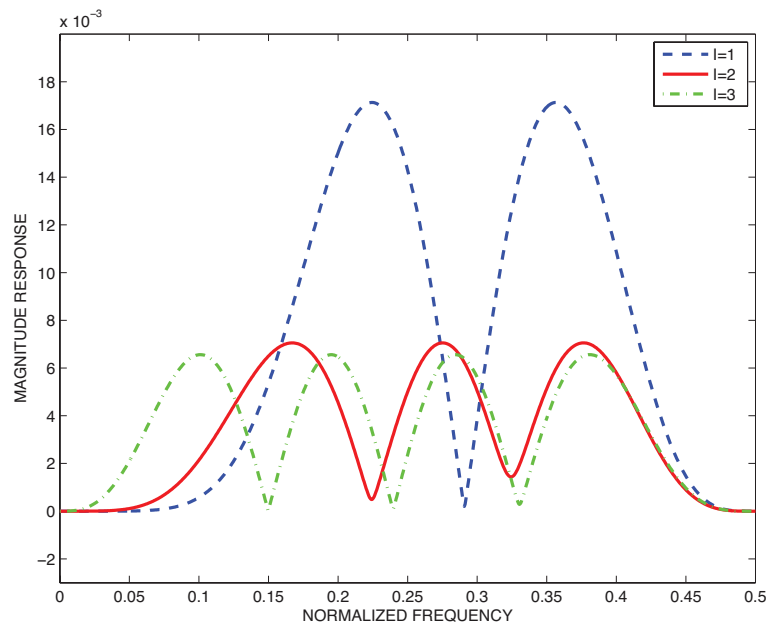
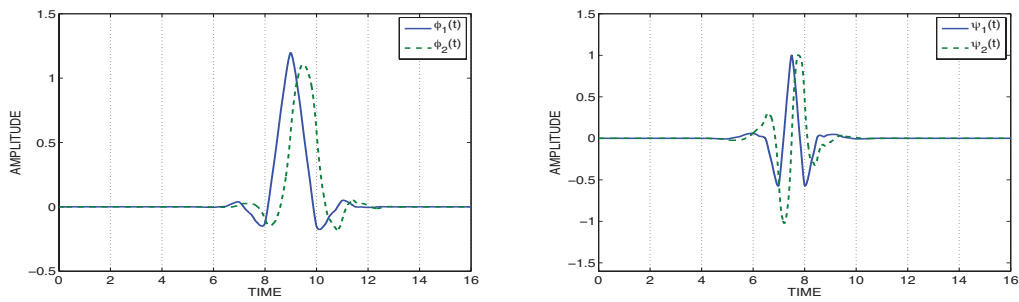
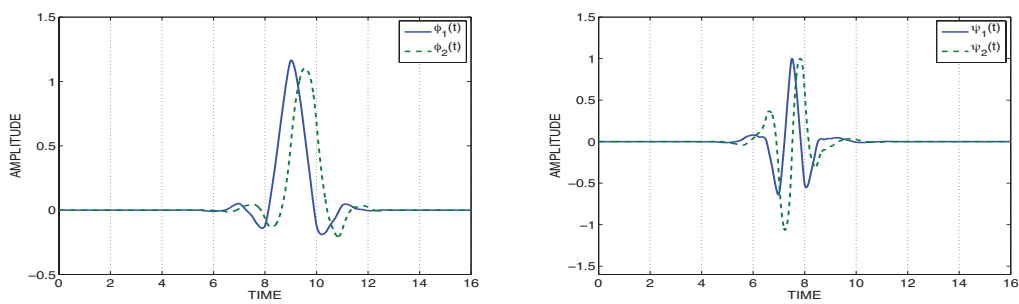


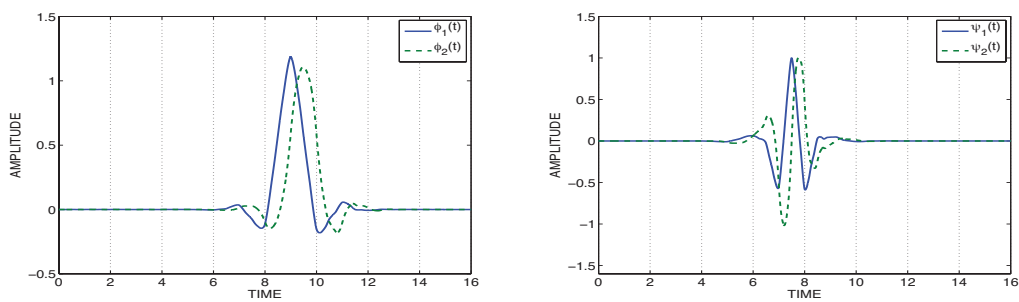
Fig.4.20 Magnitude responses of $E(\omega)$.



(a) $K = 4, L = 3, I = 1.$

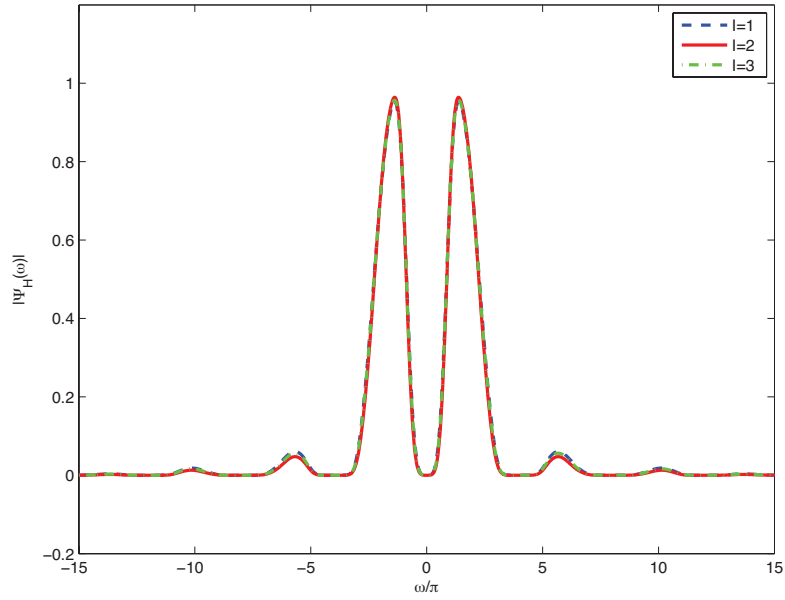
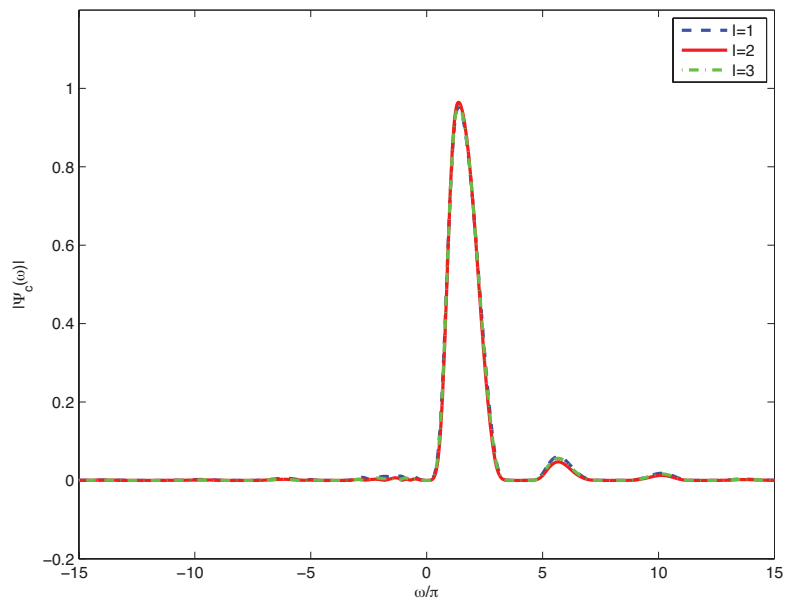


(b) $K = 4, L = 2, I = 2.$



(c) $K = 4, L = 1, I = 3.$

Fig.4.21 Scaling and wavelet functions $\phi_i(t), \psi_i(t).$

Fig.4.22 Magnitude responses of $\Psi_i(\omega)$.Fig.4.23 Magnitude responses of $\Psi_c(\omega)$.

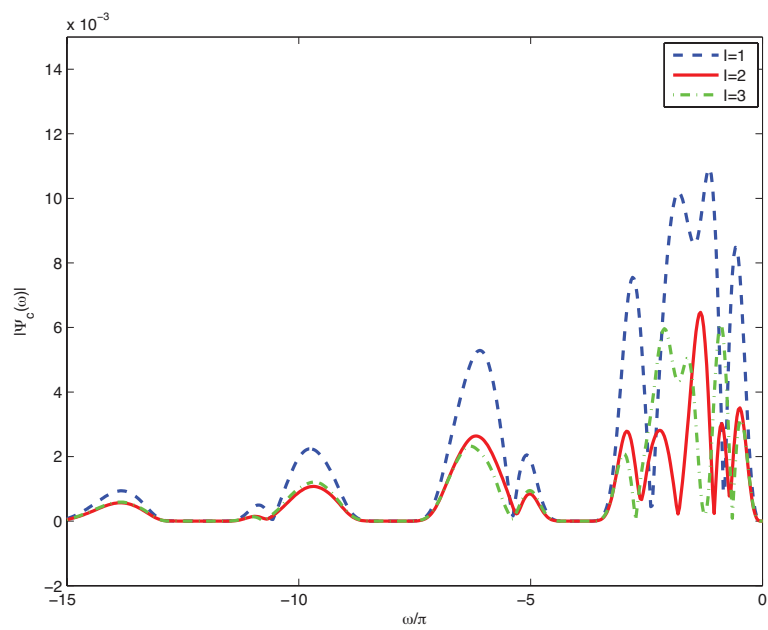


Fig.4.24 Magnitude responses of $\Psi_c(\omega)$.

Example 4.4

We consider a class of almost symmetric DTCWTs with $N = 21$, $K = 6$, $L = 3$ and $I = 2$. The group delay τ_1 is selected as $\tau_1 = 9.3$. From the half-sample delay condition, $\tau_2 = 9.8$ is selected. The magnitude responses of the scaling lowpass filters $H_i(z)$ are shown in Fig.4.25 and Fig.4.26. For comparison, the magnitude responses of other two filters with $\tau_1 = 8.1, \tau_2 = 8.6$ and $\tau_1 = 11.0, \tau_2 = 11.5$ are also shown in Fig.4.25 and Fig.4.26. The corresponding group delay responses are shown in Fig.4.27. Moreover, the magnitude responses of $E(\omega)$ are shown in Fig.4.28, and are equiripple. It is clear that the maximum error of $E(\omega)$ depends on the group delay τ_i also. In addition, the scaling functions $\phi_i(t)$ and wavelet functions $\psi_i(t)$ are given in Fig.4.29, respectively. In Fig.4.29, the scaling functions have different center of symmetry, while the center of symmetry of wavelet functions remain unchanged. However, the resulting scaling and wavelet functions have different behaviors depending on the group delays. Furthermore, the spectrum of wavelet $\Psi_i(\omega)$ and complex wavelets are given in Fig.4.30, Fig.4.31, and Fig.4.32, respectively. Finally, the analyticity measures of E_∞ and E_2 are summarized in Table 4.4.

TABLE 4.4 Analyticity Measures E_∞ and E_2 .

N	K	L	I	τ_1	$E_\infty(\%)$	$E_2(\%)$
21	6	3	2	8.1	0.380	0.372
21	6	3	2	9.3	1.251	1.092
21	6	3	2	11.0	0.740	0.634

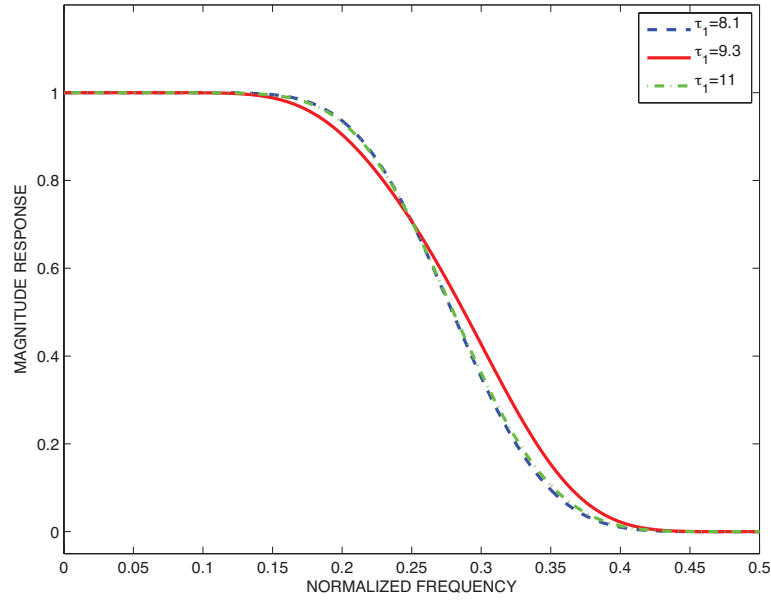


Fig.4.25 Magnitude responses of scaling lowpass filters $H_1(z)$.

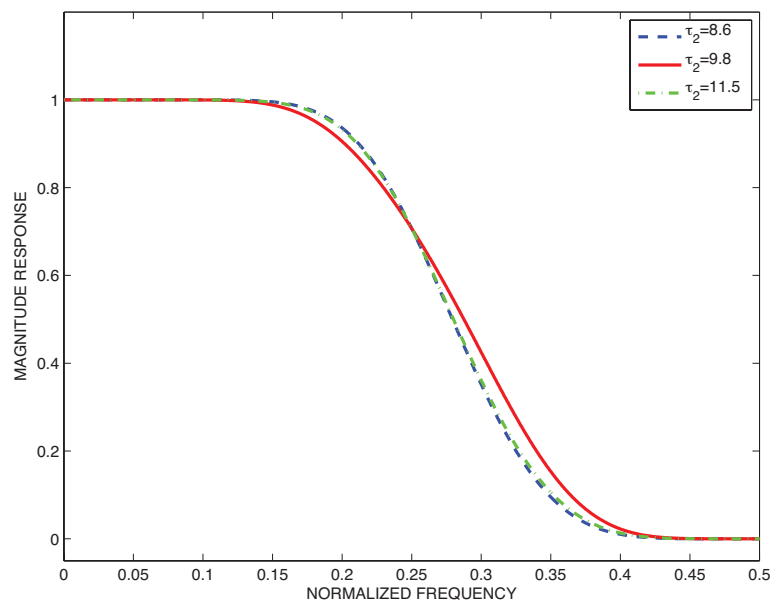


Fig.4.26 Magnitude responses of scaling lowpass filters $H_2(z)$.

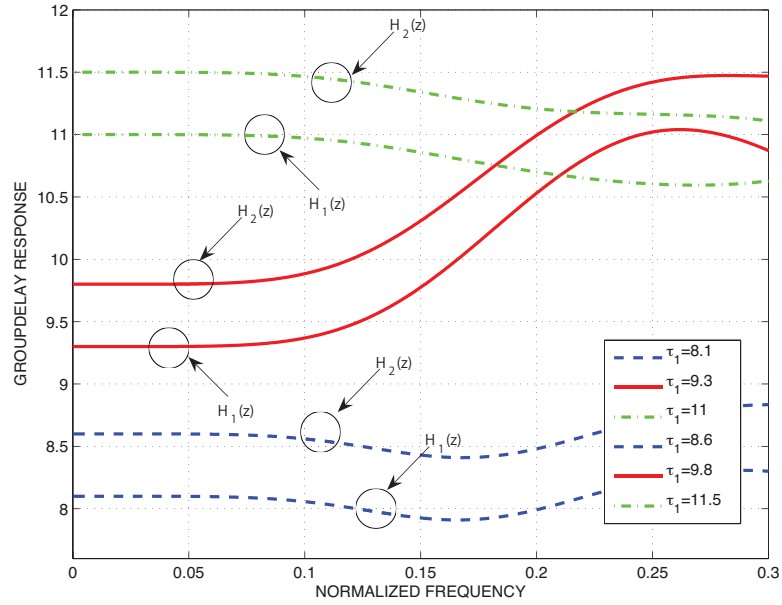


Fig.4.27 Group delay responses of scaling lowpass filters $H_i(z)$.

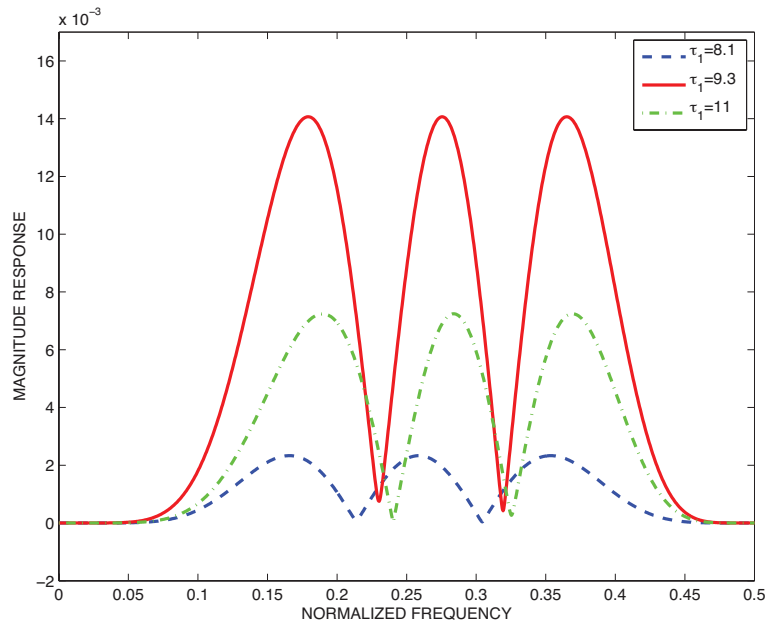
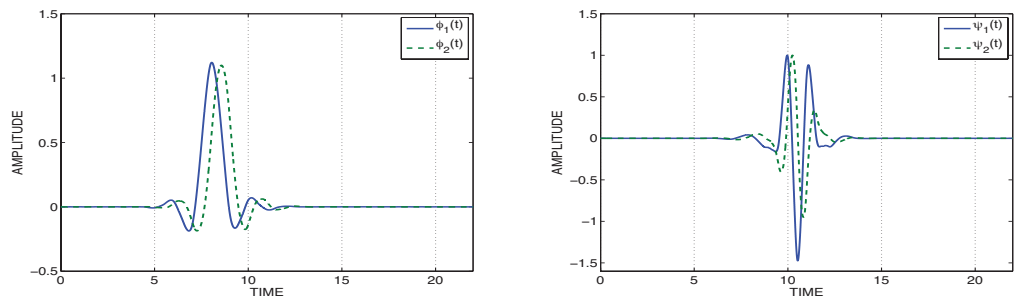
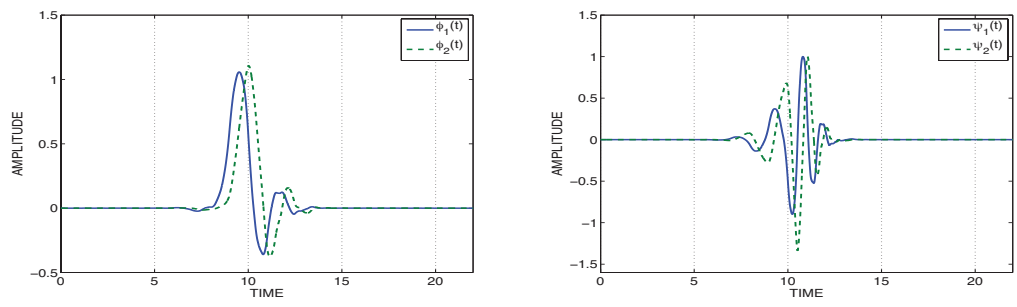


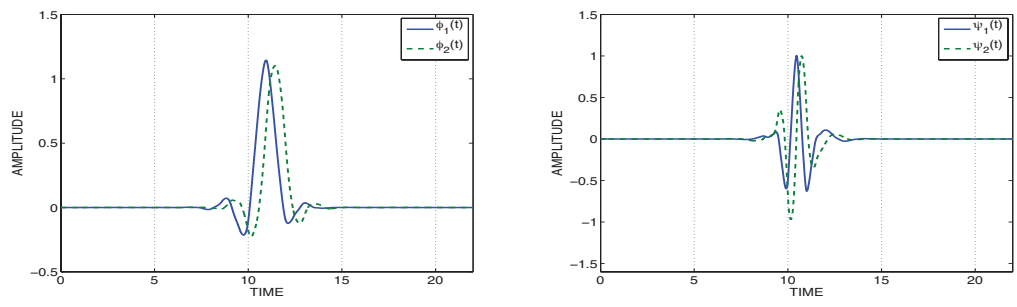
Fig.4.28 Magnitude responses of $E(\omega)$.



(a) $\tau_1 = 8.1, \tau_2 = 9.4$.

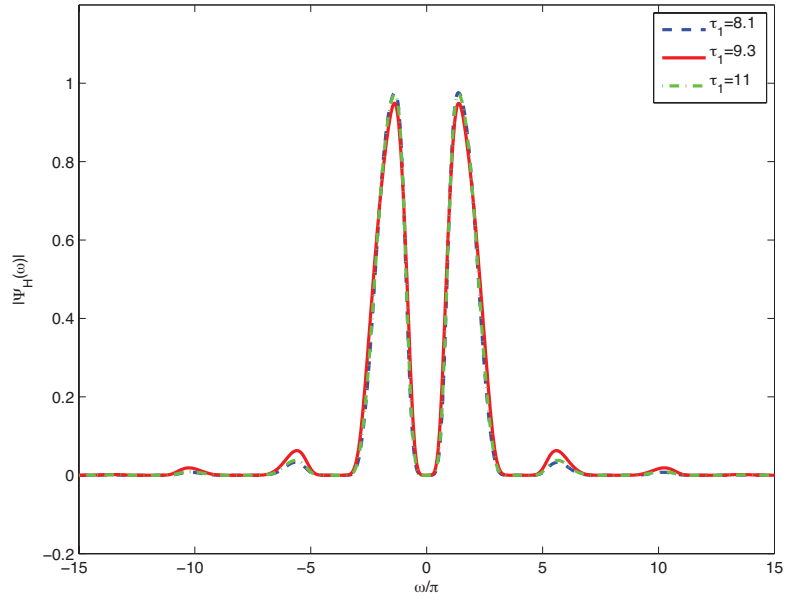
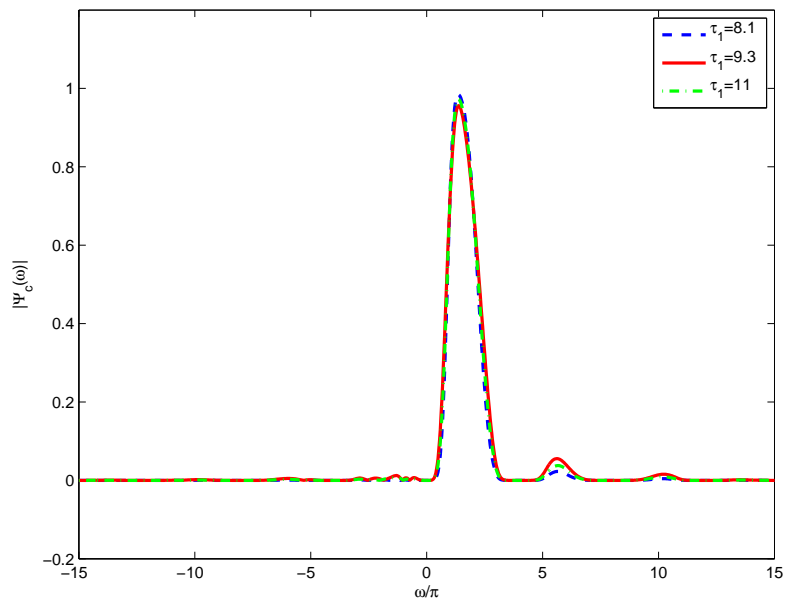


(b) $\tau_1 = 9.3, \tau_2 = 9.8$.



(c) $\tau_1 = 11.0, \tau_2 = 11.5$.

Fig.4.29 Scaling and wavelet functions $\phi_i(t), \psi_i(t)$.

Fig.4.30 Magnitude responses of $\Psi_i(\omega)$.Fig.4.31 Magnitude responses of $\Psi_c(\omega)$.

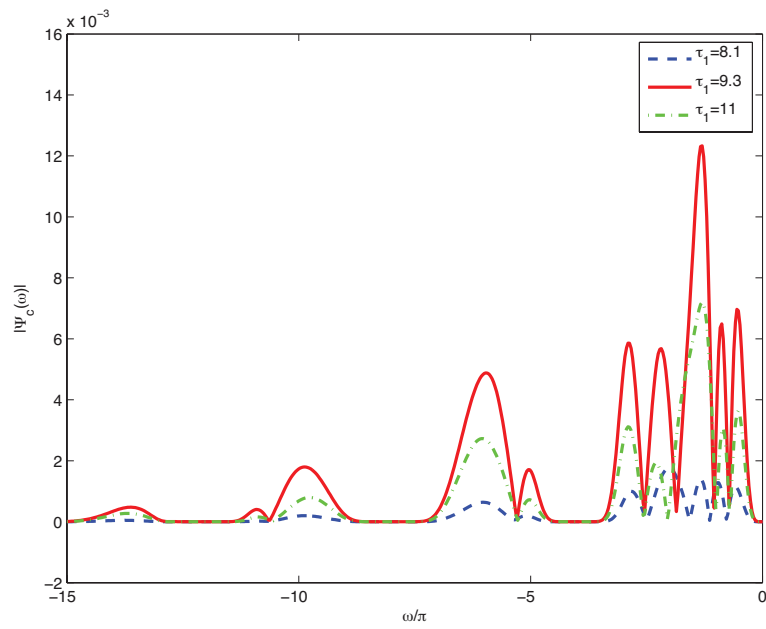


Fig.4.32 Magnitude responses of $\Psi_c(\omega)$.

Example 4.5

We have constructed a class of DTCWTs with $N = 15$, $K = 2$, $L = 3$, and $I = 3$. We set $\tau_1 = 7.25$ and $\tau_2 = 7.75$ from the half-sample delay condition. For comparison, the Q-shift filter proposed by Kingsbury in [22] is also designed, where $N = 15$, $K = 1$, $\tau_1 = 7.25$, $\tau_2 = 7.75$. The magnitude responses of the scaling lowpass filters $H_i(z)$ are shown in Fig.4.33, Fig.4.34, Fig.4.35 and Fig.4.36, respectively. It is seen in Fig.4.33 and Fig.4.35 that the Q-shift filter has a sharp magnitude response, but has only one zero at $z = -1$, which means the wavelet has only one vanishing moment. In Fig.4.33 and Fig.4.35, the magnitude responses of two filters with $\tau_1 = 6.5, \tau_2 = 7.0$ and $\tau_1 = 8.0, \tau_2 = 8.5$ are also shown. Their group delay responses are shown in Fig.4.37. It is seen that the group delay responses of the proposed filters are consistent with the specified group delays at $\omega = 0$, and more flat than the Q-shift filter. Moreover, the magnitude responses of $E(\omega)$ are shown in Fig.4.38, and are smaller than that of the Q-shift filter. In addition, the scaling functions $\phi_i(t)$ and wavelet functions $\psi_i(t)$ are shown in Fig.4.39. It is obvious that the proposed lowpass filters with different group delay responses can result in the scaling functions having different center of symmetry compared with that of Q-shift filter. Furthermore, the spectrum of wavelet function $\Psi_i(\omega)$ are shown in Fig.4.40. The complex wavelet spectrum $\Psi_c(\omega)$ and their negative spectrum are shown in Fig.4.42. The analyticity measures of E_∞ and E_2 are summarized in Table 4.5. It is clear that when $\tau_1 = 6.5$ and $\tau_2 = 7.0$ are chosen, the analyticity is the best, compared with the Q-shift and other two filters.

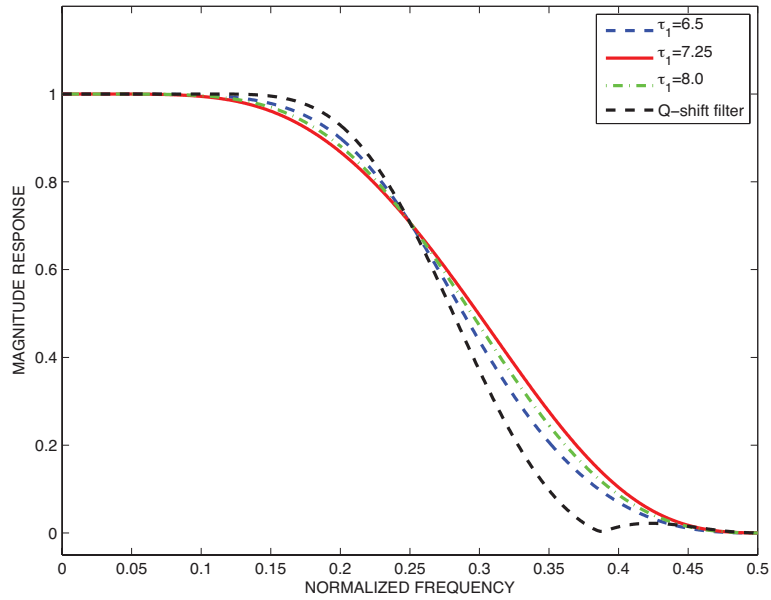


Fig.4.33 Magnitude responses of scaling lowpass filters $H_1(z)$.

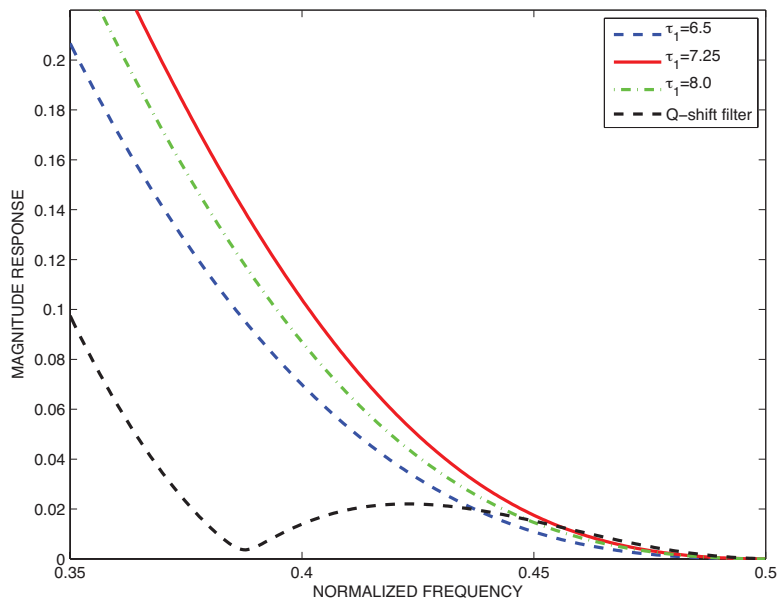


Fig.4.34 Magnitude responses of scaling lowpass filters $H_1(z)$.

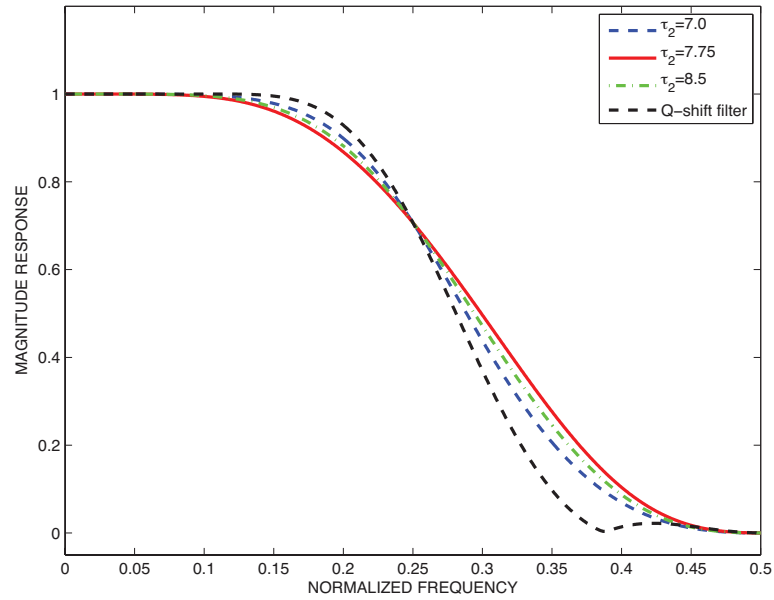


Fig.4.35 Magnitude responses of scaling lowpass filters $H_2(z)$.

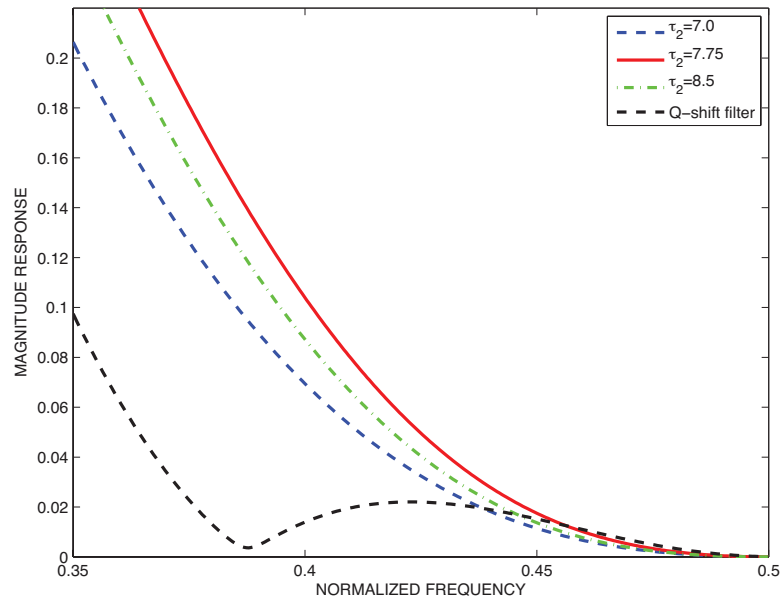


Fig.4.36 Magnitude responses of scaling lowpass filters $H_2(z)$.

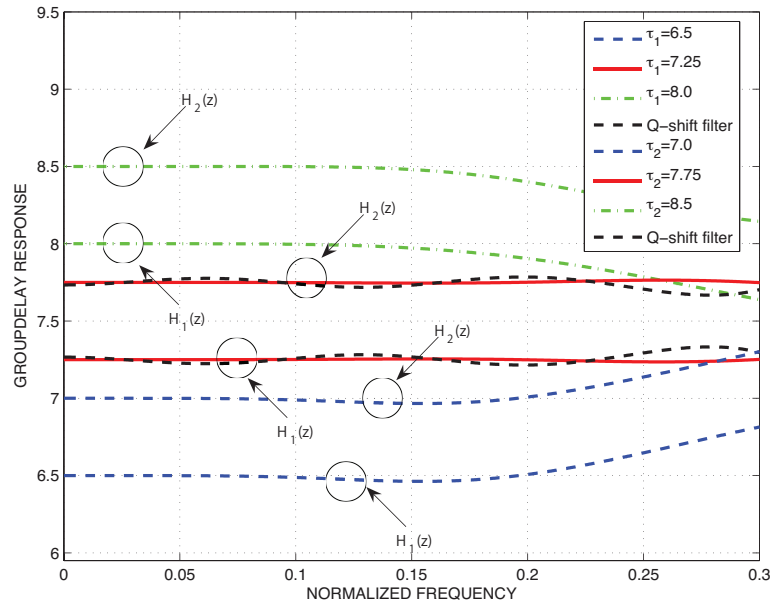


Fig.4.37 Group delay responses of scaling lowpass filters $H_1(z)$.

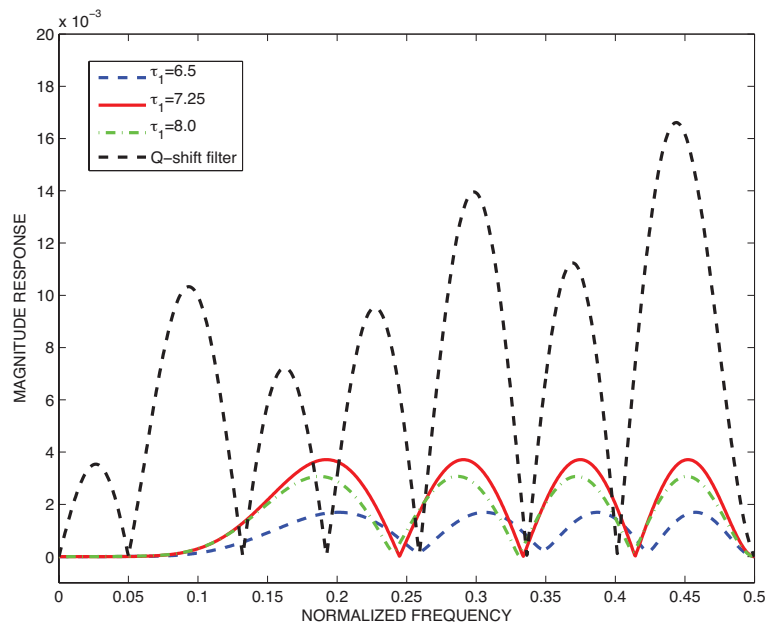
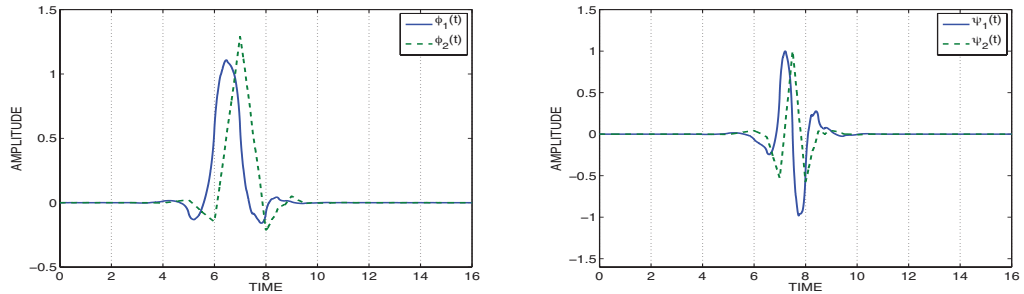
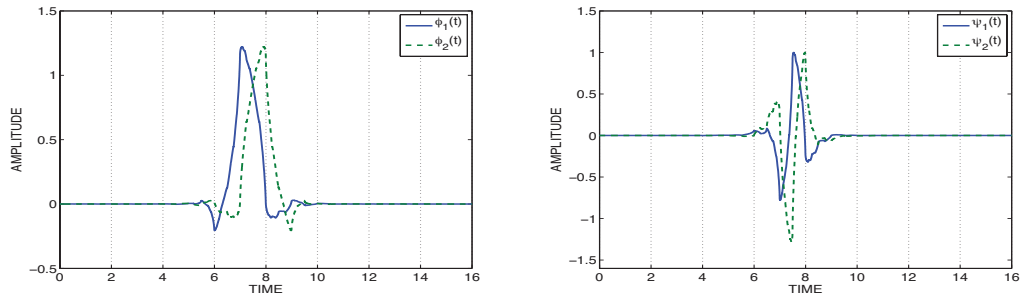


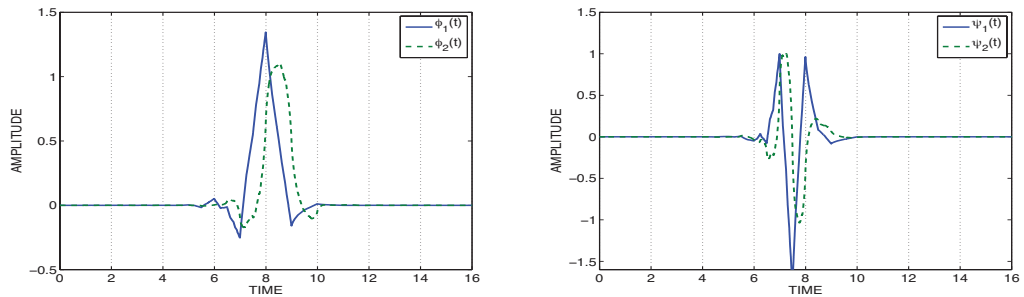
Fig.4.38 Magnitude responses of $E(\omega)$.



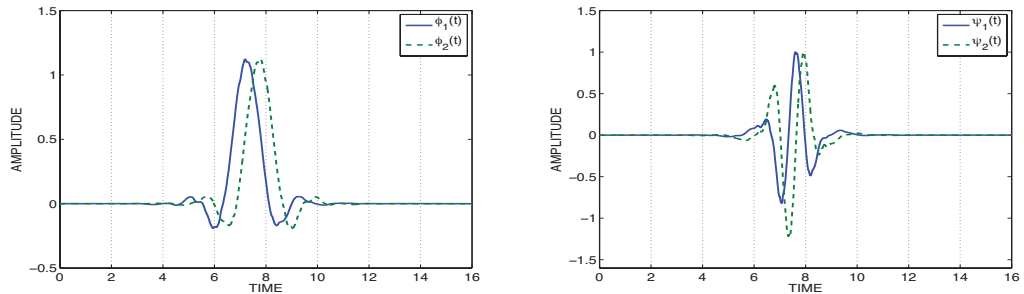
(a) $\tau_1 = 6.5, \tau_2 = 7.0$.



(b) $\tau_1 = 7.25, \tau_2 = 7.75$.



(c) $\tau_1 = 8.0, \tau_2 = 8.5$.



(d) Q-shift filter.

Fig.4.39 Scaling and wavelet functions $\phi_i(t), \psi_i(t)$.

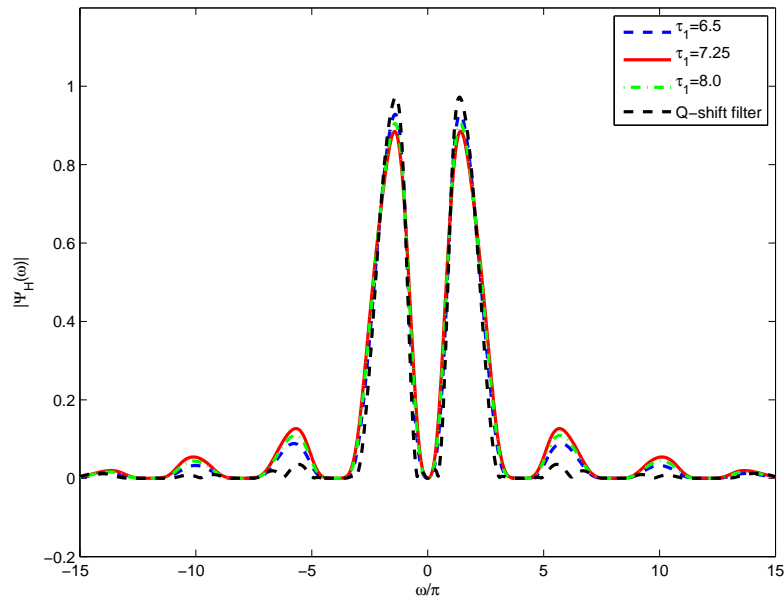


Fig.4.40 Magnitude responses of $\Psi_i(\omega)$.

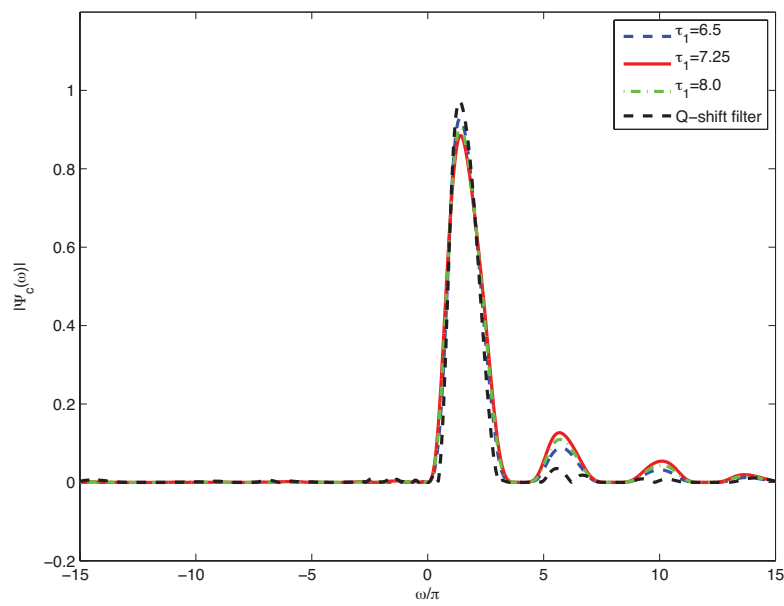
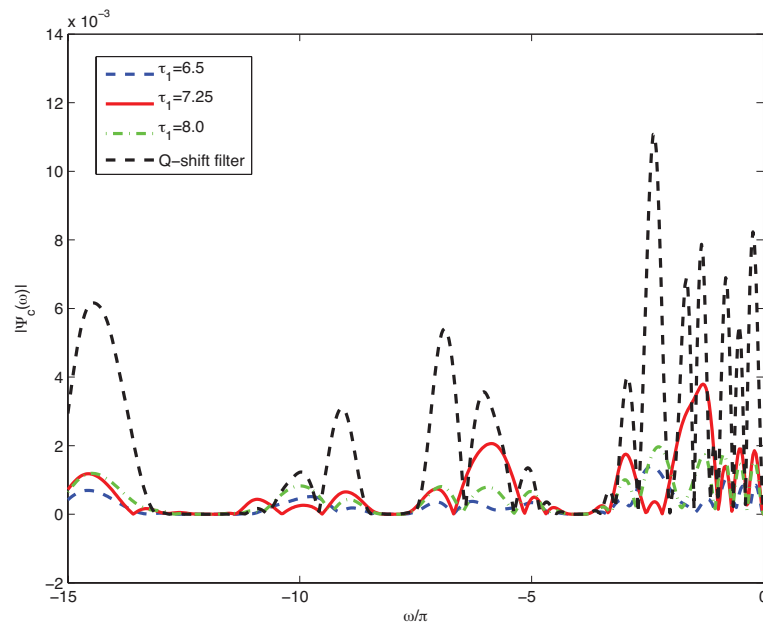


Fig.4.41 Magnitude responses of $\Psi_c(\omega)$.

TABLE 4.5 Analyticity Measures E_∞ and E_2 .

L	I	K	τ_1	τ_2	$E_\infty(\%)$	$E_2(\%)$
Q-shift filter		1	7.25	7.75	1.139	1.338
3	3	2	6.50	7.00	0.150	0.175
3	3	2	7.25	7.75	0.429	0.414
3	3	2	8.00	8.50	0.217	0.296

Fig.4.42 Magnitude responses of $\Psi_c(\omega)$.

4.5 Signal Denoising Application

In the previous section, the almost symmetric DTCWT with improved analyticity has been proposed. In this section, we review the wavelet thresholding method at first, and then introduce the DTCWT thresholding scheme. Moreover, several experiments are carried out to investigate the performance on noise reduction.

4.5.1 Denoising Using Wavelet Thresholding

In the real world, the signals are inevitably mixed with some noises. It is necessary to remove the noise corrupting a signal to recover that signal and proceed with further data analysis [15]. Wavelet thresholding scheme, which was firstly proposed by Donoho and his coworkers in [5], is considered as a preferred denoising method to suppress noise by thresholding the wavelet coefficients. Generally, wavelet thresholding scheme consists of three steps to reduce the noise, which are shown in Fig.4.43. First of all, we transform the noisy signal into wavelet domain by taking a forward DWT to obtain the approximation and wavelet coefficients, respectively. Next, we suppress the wavelet coefficients smaller than a given amplitude (using a hard or soft thresholding) to remove the noise. Finally, we take the IDWT to obtain the denoised signal.

Let $\mathcal{D}(\cdot, \cdot)$ denote the thresholding operator, then the hard thresholding



Fig.4.43 Denoising using wavelet thresholding.

can be expressed as

$$\hat{d}_{j,n} = \mathcal{D}(d_{j,n}, T) = \begin{cases} d_{j,n} & |d_{j,n}| \geq T \\ 0 & |d_{j,n}| < T \end{cases}, \quad (4.36)$$

In the case of soft thresholding,

$$\hat{d}_{j,n} = \mathcal{D}(d_{j,n}, T) = \begin{cases} d_{j,n} - T \times \text{sgn}(d_{j,n}) & |d_{j,n}| \geq T \\ 0 & |d_{j,n}| < T \end{cases}, \quad (4.37)$$

where T is the given threshold value, j is the decomposition level of DWT, and $\text{sgn}(\cdot)$ is the signum function.

4.5.2 Denoising Using DTCWT Thresholding

It has been shown in [26] that DWT is not very efficient for denoising since it is lack of shift invariance, leading to artifacts in the reconstructed signal. Denoising using DTCWT gives a substantial performance to DWT. It is effective to threshold the complex wavelet coefficients rather than its real and imaginary parts separately because the magnitude of complex wavelet coefficients are free of aliasing distortion, which results in a nearly shift-invariance.

In the previous section, we have shown that the key to obtain the shift invariance from DTCWT lies in that the corresponding wavelet functions

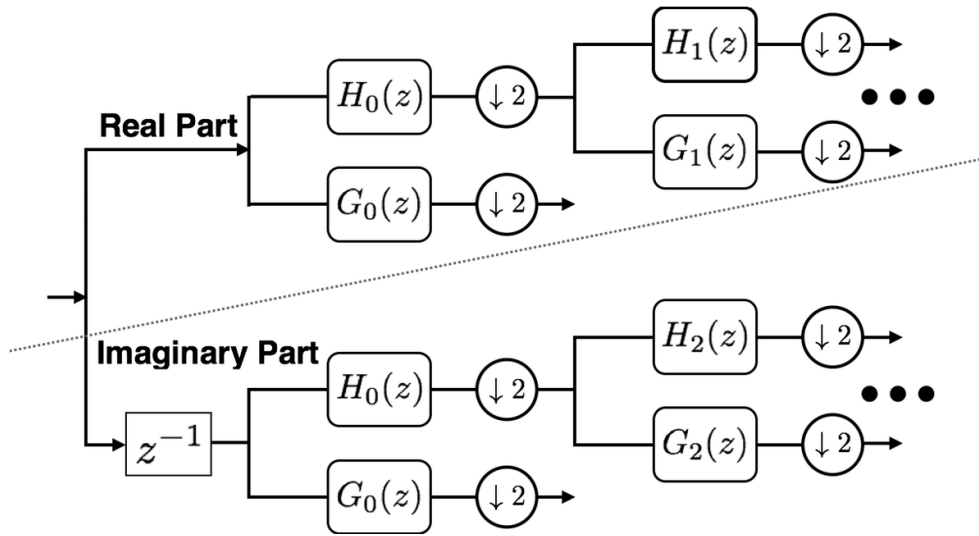


Fig.4.44 The conventional implementation of DTCWT decomposition.

are Hilbert transform pair. The necessary and sufficient condition for two wavelet bases to form a Hilbert transform pair is that two scaling lowpass filters satisfy the half-sample delay condition. For wavelet coefficients to be the Hilbert transform pair in finite levels of decomposition, it was suggested in [16] and [17] that for the first level of decomposition, the same filter bank were adopted for Tree A and Tree B, but with one sample delay difference between each other. In addition, two scaling lowpass filters, which satisfy half-sample delay condition, were adopted for the rest of levels, as shown in Fig.4.44. In [26], Selesnick had used the Daubechies length-10 filter at the first level, and the orthonormal solutions of length 12 based on the common-factor technique at the subsequent levels. However, two wavelet coefficients at the first level are not Hilbert transform pair, which results in a poor performance of noise reduction. Thus, a new scheme is proposed in the following, as shown in Fig.4.45. On the real part of DTCWT, the signal is directly inputted to the tree A of DTCWT. On the imaginary part, it is firstly through an allpass filter $A(z)$ approxi-

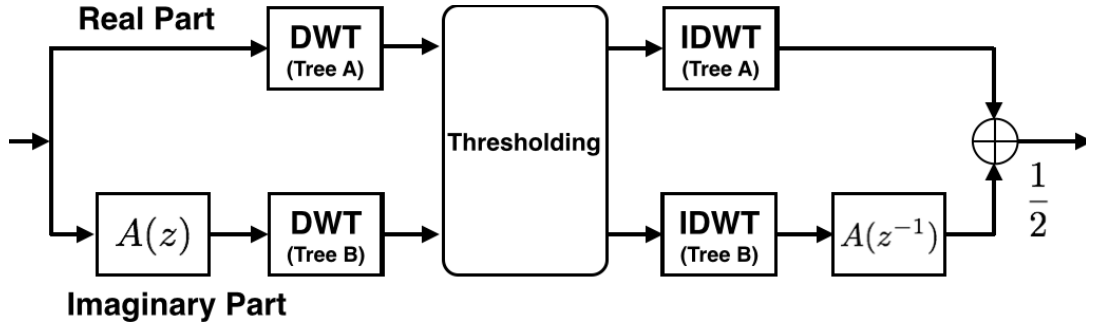


Fig.4.45 Allpass filter with approximately half-sample delay ahead of DTCWT.

mating to half-sample delay, and then inputted to the tree B. Therefore, the corresponding wavelet coefficients are Hilbert transform pair at each level. Moreover, we define the wavelet coefficients at level j from tree A as $d_{j,n}^A$ and from tree B as $d_{j,n}^B$, then the complex wavelet coefficients are $d_{j,n}^c = d_{j,n}^A + d_{j,n}^B i$. The thresholding operator $\mathcal{D}(\cdot, \cdot)$ in hard thresholding becomes

$$\hat{d}_{j,n}^c = \mathcal{D}(d_{j,n}^c, T) = \begin{cases} d_{j,n}^c & |d_{j,n}^c| \geq T \\ 0 & |d_{j,n}^c| < T \end{cases}, \quad (4.38)$$

while in the soft thresholding,

$$\hat{d}_{j,n}^c = \mathcal{D}(d_{j,n}^c, T) = \begin{cases} \frac{|d_{j,n}^c| - T}{|d_{j,n}^c|} d_{j,n}^c & |d_{j,n}^c| \geq T \\ 0 & |d_{j,n}^c| < T \end{cases}. \quad (4.39)$$

Furthermore, $A(z^{-1})$ is needed to cancel the phase of $A(z)$. $A(z^{-1})$ can be realized by reversing the input signal, passing it through $A(z)$, and then re-reversing the output signal.

4.5.3 Experiments on Signal Denoising

The noisy signal $x(n)$ is defined:

$$x(n) = x_0(n) + x_N(n), \quad (4.40)$$

where $x_0(n)$ is the original signal, $x_N(n)$ is the additive white noise with $N(0, \sigma^2)$. In the following, four specific signals, *Blocks*, *Bumps*, *Heavy Sine* and *Doppler* are used as the original signal $x_0(n)$. We generate the noisy signal $x(n)$ by adding $x_N(n)$ with $\sigma = 0.4$. First of all, we use the procedure proposed in [17] to investigate the performance of the proposed DTCWT on noise reduction by using hard thresholding. For the first level of DTCWT, we use the filter bank of length 8 proposed by Abdelnour and Selesnick in [18]. For the rest of levels, we use the Q-shift filter with $\{N = 15, K = 1, \tau_1 = 7.25\}$ proposed by Kingsbury in [22], DTCWT with $\{N = 15, K = 2, L = 3, I = 3, \tau_1 = 7.25\}$ and $\{N = 15, K = 2, L = 3, I = 3, \tau_1 = 6.5\}$ in Example 4.4.4. For the purpose of simplicity, we name DTCWT with $\tau_1 = 7.25$ as filter 1, and DTCWT with $\tau_1 = 6.5$ as filter 2. We then calculate the signal-noise ratio (SNR) by using different threshold value T from 0 to 5. SNR with the optimal threshold value is shown in Table 4.6. It is obvious that the proposed DTCWTs can achieve better performance (higher SNR) on noise reduction than Q-shift filter. Next, we use the proposed denoising scheme. We use the maximally allpass filter $A(z)$ of degree $J = 1$ with approximately half-sample delay. The results are given in Table 4.6. It is clear that the proposed denoising scheme can obtain higher SNR than the conventional scheme proposed in [17].

Moreover, we investigate the performance of DTCWTs and DWT constructed by Daubechies 9/7 filter on noise reduction. Table 4.7 summarizes the comparison of SNR using hard thresholding with optimal threshold value. It is clear that the denoising using DTCWT thresholding achieves better performance than that by DWT, averagely 2.52dB improved. Table 4.9 summarizes the comparison of SNR using soft thresholding, and denoising using DTCWT thresholding performs better. In addition, filter 2 owns the best performance on noise reduction for the most cases, since the corresponding complex wavelet is approximately analytic. The optimal threshold value of hard and soft thresholding are summarized in Table 4.8 and 4.10, respectively.

Finally, denoised signals using hard and soft thresholding are shown in Fig.4.46 ~ Fig.4.53. It is obvious that the denoised signal by using the proposed DTCWTs have little noise compared with the conventional DWT and Q-shift filters.

TABLE 4.6 Comparison of SNR(dB) for DTCWT denoising schemes using hard thresholding.

		Q-shift filter		filter 1		filter 2	
Signal	Initial SNR	Previous [17]	Proposed	Previous [17]	Proposed	Previous [17]	Proposed
<i>Blocks</i>	17.872	19.792	24.178	19.949	25.837	19.995	25.360
<i>Bumps</i>	17.866	23.140	25.830	23.302	25.700	23.105	25.911
<i>Heavy sine</i>	17.690	29.539	28.378	30.001	30.058	31.117	30.334
<i>Doppler</i>	18.087	22.476	26.065	22.062	25.624	22.486	25.956
Average	17.879	23.736	26.113	23.828	26.805	24.175	26.890

TABLE 4.7 Comparison of SNR(dB) using hard thresholding with optimal threshold value.

		D9/7 filter	Q-shift filter	filter 1	filter 2
<i>Blocks</i>	17.872	22.743	24.178	25.837	25.360
<i>Bumps</i>	17.866	23.092	25.830	25.700	25.911
<i>Heavy sine</i>	17.690	26.692	28.378	30.058	30.334
<i>Doppler</i>	18.087	23.810	26.065	25.624	25.956
Average	17.879	24.084	26.113	26.805	26.890

TABLE 4.8 The optimal threshold value of hard thresholding.

	D9/7 filter	Q-shift filter	filter 1	filter 2
<i>Blocks</i>	1.10	1.55	1.60	1.50
<i>Bumps</i>	1.15	1.45	1.75	1.50
<i>Heavy sine</i>	1.10	1.45	1.75	1.55
<i>Doppler</i>	1.20	1.65	1.45	1.50

TABLE 4.9 Comparison of SNR(dB) using soft thresholding with optimal threshold value.

		D9/7 filter	Q-shift filter	filter 1	filter 2
<i>Blocks</i>	17.872	22.291	22.859	23.684	23.369
<i>Bumps</i>	17.866	22.455	24.246	24.228	24.395
<i>Heavy sine</i>	17.690	25.468	27.318	28.075	28.099
<i>Doppler</i>	18.087	23.232	24.893	23.968	24.463
Average	17.879	23.361	24.829	24.989	25.082

TABLE 4.10 The optimal threshold value of soft thresholding.

	D9/7 filter	Q-shift filter	filter 1	filter 2
<i>Blocks</i>	0.45	0.60	0.65	0.65
<i>Bumps</i>	0.45	0.70	0.70	0.70
<i>Heavy sine</i>	0.65	0.85	0.90	0.90
<i>Doppler</i>	0.50	0.70	0.65	0.70

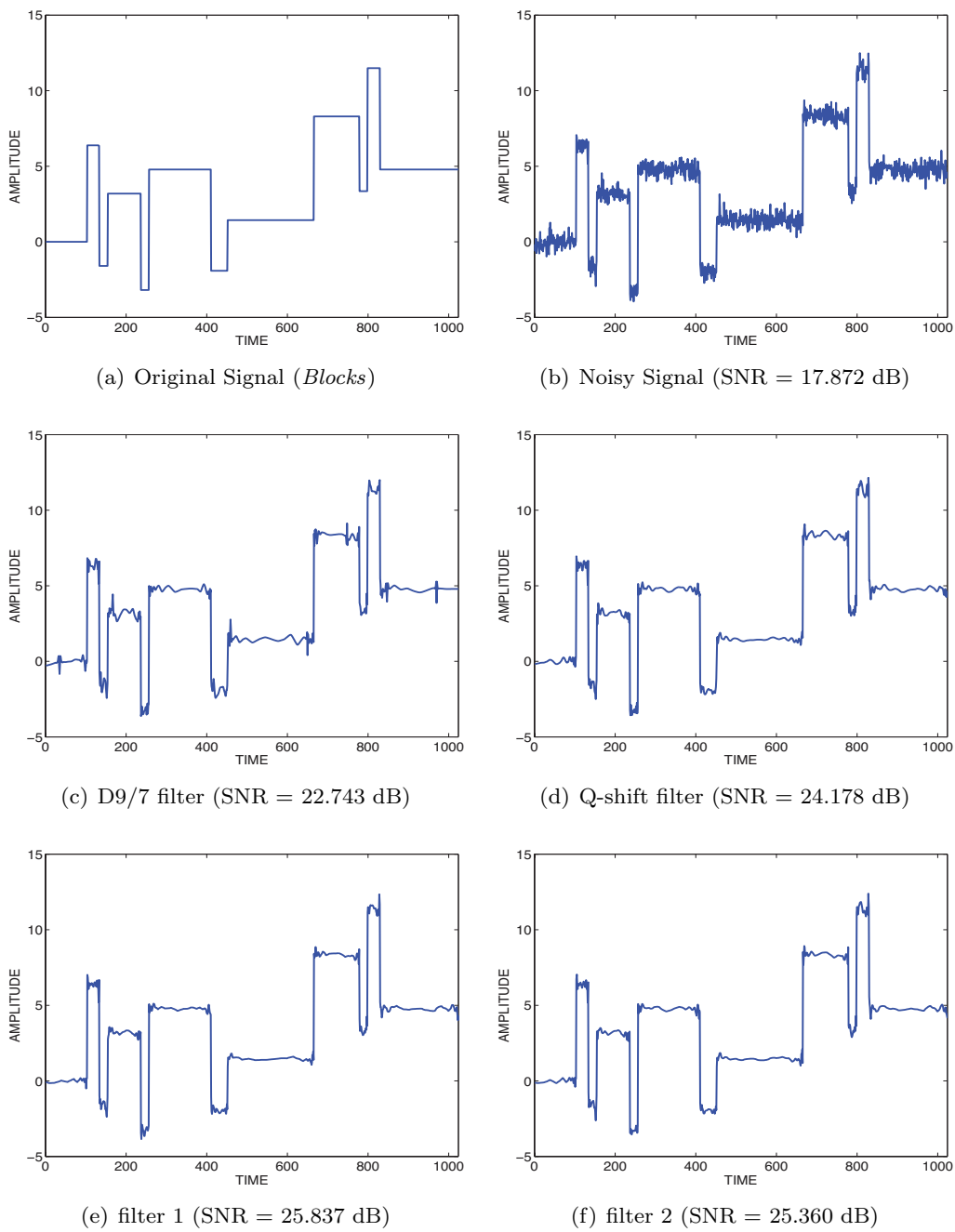
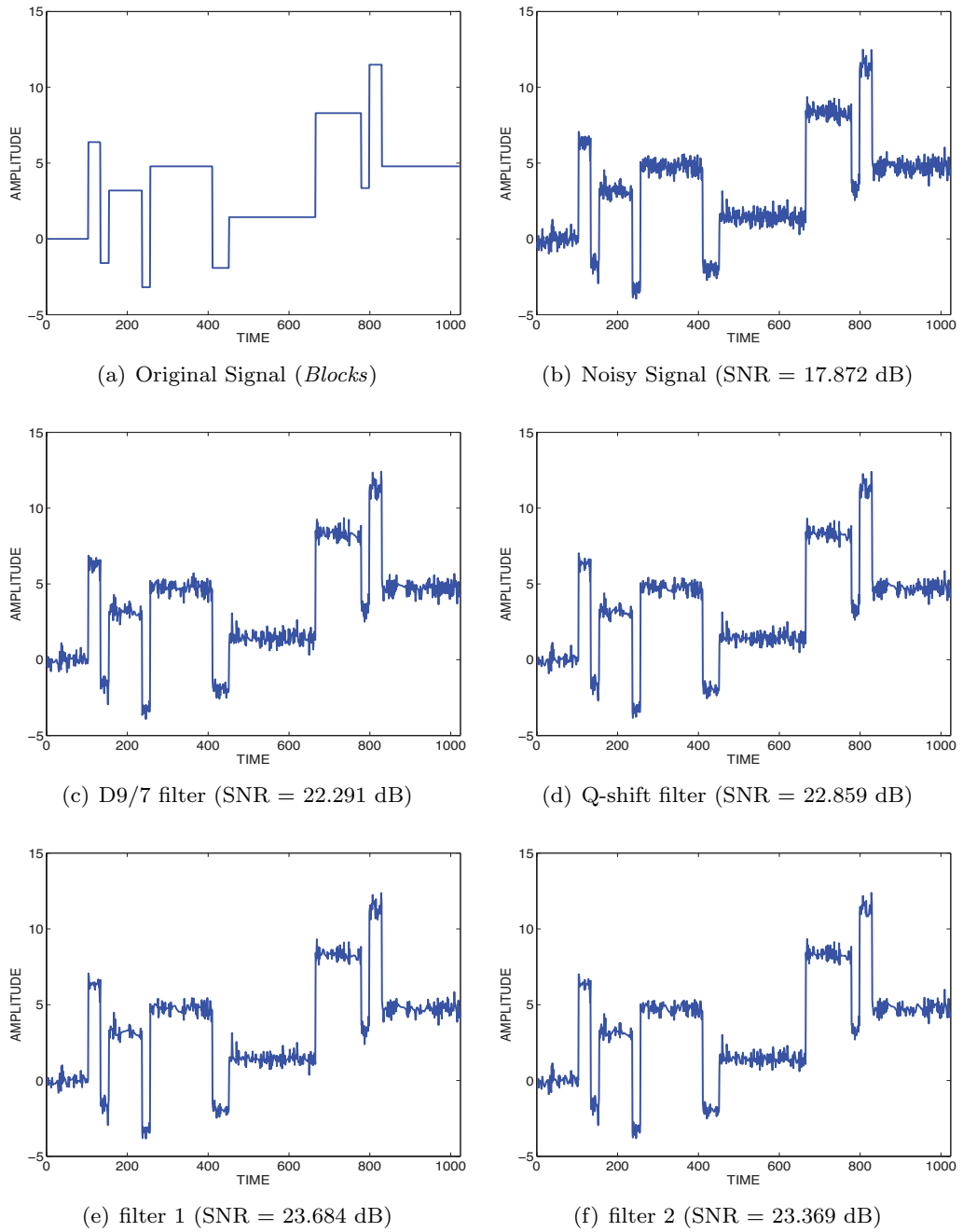
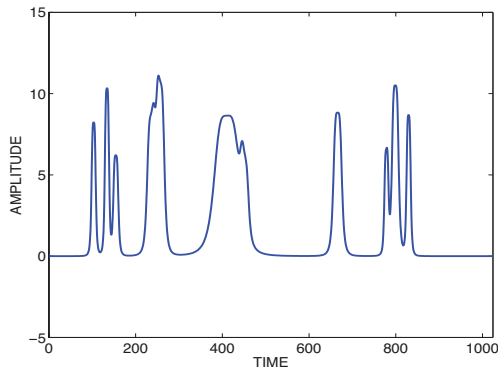
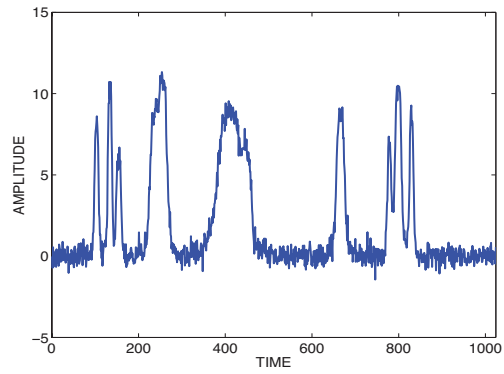


Fig.4.46 Denoising using hard thresholding for signal *Blocks*.

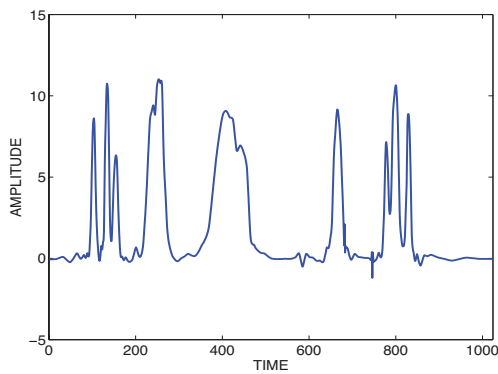
Fig.4.47 Denoising using soft thresholding for signal *Blocks*.



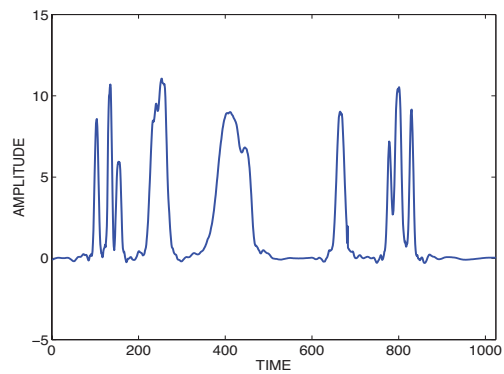
(a) Original Signal (*Bumps*)



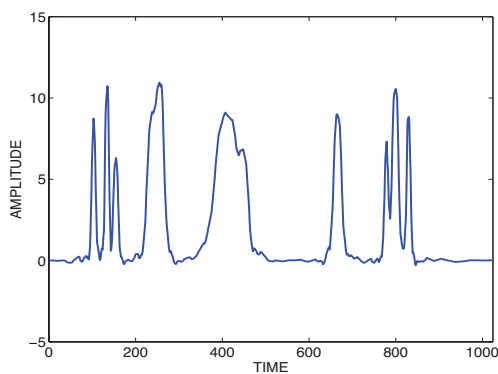
(b) Noisy Signal (SNR = 17.866 dB)



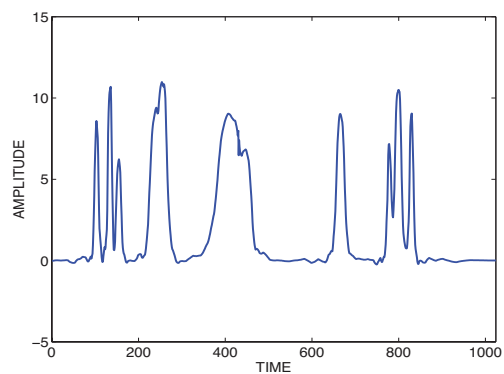
(c) D9/7 filter (SNR = 23.092 dB)



(d) Q-shift filter (SNR = 25.830 dB)

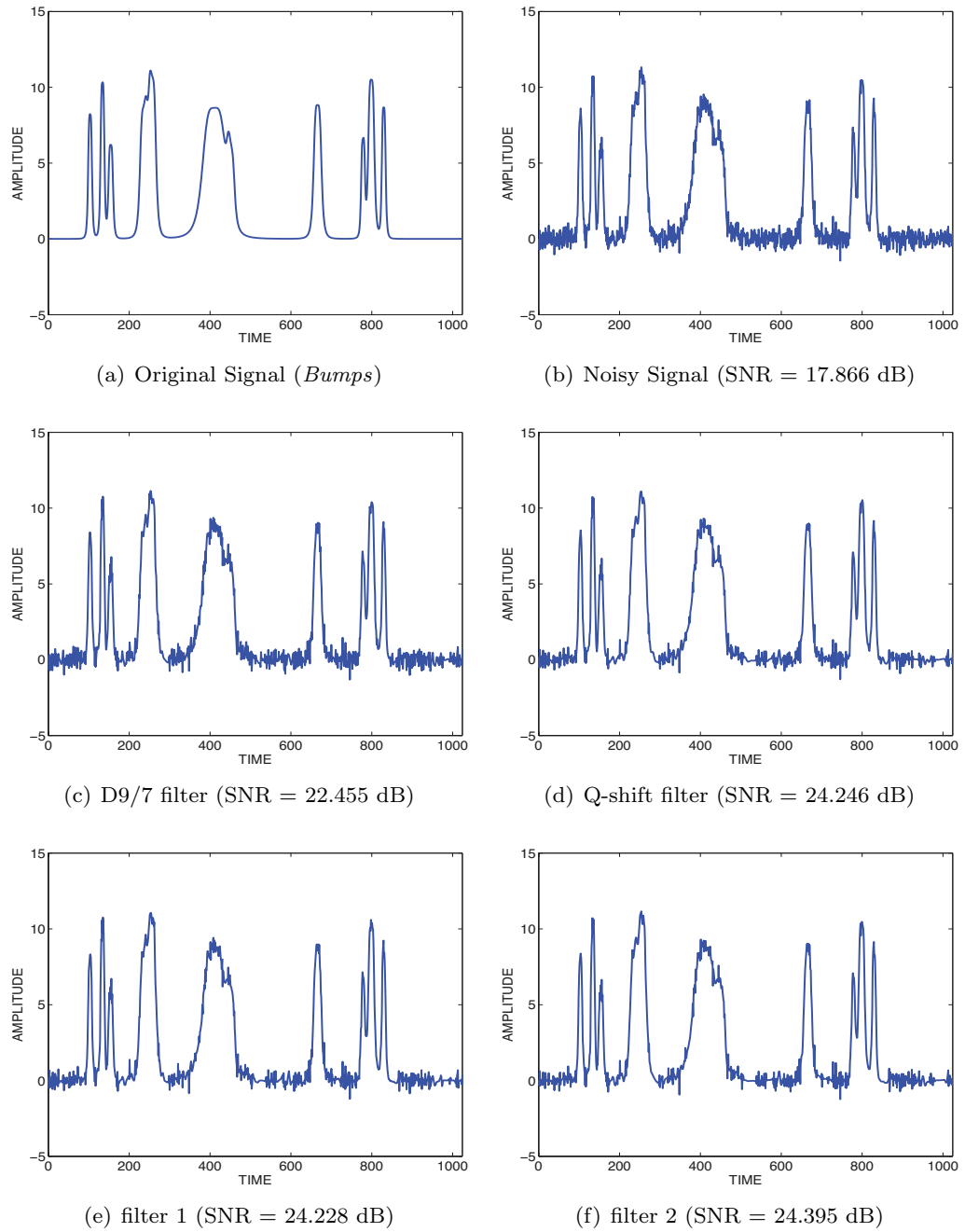


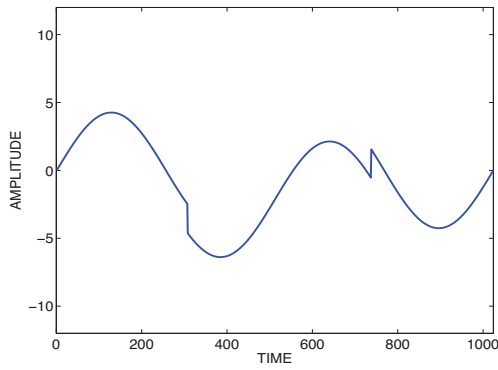
(e) filter 1 (SNR = 25.700 dB)



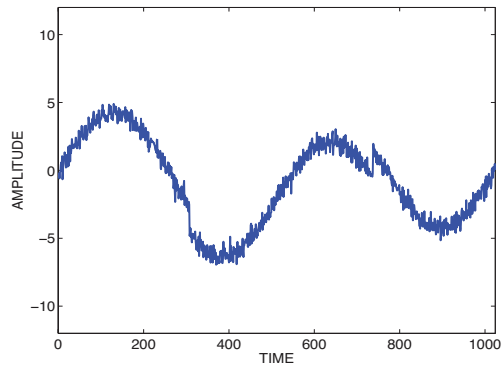
(f) filter 2 (SNR = 25.911 dB)

Fig.4.48 Denoising using hard thresholding for signal *Bumps*.

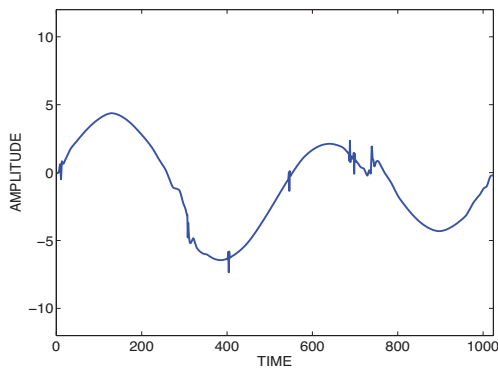
Fig.4.49 Denoising using soft thresholding for signal *Bumps*.



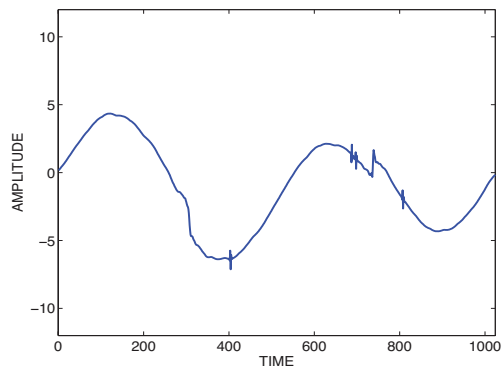
(a) Original Signal (*Heavy sine*)



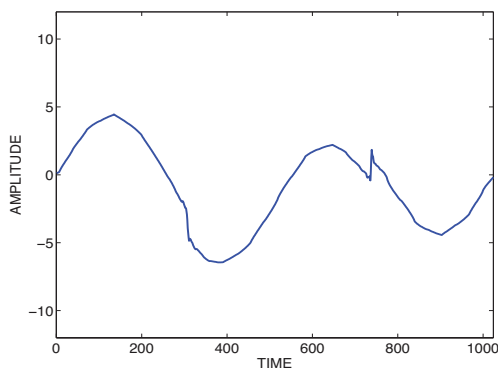
(b) Noisy Signal (SNR = 17.866 dB)



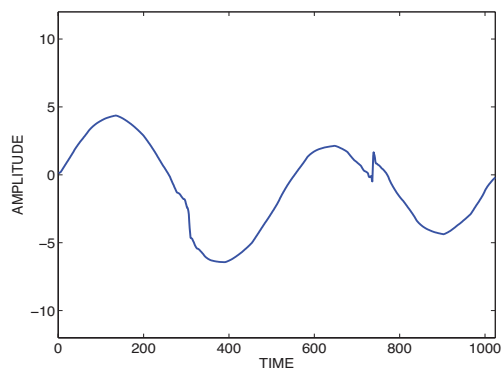
(c) D9/7 filter (SNR = 26.692 dB)



(d) Q-shift filter (SNR = 28.378 dB)



(e) filter 1 (SNR = 30.058 dB)



(f) filter 2 (SNR = 30.334dB)

Fig.4.50 Denoising using hard thresholding for signal *Heavy sine*.

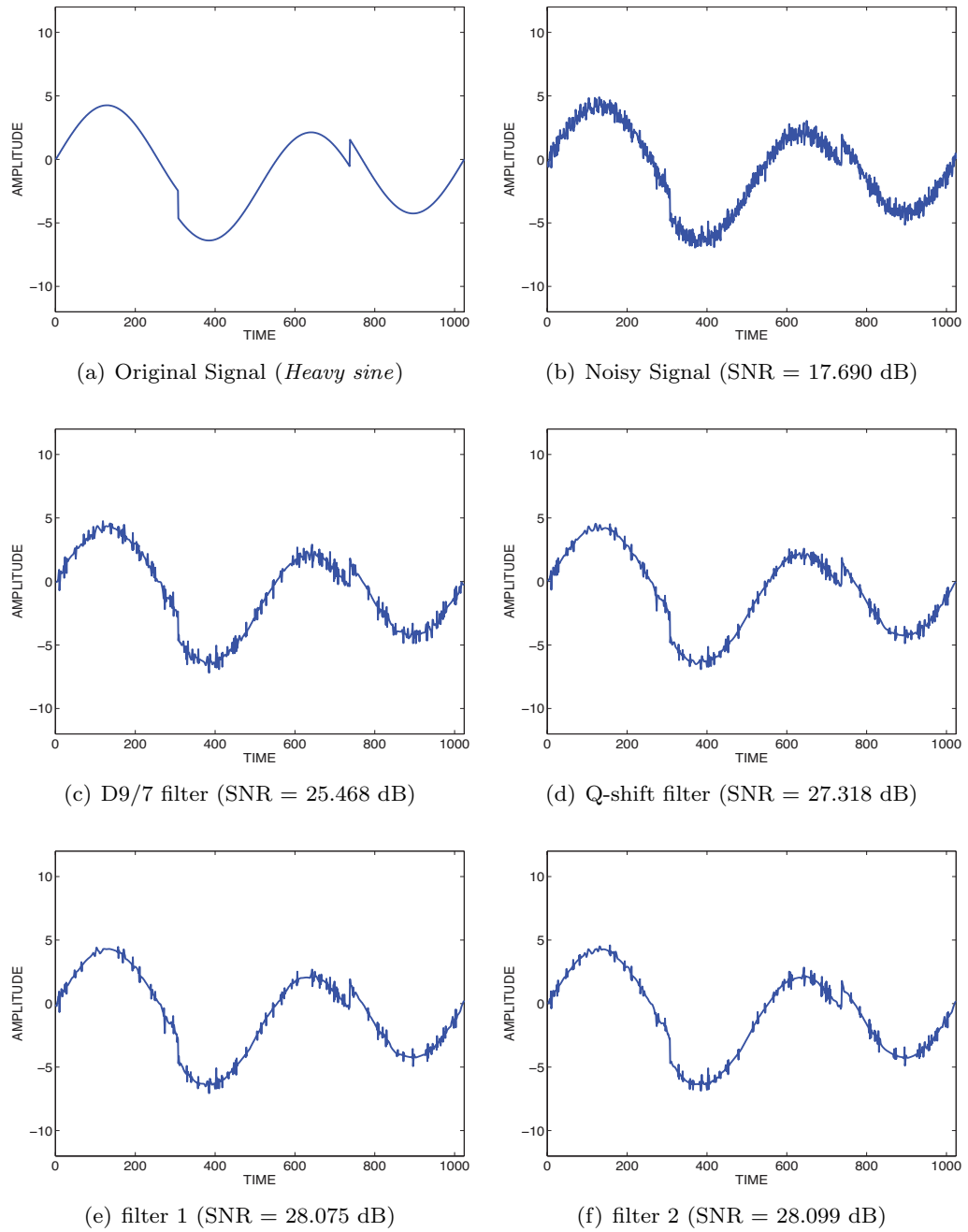


Fig.4.51 Denoising using soft thresholding for signal *Heavy sine*.

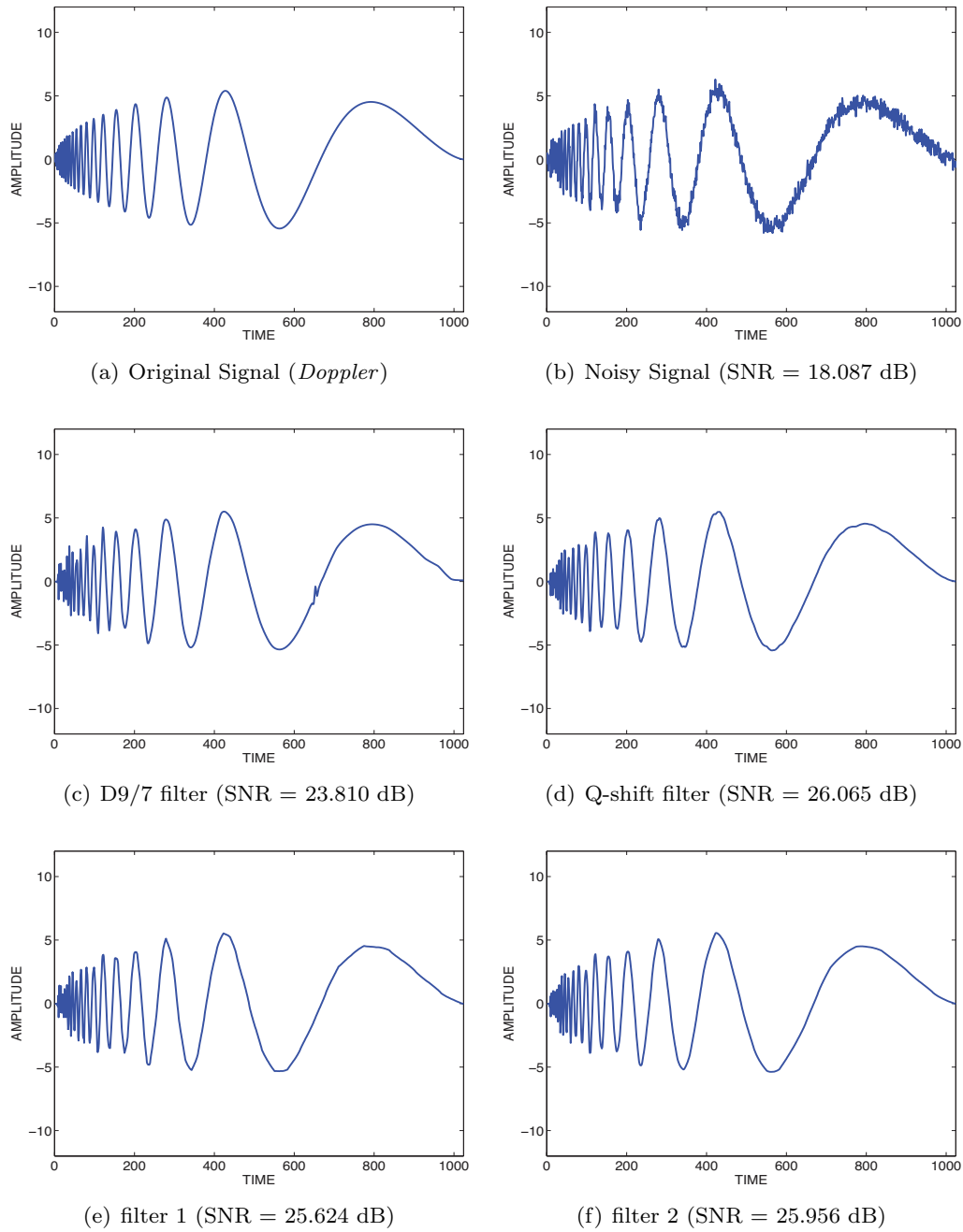
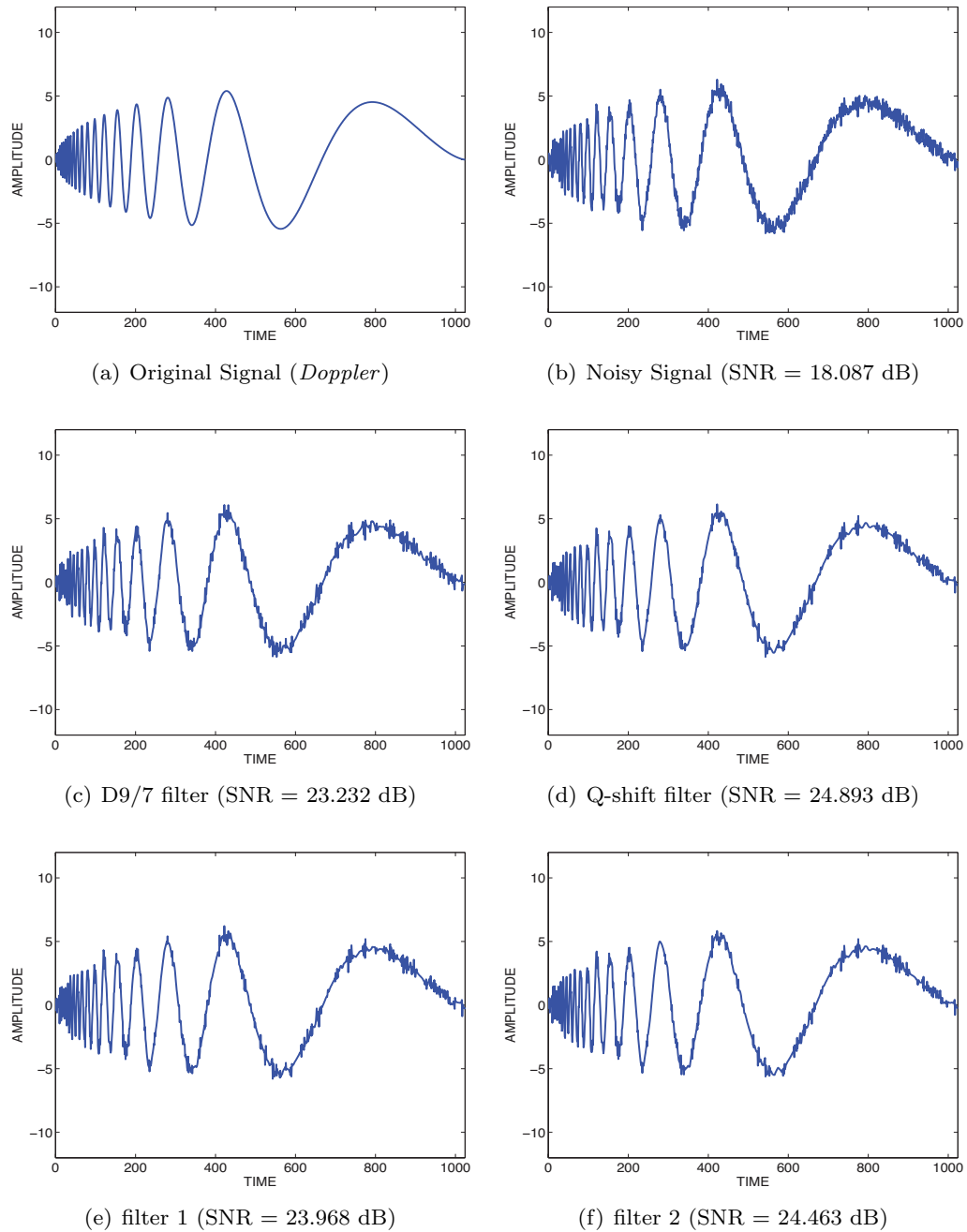


Fig.4.52 Denoising using hard thresholding for signal *Doppler*.

Fig.4.53 Denoising using soft thresholding for signal *Doppler*.

4.6 Summary

In this chapter, we have firstly reviewed the conventional Q-shift filters for DTCWTs proposed by Kingsbury in [16], [17] and [22]. We then have proposed a new method for designing DTCWTs with arbitrary center of symmetry. We have specified the degree of flatness of group delay response at $\omega = 0$, and the number of vanishing moments. Next, we have applied the Remez exchange algorithm to minimize the magnitude of the error function, resulting in the improved analyticity of complex wavelet. Two scaling lowpass filters can be obtained simultaneously by iteratively solving a set of equations. Therefore, the optimal solution is attained through a few iterations. As a result, the proposed DTCWTs are orthogonal and almost symmetric, and have the improved analyticity. Furthermore, we compared the proposed DTCWTs with Q-shift filter proposed by Kingsbury. It is obvious that the proposed DTCWTs can have arbitrary center of symmetry, while the center of symmetry of Q-shift filter remains unchanged. Finally, several experiments of signal denoising are carried out to demonstrate the efficiency of the proposed DTCWTs. It is clear that the proposed DTCWTs can achieve better performance on noise reduction.

Chapter 5 Conclusion

In this dissertation, we have proposed two new classes of DTCWTs with different improved properties. First of all, we have proposed a new class of DTCWTs with improved analyticity and frequency selectivity. Next, we have proposed another class of almost symmetric DTCWTs with arbitrary center of symmetry. The resulting DTCWTs are orthogonal and almost symmetric, and have the improved analyticities.

In Chapter 2, we have reviewed the Fourier transform and then introduced fundamentals of dual tree complex wavelet transform. The wavelet transform has been proved to be a successful tool to express the signal in time and frequency domain simultaneously. To obtain the wavelet coefficients efficiently, the discrete wavelet transform has been introduced since it can be achieved by a tree of two-channel filter banks. Then, we discussed the design conditions of two-channel filter banks, i.e., perfect reconstruction and orthogonality. Additionally, some properties of wavelet functions including orthonormality, symmetry and vanishing moments have been also given. Moreover, the structure of DTCWT was introduced, where two wavelet bases are required to form a Hilbert transform pair. Thus, the corresponding scaling lowpass filters must satisfy the half-sample delay condition. Finally, the objective measures of quality were given to evaluate the performance of the complex wavelet.

In Chapter 3, we have proposed a new class of DTCWTs with improved analyticity and frequency selectivity by using general IIR filters with numerator and denominator of different degree. The proposed DTCWTs include the conventional DTCWTs proposed by Selesnick as a special cases.

First of all, we have given a design method of allpass filters with the specified degree of flatness and equiripple phase responses in the approximation band to improve the analyticity of complex wavelets. Next, we have specified the number of vanishing moments and applied the Remez exchange algorithm to minimize the stopband error in order to improve the frequency selectivity of scaling lowpass filters. Finally, we have investigated the performance on the proposed DTCWTs, where a properly chosen approximation band can improve the analyticity of complex wavelets.

In Chapter 4, we have proposed another class of almost symmetric orthogonal DTCWTs with arbitrary center of symmetry. First of all, two scaling lowpass filters are designed separately with the specified number of vanishing moments and the specified flatness degree of group delay, which satisfy the half-sample delay condition. Next, two scaling lowpass filters are designed simultaneously by applying the Remez exchange algorithm to minimize the difference of frequency responses between two scaling lowpass filters, in order to improve the analyticity of complex wavelets. The equiripple behaviour of the error function can be obtained through a few iterations. As a result, the proposed DTCWTs are orthogonal, almost symmetric and have the improved analyticity. Differently from Q-shift filters, the group delay responses of scaling lowpass filters can be arbitrarily specified, resulting in the scaling functions having the arbitrary center of symmetry. Finally, we have introduced signal denoising by using wavelet thresholding to investigate the performance of the proposed DTCWTs on noise reduction. It is shown that the proposed DTCWTs can achieve better performance on noise reduction than the conventional DWT and Q-shift filter.

References

- [1] I. Daubechies, *Ten Lectures on Wavelets*, Philadelphia, PA: SIAM, 1992.
- [2] S. K. Mitra and J. FF. Kaiser, *Handbook for Digital Signal Processing*, Wiley, New York, 1993.
- [3] P. P. Vaidyanathan, *Multirate Systems and Filter Banks*, Englewood Cliffs, NJ: Prentice Hall, 1993.
- [4] T. W. Parks and J. H. McClellan, "Chebyshev approximation for nonrecursive digital filters with linear phase," *IEEE Trans. Circuit Theory*, vol.CT-19, no.2, pp.189-194, Mar. 1972.
- [5] D. Donoho and I. Johnstone, "Ideal spatial adaptation via wavelet shrinkage," *Biometrika*, vol.81, pp.425-455, 1994.
- [6] T. I. Laakso, V. Valimaki, M. Karjalainen and U. K. Laine, "Splitting the unit delay: Tools for fractional delay filter design," *IEEE Signal Processing Mag.*, vol.13, no.1, pp.30-60, Jan. 1996.
- [7] X. Zhang and H. Iwakura, "Design of IIR digital filters bases on eigenvalue problem," *IEEE Trans. Signal Processing*, vol.44, no.6, pp.1325-1333, June 1996.
- [8] X. Zhang and H. Iwakura, "Design of IIR digital allpass filters based on eigenvalue problem," *IEEE Trans. Signal Processing*, vol.47, no.2, pp.554-559, Feb. 1999.
- [9] P. P. Vaidyanathan and P-Q Hoang, "Lattice structures for optimal design and robust implementation of two-channel perfect reconstruc-

- tion QMF banks,” *IEEE Trans. on ASSP*, pp.81-94, Jan. 1988.
- [10] M. Lang, H. Guo, J.E. Odegard, C.S. Burrus and R.O. Wells, Jr., “Noise reduction using an undecimated discrete wavelet transform,” *IEEE Signal Processing Lett.*, vol.3, no.1, pp.10-12, Jan. 1996.
- [11] I. W. Selesnick, J. E. Odegard and C. S. Burrus, “Nearly symmetric orthogonal wavelets with noninteger DC group delay,” in *Proc. IEEE DSP Workshop*, Loen, Norway, Sep. 1996.
- [12] D. Wei and A. C. Bovik, “Generalized coiflets with nonzero-centered vanishing moments,” *IEEE Trans. Circuits and Systems II, Analog and Digital Signal Processing*, vol.45, no.8, pp.988-1001, Aug. 1998
- [13] N. G. Kingsbury, “The dual-tree complex wavelet transform: A new technique for shift invariance and directional filters,” in *Proc. 8th IEEE DSP Workshop*, Utan, no.86, Aug. 1998.
- [14] N. G. Kingsbury, “Image processing with complex wavelets,” *Phil. Trans. Royal Society London A*, no. 357, pp.2543-2560, Sep 1999.
- [15] C. Taswell, “The what, how, and why of wavelet shrinkage denoising,” *Computing in Science & Engineering*, vol.2, no.3, pp.12-19, May/June 2000.
- [16] N. G. Kingsbury, “A dual-tree complex wavelet transform with improved orthogonality and symmetry properties,” in *Proc. ICIP2000*, Vancouver, Canada, vol.2, pp.375-378, Sep. 2000.
- [17] N. G. Kingsbury, “Complex wavelets for shift invariant analysis and filtering of signals,” *Appl. Comput. Harmon. Anal.*, vol.10, no.3, pp.234-253, May 2001.
- [18] A. F. Abdelnour and I. W. Selesnick, “Design of 2-band orthogonal

- near-symmetric CQF,” in Proc. ICASSP2001, Salt Lake City, USA, vol.6, pp.3693-3696, May 2001.
- [19] I. W. Selesnick, “Hilbert transform pairs of wavelet bases,” IEEE Signal Processing Letters, vol.8, no.6, pp.170-173, Jun. 2001.
- [20] I. W. Selesnick, “The design of approximate Hilbert transform pairs of wavelets bases,” IEEE Trans. Signal Processing, vol.50, no.5, pp.1144-1522, May 2002.
- [21] I. W. Selesnick, “A new complex-directional wavelet transform and its application to image demonising,” in Proc. ICIP2002, vol.3, pp.573-576, 2002.
- [22] N. G. Kingsbury, “Design of Q-shift complex wavelets for image processing using frequency domain energy minimization,” in Proc. ICIP2003, Barcelona, Spain, vol.1, pp.1013-1016, Sep. 2003.
- [23] H. Ozkaramanli and R. Yu, “On the phase condition and its solution for Hilbert transform pairs of wavelet bases,” IEEE Trans. Signal Processing, vol.51, no.12, pp.3293-3294, Dec. 2003.
- [24] D. B. H. Tay, M. Palaniswami, “Hilbert pair of wavelets via the matching design technique,” in Proc. ISCAS2005, Kobe, Japan, vol.3, pp.2303-2306, May 2005.
- [25] K. Kawada, X. Zhang, T. Yoshikawa, Y. Takei and Y. Sugita, “Design of Hilbert transform pairs of wavelet bases using IIR filters,” Technical Report of IEICE, no.CAS2005-44, Sep. 2005.
- [26] I. W. Selesnick, R. G. Baraniuk and N. G. Kingsbury, “The dual-tree complex wavelet transform,” IEEE Signal Processing Mag., vol.22, no.6, pp.123-151, Nov. 2005.

- [27] R. Yu and H. Ozkaramanli, "Hilbert transform pairs of orthogonal wavelet bases: Necessary and sufficient conditions," *IEEE Trans. Signal Processing*, vol.53, no.12, pp.4723-4725, Dec. 2005.
- [28] D. B. H. Tay, "Least squares design of orthonormal wavelets via the zero-pinning technique," in *Proc. ICASSP2006*, Toulouse, France, vol.3, pp.213-216, May 2006.
- [29] C. Chaux, L. Duval and J. -C. Pesquet, "Image analysis using a dual-tree M-band wavelet transform," *IEEE Trans. Image Processing*, vol.15, no.8, pp.2397-2412, Aug. 2006.
- [30] D. B. H. Tay, N. G. Kingsbury and M. Palaniswami, "Orthonormal Hilbert pair of wavelets with (almost) maximum vanishing moments," *IEEE Signal Process. Lett.*, vol.13, no.9, pp.533-536, Sep. 2006.
- [31] B. Dumitrescu, I. Bayram and I. W. Selesnick, "Optimization of symmetric self-Hilbertian filters for the dual-tree filter complex wavelet transform," *IEEE Signal Process. Lett.*, vol.15, pp.146-149, Jan. 2008.
- [32] I. A. El-shehaby and T. D. Tran, "Local computation and estimation of wavelet coefficients in the dual-tree complex wavelet transform," in *Proc. ISCAS2008*, Seattle, WA, USA, pp.2877-2880, May 2008.
- [33] H. L. Shi, B. Hu and J. Q. Zhang, "A novel scheme for the design of approximate Hilbert transform paris of orthonormal wavelet bases," *IEEE Trans. Image Processing*, vol.56, no.6, pp.2289-2297, June 2008.
- [34] X. Zhang, "Design of Hilbert transform pairs of orthonormal wavelet bases using Remez exchange algorithm," in *Proc. ICIP2009*, Cairo, Egypt, pp.3813-3816, Nov. 2009.
- [35] B. Goossens, A. Pizurica and W. Philips, "A filter design technique

- for improving the directional selectivity of the first scale of the Dual-Tree complex wavelet transform,” in Proc. ICIP2009, Cairo, Egypt, pp.3805-3808, Nov. 2009.
- [36] X. Zhang and D. W. Wang, “Design of dual tree complex wavelet transforms using IIR digital filters,” in Proc. of 3rd International Symposium on Robot and Artificial Intelligence, Shanghai, China, June 2010.
- [37] D. W. Wang and X. Zhang, “Design of Hilbert transform pairs of orthonormal wavelet bases using IIR filters,” in Proc. ISCIT2010, Tokyo, Japan, pp.554-559, Oct. 2010.
- [38] D. B. H. Tay, “A new approach to the common-factor design technique for Hilbert-pair of wavelets,” *IEEE Signal Process. Lett.*, vol.17, no.11, pp. 969-972, Nov. 2010.
- [39] X. Zhang, “Design of Hilbert transform pairs of orthonormal wavelet bases with improved analyticity,” in Proc. ICASSP2011, Prague, Czech Republic, pp.4384-4387, May 2011.
- [40] D.W. Wang and X. Zhang, “Design of DTCWT with improved analyticity and frequency selectivity,” in Proc. of 26th SIP Symposium, Hokkaido, Japan, Nov. 2011.
- [41] X. Zhang, “Design of Q-shift filters with improved vanishing moments for DTCWT,” in Proc. ICIP2011, Brussels, Belgium, pp.257-260, Sep. 2011.
- [42] X. Zhang and H. Morihara, “Design of Q-shift filters with flat group delay,” in Proc. ISCAS2012, Seoul, Korea, pp.2337-2340, May 2012.

- [43] D. W. Wang and X. Zhang, "Performance investigation on DTCWT based on the common factor technique," in Proc. ICASSP2012, Kyoto, Japan, Mar. 2012.
- [44] D. W. Wang and X. Zhang, "IIR-based DTCWTs with improved analyticity and frequency selectivity," *IEEE Trans. Signal Processing*, vol.60, no.11, pp.5764-5774, Nov. 2012.
- [45] D. B. H. Tay, "Symmetric self-Hilbertian filters via extended zero-pinning," *Signal Process.*, vol.92, no.2, pp.392-400, Feb. 2012.
- [46] Murugesan and D. B. H. Tay, "Design of almost symmetric orthogonal wavelet filter bank via direct optimization," *IEEE Trans. Image Processing*, vol.21, no.5, pp.2474-2480, May 2012.
- [47] D. B. H. Tay, "Symmetric self-Hilbertian wavelets via orthogonal lattice optimization," *IEEE Signal Process. Lett.*, vol.19, no.7, pp.387-390, Jul. 2012.
- [48] D. W. Wang and X. Zhang, "Hilbert pair of almost symmetric orthogonal wavelets with arbitrary center of symmetry," in Proc. AP-SIPA ASC, Kaohsiung, Taiwan, Oct. 2013.

Acknowledgements

This dissertation is a summary of my doctoral study from October 2011 to October 2014 at the Department of Communication Engineering and Informatics, University of Electro-Communications, Tokyo, Japan. I am grateful to a large number of people who have directly and indirectly helped me finish this work.

First of all, I would like to express my deep gratitude to Professor Xi Zhang, my supervisor, who has granted me the change to start this research, and has given me innumerable advices and unrelenting encouragements throughout the whole work. I am also deeply indebted to Professor Wataru Mitsuhashi, Professor Takayuki Nagai, Associate Professor Kota Takahashi, Associate Professor Hideyuki Nomura, members of the supervisory committee, for their helpful comments and advices. It is a pleasure to acknowledge the hospitality and encouragement of the members of the Zhang Laboratory.

I would like to give special thanks to my friends and my parents, in appreciation of their generous support, continuous encouragement.

Daiwei Wang

University of Electro-Communications

2014. 7. 29

Author Biography

Daiwei Wang was born in Harbin, China, on October 20, 1986. He received his B.E. degree in information and communication engineering, from Harbin Engineering University (HEU), China, in 2009 and the M.E. degree in communication and informatics from University of Electro-Communications (UEC), Tokyo, Japan, in 2011. He has been with the Department of Communication Engineering and Informatics, University of Electro-Communications, working towards the Ph.D. degree. His current research interests are digital signal processing, filter design theory, filter banks and wavelets.

List of Publications

- [1] D. W. Wang and X. Zhang, "IIR-based DTCWTs with improved analyticity and frequency selectivity," *IEEE Trans. Signal Processing*, vol.60, no.11, pp.5764-5774, Nov. 2012.
- [2] X. Zhang and D. W. Wang, "Design of dual tree complex wavelet transforms using IIR digital filters," in *Proc. of 3rd International Symposium on Robot and Artificial Intelligence*, Shanghai, China, June 2010.
- [3] D. W. Wang and X. Zhang, "Design of Hilbert transform pairs of orthonormal wavelet bases using IIR filters," in *Proc. of ISCIT2010*, pp.554-559, Tokyo, Japan, Oct. 2010.
- [4] D.W. Wang and X. Zhang, "Design of DTCWT with improved analyticity and frequency selectivity," in *Proc. of 26th SIP Symposium*, Hokkaido, Japan, Nov. 2011.
- [5] D. W. Wang and X. Zhang, "Performance investigation on DTCWT based on the common factor technique," in *Proc. of ICASSP2012*, Kyoto, Japan, Mar. 2012.
- [6] D. W. Wang and X. Zhang, "Hilbert pair of almost symmetric orthogonal wavelets with arbitrary center of symmetry," in *Proc. AP-SIPA ASC*, Kaohsiung, Taiwan, Oct. 2013.